UNIVERSITAT POLITÈCNICA DE CATALUNYA
BARCELONATECH

Autonomous and reliable operation of multilayer optical networks

Sima Barzegar

Universitat Politècnica de Catalunya

Optical Communications Group

Autonomous and Reliable Operation of Multilayer Optical Networks

Sima Barzegar

Advisor:

Dr. Luis Velasco

Co-advisor:

Dr. Marc Ruiz

A thesis presented in partial fulfilment of the requirements for the degree of

Philosophy Doctor

April 19, 2022

Optical Communications Group (GCO)

Universitat Politècnica de Catalunya (UPC)

C/ Jordi Girona, 1-3

Campus Nord, D4-2013

08034 Barcelona, Spain

UNIVERSITAT POLITÈCNICA DE CATALUNYA
BARCELONATECH
Escola de Doctorat

Acta de calificación de tesis doctoral

Curso académico:

Nombre y apellidos

Programa de doctorado

Unidad estructural responsable del programa

Resolución del Tribunal

Reunido el Tribunal designado a tal efecto, el doctorando / la doctoranda expone el tema de la su tesis doctoral titulada ____

____.

Acabada la lectura y después de dar respuesta a las cuestiones formuladas por los miembros titulares del tribunal, éste otorga la calificación:

☐ NO APTO ☐ APROBADO ☐ NOTABLE ☐ SOBRESALIENTE

(Nombre, apellidos y firma) Presidente/a	(Nombre, apellidos y firma) Secretario/a

(Nombre, apellidos y firma) Vocal	(Nombre, apellidos y firma) Vocal	(Nombre, apellidos y firma) Vocal

______________________, _______ de __________________ de _______________

El resultado del escrutinio de los votos emitidos por los miembros titulares del tribunal, efectuado por la Escuela de Doctorado, a instancia de la Comisión de Doctorado de la UPC, otorga la MENCIÓN CUM LAUDE:

☐ SÍ ☐ NO

(Nombre, apellidos y firma) Presidente de la Comisión Permanente de la Escuela de Doctorado	(Nombre, apellidos y firma) Secretaria de la Comisión Permanente de la Escuela de Doctorado

Barcelona a _______ de ____________________ de __________

Acknowledgements

First and foremost, I am extremely grateful to my supervisors, Prof. Luis Velasco and Dr. Marc Ruiz for their invaluable advice, continuous support, and patience during my PhD study. Their immense knowledge and plentiful experience have encouraged me in all the time of my academic research and daily life. I would also like to thank Dr. Filippo Cugini and Dr. Matias Richart for accepting and supporting me to work within their group in CNIT, Italy and Universidad de la República, Uruguay; these stays provided me bunch of skills and experiences in my carrier and in my life.

I would like to thank all the colleagues, Fatemeh, Morteza, Mariano, Masab, Diogo, Hailey, Shaoxuan and Pol for the cherished time spent together in the GCO lab, and all my colleagues in Italy and Uruguay whose contribution in my life is unforgettable.

Finally, I would like to express my gratitude to my parents, my brother, my family and my friends. Without their tremendous understanding and encouragement in the past few years, it would be impossible for me to complete my study.

This PhD thesis is dedicated to my dear parents, Khadijeh and Ahmad,

and my dear brother, Salar, who have taught me how to live, be strong and love unconditionally.

Abstract

This Ph.D. thesis focuses on the reliable autonomous operation of multilayer optical networks.

The first objective focuses on the reliability of the optical network and proposes methods for health analysis related to Quality of Transmission (QoT) degradation. Such degradation is produced by soft-failures in optical devices and fibers in core and metro segments of the operators' transport networks. Here, we compare estimated and measured QoT in the optical transponder by using a QoT tool based on GNPy. We show that the changes in the values of input parameters of the QoT model representing optical devices can explain the deviations and degradation in performance of such devices. We use reverse engineering to estimate the value of those parameters that explain the observed QoT. We show by simulation a large anticipation in soft-failure detection, localization and identification of degradation before affecting the network. Finally, for validating our approach, we experimentally observe the high accuracy in the estimation of the modeling parameters.

The second objective focuses on multilayer optical networks, where lightpaths are used to connect packet nodes thus creating virtual links (vLink). Specifically, we should study how lightpaths can be managed to provide enough capacity to the packet layer without detrimental effects in their Quality of Service (QoS), like added delays or packet losses, and at the same time minimize energy consumption. Such management must be as autonomous as possible to minimize human intervention. In addition, the relation between the packet and the optical layer should be considered, as it can bring global optimal solutions. We study the autonomous operation of optical connections based on digital subcarrier multiplexing (DSCM). We propose several solutions for the autonomous operation of DSCM systems. In particular, the combination of two modules running in the optical node and in the optical transponder activate and deactivate subcarriers to adapt the capacity of the optical connection to the upper layer packet traffic. The module running in the optical node is part of our Intent-based Networking (IBN) solution and implements prediction to anticipate traffic changes. Our comprehensive study demonstrates the feasibility of DSCM autonomous operation and shows large cost savings in terms of energy consumption. In addition, our study provides a guideline to help vendors and operators to adopt the proposed solutions.

The final objective targets at automating packet layer connections (PkC). Automating the capacity required by PkCs can bring further cost reduction to network operators, as it can limit the resources used at the optical layer. However, such automation requires careful design to avoid any QoS degradation, which would impact Service Level Agreement (SLA) in the case that the packet flow is related to some customer connection. We study autonomous packet flow capacity management. We apply RL techniques and propose a management lifecycle consisting of three different phases: 1) a self-tuned threshold-based approach for setting up the connection until enough data is collected, which enables understanding the traffic characteristics; 2) RL operation based on models pre-trained with generic traffic profiles; and 3) RL operation based on models trained with the observed traffic. We show that RL algorithms provide poor performance until they learn optimal policies, as well as when the traffic characteristics change over time. The proposed lifecycle provides remarkable performance from the starting of the connection and it shows the robustness while facing changes in traffic. Finally, we take advantage of our experience and revisit our proposed solutions for autonomous vLink operation supported by DSCM systems. The contribution is twofold: 1) and on the one hand, we propose a solution based on RL, which shows superior performance with respect to the solution based on prediction; and 2) because vLinks support packet connections, coordination between the intents of both layers is proposed. In this case, the actions taken by the individual PkCs are used by the vLink intent. The results show noticeable performance compared to independent vLink operation.

Resumen

Esta tesis doctoral se centra en la operación autónoma y confiable de redes ópticas multicapa.

El primer objetivo se centra en la fiabilidad de la red óptica y propone métodos para el análisis del estado relacionados con la degradación de la calidad de la transmisión (QoT). Dicha degradación se produce por fallos en dispositivos ópticos y fibras en las redes de transporte de los operadores que no causan corte de la señal. Aquí, comparamos el QoT estimado y medido en el transpondedor óptico mediante el uso de una herramienta de QoT basada en GNPy. Mostramos que los cambios en los valores de los parámetros de entrada del modelo QoT que representan los dispositivos ópticos pueden explicar las desviaciones y la degradación en el rendimiento de dichos dispositivos. Usamos ingeniería inversa para estimar el valor de aquellos parámetros que explican el QoT observado. Mostramos, mediante simulación, una gran anticipación en la detección, localización e identificación de fallos leves antes de afectar la red. Finalmente, validamos nuestro método de forma experimental y comprobamos la alta precisión en la estimación de los parámetros de los modelos.

El segundo objetivo se centra en las redes ópticas multicapa, donde se utilizan conexiones ópticas (lightpaths) para conectar nodos de paquetes creando así enlaces virtuales (vLink). Específicamente, estudiamos cómo se pueden gestionar los lightpaths para proporcionar suficiente capacidad a la capa de paquetes sin efectos perjudiciales en su calidad de servicio (QoS), como retardos adicionales o pérdidas de paquetes, y al mismo tiempo minimizar el consumo de energía. Dicha gestión debe ser lo más autónoma posible para minimizar la intervención del operador. Además, se debe considerar la relación entre las capas de paquetes y óptica, ya que pueden obtenerse soluciones óptimas globales. Estudiamos el funcionamiento autónomo de conexiones ópticas basadas en multiplexación de subportadoras digitales (DSCM).

Proponemos varias soluciones para el funcionamiento autónomo de los sistemas DSCM. En particular, la combinación de dos módulos que se ejecutan en el nodo óptico y en el transpondedor óptico activan y desactivan subportadoras para adaptar la capacidad de la conexión óptica al tráfico de paquetes de la capa superior. El módulo que se ejecuta en el nodo óptico es parte de nuestra solución de red basada en intención (IBN) e implementa predicción para anticipar los cambios de tráfico. Nuestro estudio integral demuestra la viabilidad de la operación autónoma de DSCM y muestra un gran ahorro de costos en términos de consumo de energía. Además, nuestro estudio proporciona una guía para ayudar a los proveedores y operadores a adoptar las soluciones propuestas.

El objetivo final es la automatización de conexiones de capa de paquetes (PkC). La automatización de la capacidad requerida por las PkC puede generar una mayor reducción de costes para los operadores de red, ya que puede limitar los recursos utilizados en la capa óptica. Sin embargo, dicha automatización requiere un diseño cuidadoso para evitar cualquier degradación de QoS, lo que afectaría acuerdos de nivel de servicio (SLA) en el caso de que el flujo de paquetes esté relacionado con alguna conexión del cliente. Estudiamos la gestión autónoma de la capacidad del flujo de paquetes. Aplicamos técnicas de aprendizaje por refuerzo (RL) y proponemos un ciclo de vida de gestión que consta de tres fases diferentes: 1) un enfoque basado en umbrales auto ajustados para configurar la conexión hasta que se recopilen suficientes datos, lo que permite comprender las características del tráfico; 2) operación RL basada en modelos pre-entrenados con perfiles de tráfico genéricos; y 3) operación de RL en base a modelos entrenados con el tráfico observado. Mostramos que los algoritmos de RL ofrecen un desempeño deficiente hasta que aprenden las políticas óptimas, así como también cuando las características del tráfico cambian con el tiempo. El ciclo de vida propuesto proporciona un rendimiento notable desde el inicio de la conexión y muestra la robustez frente a cambios en el tráfico. Finalmente, aprovechamos nuestra experiencia y revisamos las soluciones propuestas para la operación autónoma de vLink respaldada por sistemas DSCM. La contribución es doble: 1) por un lado, propusimos una solución basada en RL, que muestra un rendimiento superior con respecto a la solución basada en predicción; y 2) debido a que los vLinks admiten conexiones de paquetes, se propone la coordinación entre las intenciones de ambas capas. En este caso, la intención de vLink utiliza las acciones realizadas por los PkC individuales. Los resultados muestran un rendimiento notable en comparación con la operación independiente de vLink.

Table of Contents

List of Figures

Page

List of Tables

Chapter 1

Introduction

1.1 Motivation

The massive application of the optical technology [EON16], not only in the core segment of the operators' transport networks, but also in the metro and even in the access segments [Ve13], is a clear consequence of its characteristic high bandwidth, low latency, and high reliability.

One ingredient of the optical technology is that of the Forward Error Correction (FEC) techniques [Ty06] that allow to correct errors in the optical transmission. FEC techniques are applied in the end Optical Transponders (TRX) of optical connections (*lightpath*) to guarantee zero post-FEC Bit Error Rate (BER) transmission provided that pre-FEC BER is below some BER threshold; when such threshold is exceeded, zero post-FEC error cannot be achieved (FEC limit) and the lightpath will be consequently torn down.

Although degradation of the Quality of Transmission (QoT) is related to linear and Non-Linear (NL) optical impairments, other effects like optical fiber and devices aging have a great impact as well. Aging effects are usually considered by means of costly system margins [Po17]; examples include the increasing fiber losses due to splices to repair fiber cuts, degradation of Optical Amplifiers (OA) noise factor, and detuning of the lasers in the TRXs leading to misalignment with filters in Wavelength Selective Switches (WSS). If those degradations (soft-failures) are not corrected (e.g., by retuning, repairing or replacing the related optical device/fiber), they can degenerate into hard-failures and affect a number of lightpaths supporting a large amount of network services; therefore, it is of paramount importance not only to detect any QoT degradation as soon as possible [APV17], but also to localize the device/fiber causing the degradation to facilitate maintenance [APV18].

For such detection and localization to be possible, the control plane of the optical network, which based on the Software-Defined Networking (SDN) concept [Ne17], needs to be enriched with Monitoring and Data Analytics (MDA) capabilities [Ve19.1]. Once monitoring data have been collected from the data plane, data analytics algorithms, e.g., based on Machine Learning (ML) [Ra18.1], can analyze them either as soon as they are available or periodically to proactively detect the degradation and anticipate hard-failures before they actually happen; once detected, recommendations can be issued to the network controller so it can make decisions about rerouting and/or reconfiguring the network [Ve17], as well as to notify the management plane for scheduling maintenance.

Further, a considerable effort is being payed towards disaggregating the optical layer to enrich the offer of available solutions and to enable the deployment of optical nodes that better fit optical network operators' needs [Ve18]. Such disaggregation, however, tends to make network surveillance and maintenance more complex in general.

From the operation perspective, the optical network is becoming more and more are complex, since it interacts with many other systems to provide end-to-end services. With localized and highly engineered operational tools, it is typical of these networks to take several weeks to months for any changes, upgrades or service deployments to take effect. However, as the dynamicity of the traffic increases, the need for self-network operation becomes more evident. In this regard, advances in network automation [Ra18.1] are receiving considerable attention from the industry as the complexity of the network increases and the requirements from the services become more stringent and diverse. Autonomous network operation evolves from SDN and promises to reduce operational expenditures by implementing *closed loops* based on data analytics [Ve19.1], [Bo21]; network automation entails the collection of performance monitoring data that are analyzed, and the extracted knowledge is used to make decisions (control loop). Machine Learning (ML), a sub-domain of Artificial Intelligence (AI), is highly suitable for complex system representation [Ra18.1]. Using ML algorithms for network automation entails analyzing heterogeneous data collected from monitoring points in network devices.

Among the large number of use cases for autonomous optical network operation, three major categories covering the entire lifecycle of optical connections are highlighted in [Ve19.1]. The first category refers to the automation of connectivity provisioning, when the provisioning process itself requires meeting some performance, e.g., achieve resource efficiency or minimize connection blocking [Da15], [Ch19.1]. In addition, monitoring and estimation of QoT is of paramount importance for both connection provisioning and reconfiguration. A second category is related to the dynamic network adaptation, which entails monitoring one or more network entities (e.g., an optical connection) and make decisions to achieve some target performance. The target is to deal with situations ranging from those that require scaling or reallocating resources to elastically adjust to demand variations in volume and direction, to those that require healing and recovery. Examples include QoT degradation and connection rerouting [Ve18.2], in-operation network planning [Ve17], dynamic capacity allocation of virtual links supported by one or more optical connections or even reconfigure a virtual network topology [Mo17], [Ve18.1]. Finally, as a third category, degradation detection can be used also for failure localization [Sh19]. Here, the performance to be achieved is related, e.g., to availability metrics.

However, the drawback is the proliferation of individual control loops, which brings also complexity to network management. In addition, defining how to achieve operational goals is very complex. To address some of these issues, Intent-Based Networking (IBN) [Cl21], [Ve21] allows the definition of operational objectives that a network entity, e.g., a lightpath or a traffic flow, has to meet without specifying how to meet them. IBN implements and enforces those objectives, often with the help of ML. This strategy reduces human intervention and paves the way to the application of AI/ML techniques.

Another issue is that of data availability, since AI/ML usually require a large dataset for training purposes, which is difficult to obtain. The lack of data can be compensated with the use of tools that include analytic models to explain the data plane, e.g., GNPy [Fi18] for the optical and CURSA-SQ [Ru18] to generate packet traffic and measure Quality of Service (QoS) related performance. Such tools can run in sandbox domains [Ru20.1] and used for training AI/ML algorithms (see [ITU20]).

1.2 Goals of the thesis

In light of the above, this Ph.D. thesis focuses on the reliable autonomous operation of multilayer optical networks. Specifically, the following goals are defined to achieve this main objective:

G.1 – Optical Network Health Analysis

This first objective focuses on the reliability on the optical network and proposes methods for health analysis related to QoT degradation. Such degradation is produced by soft-failures in optical devices and fibers in core and metro segments of the operators' transport networks. This goal targets at several aspects related to QoT degradation, including:

- Detecting and localizing soft-failures that impact on the optical layer.
- Finding the likely configuration of the optical devices and fibers that are the cause of a soft-failure, while minimizing both the computation requirements and the time needed for that.

- Estimating the severity of the soft-failure, defined as the time when some threshold value will be exceeded. The intention is to evaluate the urgency for making the proper decision to avoid disruption, including re-tuning, re-routing, maintenance, etc.
- Comparing estimation results to real test bed measurement for validating the accuracy of the proposed methods.

G.2 – Reliable vLink Autonomous Operation

This goal focuses on multilayer optical networks, where lightpaths are used to connect packet nodes thus, creating virtual links (vLink). Specifically, we should study how lightpaths can be managed to provide enough capacity to the packet layer without detrimental effects in their QoS, like added delays or packet losses, and at the same time minimize energy consumption. Such management must be as autonomous as possible to minimize human intervention. In addition, the relation between the packet and the optical layer should be considered, as it can bring global optimal solutions.

G.3 – Autonomous Packet Flow Capacity Management

This final goal targets at automating packet layer connections (PkC). Automating the capacity required by PkCs can bring further costs reduction to network operators, as it can limit the resources used at the optical layer. However, such automation requires careful design to avoid any QoS degradation, which would impact Service Level Agreement (SLA) in the case that the packet flow is related to some customer connection.

A summary of the goals of the Ph.D. thesis is presented in Table 1-1.

Table 1-1: Thesis goals

Goals
G.1 **Optical Network Health Analysis**
G.2 **Reliable vLink Autonomous Operation**
G.3 **Autonomous Packet Flow Capacity Management**

1.3 Methodology

This Ph.D. thesis assumes the architecture in Figure 1-1, where the optical layer consists of a disaggregated set of ROADMs and TRXs, and a set of optical links interconnecting ROADMs with a number of OAs. On top of the optical layer, a packet layer is configured, where the packet nodes are connected through the optical layer. The control plane includes:

i) a Network Controller to program the network devices;

ii) an MDA system [Ve19.1] that collates measurements from the data plane, analyses the data and issues recommendations to the network controller;

iii) a QoT tool that estimates the SNR of the lightpaths and it is used for connection provisioning, as well as for diagnosis and failure localization.

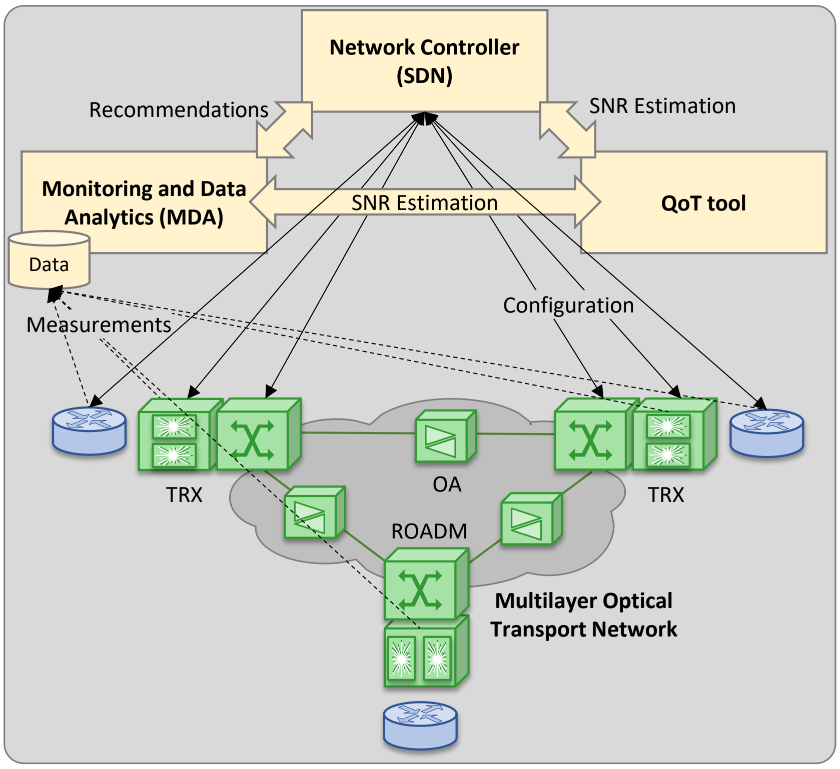

Figure 1-1: Overview of the proposed architecture

To carry out the studies needed to meet the goals of this thesis, the methodology in Figure 1-2 will be followed.

As the starting point of every study, one or more topologies and scenarios will be conceived. Then, due to the nature of this Ph.D. thesis' goals, performance data will be generated, where configuration parameters of the optical devices and fibers or the packet traffic itself will be varied. Such initial data set will be the input for a data generator that will produce performance or traffic data that evolved with the time following some predefined profile.

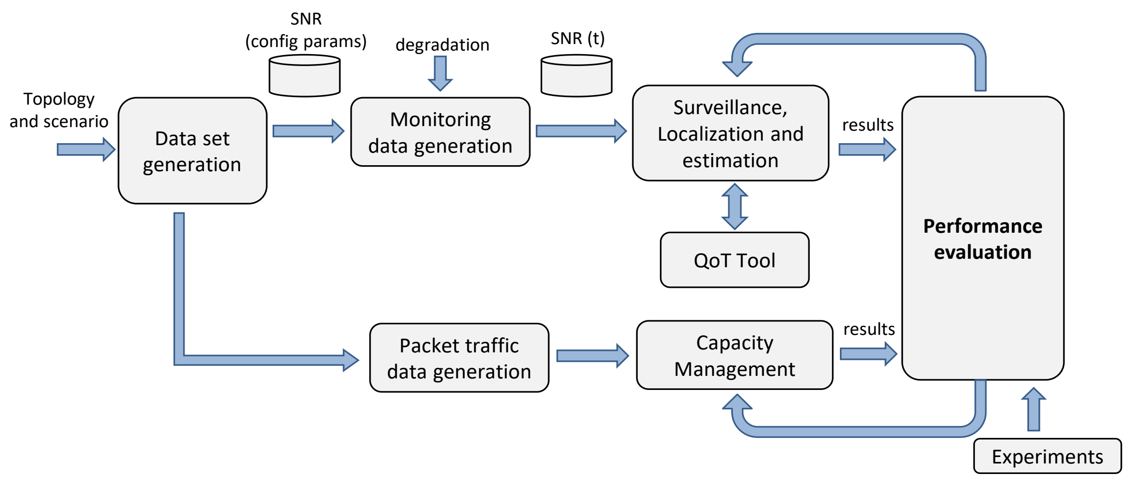

Figure 1-2: Methodology to be followed in this Ph.D. thesis

The main algorithms developed in this Ph.D. thesis will concentrate on the surveillance, localization and estimation on the one hand, and on the other, on the capacity management for autonomous operation. The former algorithms will receive the evolution of the performance and use an external QoT for estimating the likely configuration parameters of the optical devices and fibers, whereas the latter, will receive the packet traffic and compute the capacity of the lightpath or packet flow to guarantee the committed performance.

Finally, the results obtained in the previous steps will be evaluated through experiments carried out in a real test bed. Such evaluation will help the improvement of the algorithms.

The results will be disseminated and considered as the conception of new ideas requiring further research.

1.4 Thesis outline

The remainder of this Ph.D. thesis is organized as follows.

Chapter 2 provides the needed background on AI/ML methods, SDN and IBN concepts.

Chapter 3 briefly reviews the state-of-the-art related to the objectives of this Ph.D. thesis such as optical network health analysis and Autonomous Operation in multilayer optical networks and highlighting the niches to be covered.

Chapter 4 focuses on goal G.1 and covers optical network health analysis. This chapter is based on the journal publication [TNSM21].

Chapter 5 relates to goal G.2 and investigates vLink autonomous operation based on predefined policies and simple ML techniques. This chapter is based on one journal publication [JSAC21].

Chapter 6 concentrates on goal G.3 and is devoted to the application of apply Reinforcement Learning (RL) for the autonomous packet flow capacity management. This chapter is based on the journal publication [SENSORS21].

Chapter 7 aims the complete achievement of goal G.2, where we apply RL for reliable vLink autonomous operation. In addition, cooperation between PkC and vLink intents is proposed. This chapter is based on the journal papers [JSAC21] and [JOCN22].

Finally, Chapter 8 concludes this Ph.D. thesis.

1.5 Contributions and References from the Literature

For the sake of clarity and readability, references contributing to this Ph.D. thesis are labelled using the following criteria: [<conference/journal> <Year(yy)[.autonum]>], e.g., [ECOC20] or [JSAC21]; in case of more than one contribution with the same label, a sequence number is added.

The rest of the references to papers or books, both auto references not included in this Ph.D. thesis and other references from literature are labelled with the initials of the first author's surname together with its publication year, e.g., [Ve17].

Chapter 2

Background

In this chapter, we introduce the needed background on the IBN paradigm. IBN targets at defining high-level abstractions, so network operators can define what are their desired outcomes without specifying how they would be achieved. The latter can be achieved by leveraging network programmability, monitoring and data analytics, as well as the key assurance component.

IBN relates to AI/ML techniques and those need large datasets for training purposes. In this chapter, we cover the AI/ML techniques that we consider for the solutions proposed in this Ph.D. thesis, as well as some challenges and solutions for the generation of accurate synthetic data.

2.1 Toward Network Automation

2.1.1 Previous Architectures

Network automation has been long time envisioned. In fact, the Telecommunications Management Network (TMN), defined by the International Telecommunication Union in [ITU00], is a hierarchy of management layers (network element, network, service, and business management), where high-level operational goals propagate from upper to lower layers.

In the way toward autonomic adaptation to changes, while hiding intrinsic complexity to operators and users, the Internet Engineering Task Force developed the concept of Policy-Based Network Management (PBNM) [St04]. PBNM separates the rules governing the behavior of a system from its functionality. In PBNM, high-level management *policies* are broken down into low-level configurations and control logic (*policy rules*) to ensure that the network provides the required services. Policies can be defined as a set of simple *control loops*; each policy rule consists of a set of events and conditions and a corresponding set of actions, where each condition defines *when* the policy rule is applicable.

The most extended PBNM architecture consists of four systems (Figure 2-1): *i*) the policy management tool allows operators to define and update policies and it translates and validates policy rules; *ii*) the policy repository that stores the policies; *iii*) a set of policy decision points, which interprets the policies, translates them into a device-specific representation, and triggers the execution of the related actions whenever they satisfy the specified conditions; and *iv*) the policy enforcement points running on a policy-aware node that executes the policies. The drawback of PBNM is solving conflicts that might arise within or among policies; conflict resolution requires some external system or iterations with operators and/or users.

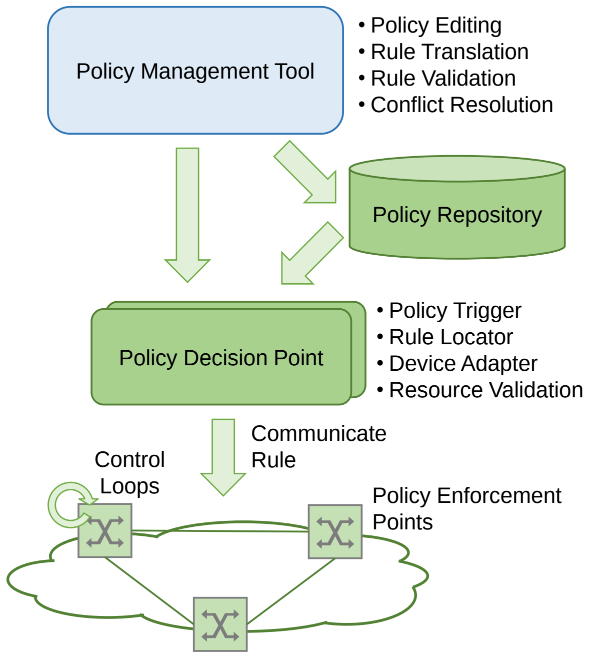

Figure 2-1 Policy-Based Network Management

2.1.2 Software-Defined Networking (SDN)

The network management architecture has evolved with the development of the Software-Defined Networking (SDN) [Ne17] concept. SDN brings programmability to simplify configuration (it breaks down high-level service abstraction into lower-level device abstractions), orchestrates operation, and automatically reacts to changes or events. SDN defines a centralized control plane architecture with global network vision, which can achieve optimal routing at provisioning time and during reconfiguration [Ve14]. Placed besides the SDN controller, a Monitoring and Data

Analytics (MDA) system was proposed in [Gi18] and [Ve19.1] to collect monitoring data, analyze such data, and make decisions (control loop) (Figure 2-2). Such data analysis can be based on AI / ML algorithms [Ra18.1], which enable network automation solutions, aiming at reducing operational costs.

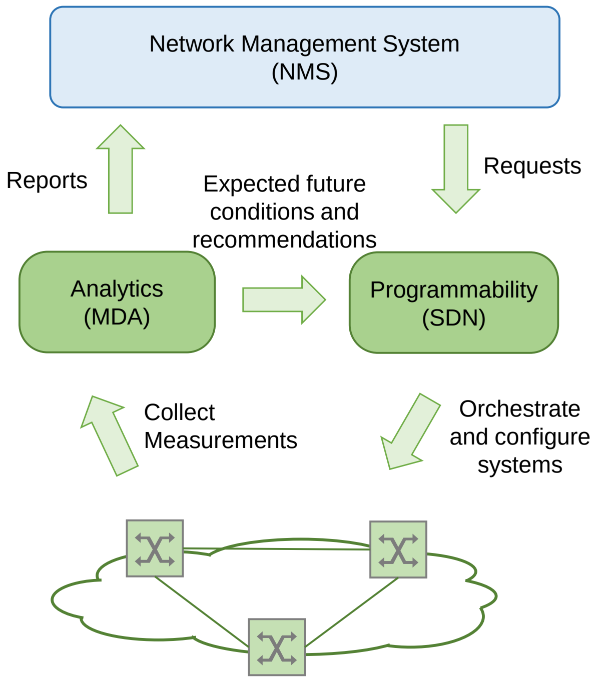
Network Management System (NMS)
Reports
Requests
Expected future conditions and recommendations
Analytics (MDA)
Programmability (SDN)
Collect Measurements
Orchestrate and configure systems

Figure 2-2 Software-Defined Networking and Monitoring and Data Analytics

The MDA complements the SDN controller, so the network becomes proactive. Being proactive is of paramount importance, as the analytics system could anticipate anomalies and degradations (soft-failures) before they cause major problems or become hard-failures. Upon the detection, the analytics system can issue proper recommendations to the SDN controller, which can take the most appropriate action. Additionally, such analysis can be extended to forecasting network conditions that can be used to improve resource efficiency. In this architecture, control loops can be defined at various levels, from the device [APV17.2] to the network, depending on the use case [APV18], [APV17.1], as monitoring is collected and can be analyzed locally and/or network-wide.

The drawback of this architecture is that the analytics system needs to combine information about services and the network itself, which, in practice, requires redesigning that and other control and management systems.

2.1.3 Intent-Based Networking

Another approach for network automation is IBN [Cl21], [Ve21]. In IBN intents are defined as high-level abstractions that allow network operators to define *what* are their desired outcomes, without specifying *how* they would be achieved.

In an IBN environment thus, operators provide intents as inputs to guide content-based systems to implement them without human intervention. Intents allow to define the goals and outcomes and provide: *i*) data abstraction to avoid users and operators to take care of specific device configuration; and *ii*) functional abstraction to avoid users and operators being concerned with how to achieve the goals.

IBN complements SDN control and orchestration by allowing a declarative syntax while abstracting the operational process and focusing on behavior. Service definition can be based on templates to define resources and relationships for the service and allow specifying the Intent in terms of policy rules that guide the service behavior, specifying the applications, analytics and closed control loop events needed for the elastic management of the service.

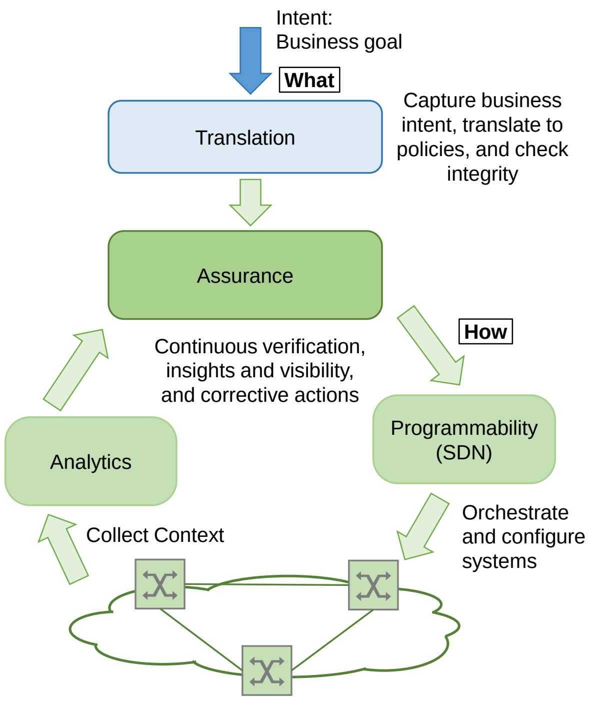
Intent:
Business goal
What
Translation
Capture business intent, translate to policies, and check integrity
Assurance
How
Continuous verification, insights and visibility, and corrective actions
Programmability (SDN)
Analytics
Collect Context
Orchestrate and configure systems

Figure 2-3 Intent-Based Networking

A *translation* mechanism is needed to convert the intent into a network configuration to be automatically deployed within the network infrastructure and a set of policies that the IBN needs to verify that such policies can be executed (Figure 2-3). During the service lifecycle, the service *assurance* system makes sure that the network continues to deliver on that intent based on the specified design, analytics, and policies and with the help of ML algorithms. Intent-Based ML algorithms find the right knowledge and data to identify conditions with significant semantic value (insights) from raw telemetry, without being explicitly programmed. Actionable insights and rich context together with policy-driven closed loops can take automated actions whenever the network deviates from the intent. Reporting is intended to generate descriptive outputs, e.g., statistical summaries, as well as knowledge transfer of main key performance indicators of the service. Differentiated reports can be generated, so applications can reconfigure policies to adjust to service requirements and the network management can gather knowledge transferred for different services and processed jointly to improve actions [Ch21], [Ru20.2], [Ta21].

Finally, the IBN architecture can be complemented with sandbox domains, where model training will be performed with data from a data lake populated from heterogeneous data and context sources, including network, applications, and other systems, and augmented with data from simulation [Ve19.2], [Be20].

2.2 Advanced ML Techniques

Many intent-based solutions need from ML techniques as a way to implement proactive approaches. In this section, we give some background on advanced ML techniques that are used in the applications that are presented in the next sections. Note that simpler (but not necessarily less effective) ML techniques for network automation can be found in [Ra19].

2.2.1 Regression for Time Series

Time series forecasting covers those methodologies that predict future events as a function of previous observations, as well as some additional features that may or not depend on time. Traditionally, Autoregressive Integrated Moving Average (ARIMA) models [ShSt17] have been proposed for time series forecasting, due to several key characteristics, such as easiness of interpretability and the ability to provide probability distributions of the predicted events. They assume linearity between features and need some data pre-processing to remove important components out of the model (such as trend or heteroscedasticity), which reduces their applicability for more complex time series events.

Deep learning techniques can be applied to predict complex future events without considering strongly limiting assumptions. In particular, the use of feed-forward neural networks (FFNN) [ZhQi05] allows considering complex nonlinear relations among input features and the predicted future event. Moreover, they facilitate working with a mix of numerical and categorical inputs, as well as making predictions for several steps ahead, i.e., multi-step prediction.

In general, FFNNs work better with pre-processed features that summarize the input information to be considered for prediction, e.g., some statistics and trend of the last observed events. This can be a limiting factor if features are not well designed. Another approach is to use raw data, e.g., all data observed in a large past window. In this regard, convolutional neural networks (CNN) have the inherent ability to learn and automatically extract features from raw input data [Ag18]. By means of hidden convolutional layers, automatic identification and extraction of relevant features is produced in an unsupervised manner.

Although both FFNN and CNN can be designed and trained to predict time series events, they were devised for applications that do not depend on time. On the contrary, Recurrent Neural Networks (RNN) [MaCh01] have been proposed specifically to deal with time series events, since they can explicitly manage the ordering among inputs. RNNs implement knowledge persistence, so it can be used for predictions. However, in general, this memory is short and knowledge vanishes with time. To improve RNNs, Long Short-Term Memory (LSTM) networks [MaCh01] were proposed to expand temporal dependence learning. LSTM units consist of a set of different complex gates, namely input, output, and forget gates and the coefficients of the network are dynamically managed to keep long term memory. LSTMs provide accurate prediction of time series with complex temporal correlation, e.g., periodical sharp changes [GuTh19].

2.2.2 Reinforcement Learning

Reinforcement Learning (RL) considers the paradigm of an intelligent agent that takes actions in an *environment*. At every discrete time step t, with a given state *s*, the agent selects action a with respect to a policy, and it receives from the environment a reward r and the new state *s'*. The objective is to find the optimal policy that maximizes a cumulative reward function. RL fits perfectly as part of intent agents, as the related problems can be usually stated in the form of a Markov decision process and they can be solved RL using dynamic programming techniques. In addition, in contrast to supervised learning, RL does not need labeled datasets and it can correct sub-optimal actions through exploration.

The simplest RL is Q-learning [SuBa18], which is a model-free discrete RL method that uses a Q-table to represent the learned policy, where every pair *<s, a>* contains a *q* value. Being at state *s*, the action a to be taken is the one with the highest q value (or it is chosen randomly). Once the action is implemented and the new state *s'* and the gained reward *r* are received from the environment, the agent updates the corresponding *q* value in the Q-table. Q-learning works efficiently for problems where both states and actions are discrete and finite. However, it usually introduces overestimation, which leads to suboptimal policies, and the Q-table grows with the number of states.

Deep Q-learning (DQN) substitutes the Q-table by a FFNN that receives a continuous representation of the state and returns the expected *q* value for each discrete action [SuBa18]. However, the FFNN tends to make learning unstable, so a *replay buffer* can be used to retrain the FFNN. Double DQN [Ha16] uses two different FFNNs (*learning and target*) to avoid overestimation, which happens when a non-optimal action is quickly biased (due to noise or exploration) with a high q value that makes it preferably selected. The learning model is updated using the q values retrieved from the target model, which is just a simple copy of the learning model and it is periodically updated. Finally, D3QN [Wa16] uses two different estimators to compute the q value of a pair <*s, a*>: *i*) the *value* estimator, an average *q* value of any action taken at state *s*; and *ii*) the *advantage* estimator, which is the specific state-action dependent component. The sum of both components returns expected q values.

DQN-based methods assume a finite discrete action space. Nonetheless, other approaches, such as *Actor-Critic* methods [Fu18], use continuous state and action spaces. *Actor-Critic* methods train two different types of models separately: *i*) *actors*, which compute actions based on states, and *ii*) *critics* that evaluate the actions taken by actors, i.e., compute q values. Both actor and critic models can be implemented by means of FFNNs. Aiming at reducing overestimation, the TD3 method [Fu18] considers one single actor and two different critic models, where the minimum value from the two critics is used for learning the optimal policy.

2.3 Examples of Autonomous Network Operation

Autonomous network operation can be *reactive* (i.e., in response to events) or *proactive* (i.e., acting ahead of time). Let us illustrate the difference with an example, where a packet connection (*PkC*) is established and conveys a traffic flow with unknown traffic characteristics. Our target here is to allocate just enough capacity to ensure the required performance, which would optimize resource utilization. However, every different PkC supports services with different operational goals in terms of delay and throughput (e.g., keeping the total delay below a given maximum, or minimizing the capacity while ensuring zero packet losses, etc.), and so, the tailored capacity dimensioning is required.

Imagine that a policy-based management based on a fixed threshold (e.g., defined in terms of the ratio traffic volume over capacity) is set to operate the capacity of a PkC. Note that such operation can be highly reliable and it is based on a specific rule that is easily understood by human operators. However, deciding the value of the threshold requires knowledge of the traffic: *i*) a high threshold value (e.g., 90%) would result into poor performance coming from high delay, and it can be worse when the variability of the traffic is high; and *ii*) a low threshold value (e.g., 60%) would result into poor resource utilization. Therefore, some traffic analysis would be required. Further, since traffic characteristics can change over time, such analysis need to be continuously performed to change the operating model, when needed.

When PkCs are routed on top of virtual networks, where vLink are supported by the optical layer, capacity might not be instantly allocated. Let us illustrate this problem with an example. Figure 2-4a shows two PkCs (DC1-DC4 and DC2-DC3) that are established on top of a virtual network. Packet nodes are connected through vLinks, each supported by lightpaths on the optical layer. To minimize overprovisioning, such capacity is dynamically adjusted, thus enabling the dynamic vLink capacity management, e.g., by establishing and releasing parallel lightpaths between the end packet nodes or activating and deactivating subcarriers in DSCM systems.

Note that modifying the capacity of a PkC entails programming some rules in packet nodes and new capacity becomes immediately available. In contrast, adding more capacity to the vLink entails establishing a new lightpath, which requires some time (e.g., one minute). Therefore, vLink intents must make decisions with enough time to guarantee capacity availability. Such time depends, among others, of the packet traffic variation and thus, the value of the configured threshold could result into high delay and packet loss.

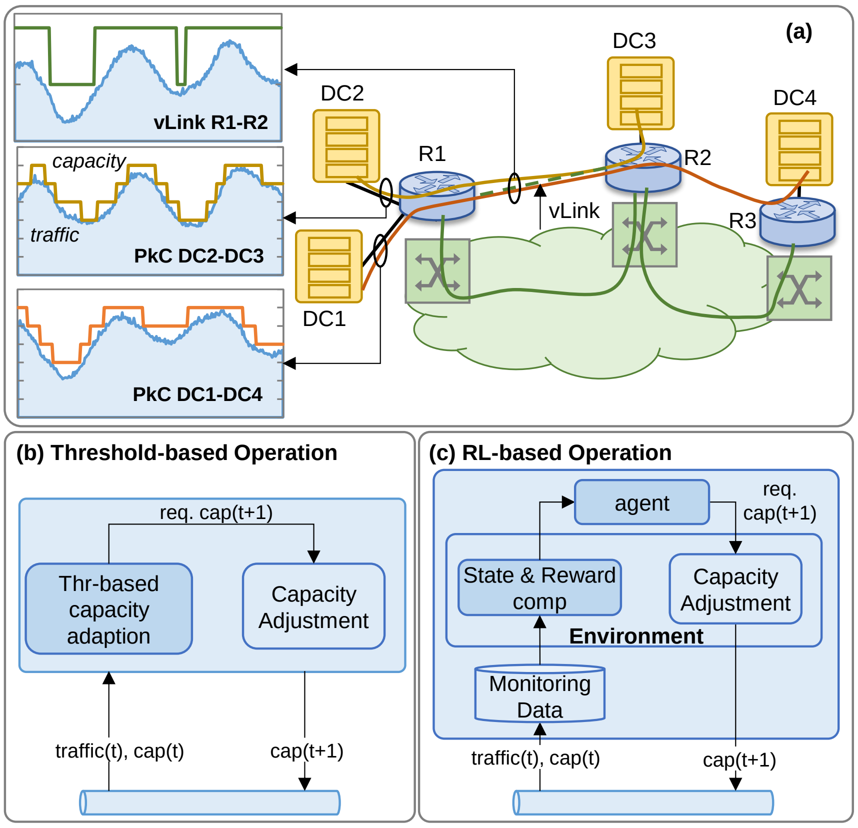

Figure 2-4 Capacity operation of PkCs and vLinks

The inner graph for PkC DC2-DC3 in Figure 2-4a shows the capacity adjustments performed assuming that the operational goal of the PkC is to minimize the allocated capacity to reduce connectivity costs, by following as close as possible the input traffic, while avoiding traffic loss. Figure 2-4b-c present two alternative approaches to operate the capacity of the PkCs, based on a simple threshold rule or based on an intelligent ML-based algorithm, in this case, RL. Every connection (PkC or vLink) intent agent collects the amount of input traffic that is injected to the connection, as well as some other measurements, like packet loss and delay, and it determines the capacity of the connection that will be needed to meet the given operational goals for the next period (e.g., one minute). Such capacity can be used to program some rules in the packet nodes not only to increment the capacity but also, e.g., to adjust the amount of buffer at the input of the connection.

2.4 Digital Subcarrier Multiplexing (DSCM)

DSCM systems, based on advanced digital signal processing (DSP) modules, represent a key technology to transparently route heterogenous data in an efficient and cost-effective way [Zh11], [Ra16]. The key-aspect of DSCM with respect to single wavelength transmission is the usage of one single laser to digitally generate multiple Nyquist SC, e.g., 4, 8 or more, instead of a single one [Kr17], [Su20].

One of the major advantages of using DSCM in optical transport networks is to keep high data-rates (e.g., 400 Gb/s) while using lower symbol rates (SR) per SC (e.g., 8 or 11 GBaud). As an example, a 32 GBaud system can be implemented using 4×8 GBaud SCs, multiplexed at near Nyquist sub-carrier spacing. This lowers the penalties caused by fiber propagation impairment, such as dispersion and nonlinear Kerr effects [Qi14]. The DSCM is realized at the transmitter (Tx) side and each SC is individually detected and post-processed at the coherent receivers (Rx); SCs with different modulation format (MF), SR, and FEC overhead can coexist. Figure 2-5 illustrates a DSCM system with 4 SCs, where each Sc can be independently modulated using Quadrature Phase-Shift Keying (QPSK) and Quadrature Amplitude Modulation (QAM). For an introduction to DSCM, we refer the reader to [Su20] and the guide in [Infinera].

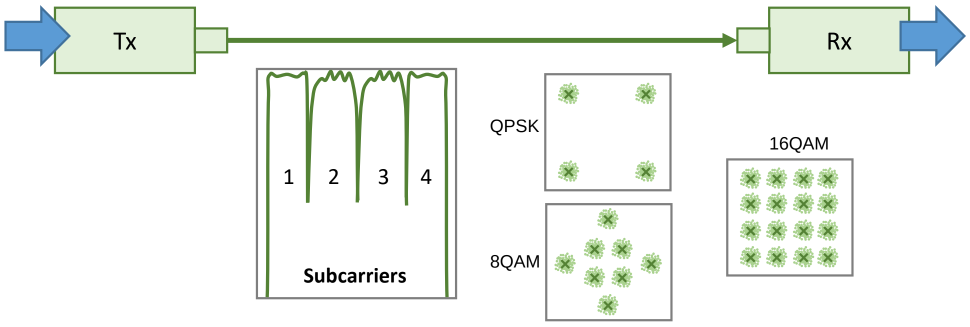

Figure 2-5 Example of a DSCM system

The flexibility provided by DSCM systems can be used to substantially reduce the energy consumption; for example, in case the actual amount of traffic that the lightpath needs to transport is low, the number of SCs that are active can be reduced. This represents a step further in terms of flexibility with respect to the sliceable-bandwidth variable transponder proposed in [Sa15], by achieving a higher granularity and increasing the flexibility thanks to the digital generation of the SCs; this might be useful, especially for metro applications [Ve13].

2.5 Generation of Reliable and Accurate Synthetic Data

How to gather data for training ML algorithms is one of the main challenges that need to be solved for the deployment of network automation solutions. The objectives to be achieved include not only the quality of such dataset, which is directly related to the final accuracy of the prediction for network operation, but also the time needed for that collection. Note that in many cases, performance-related data heavily depends on the actual characteristics of the network entity of interest and are only available when such entity is set-up. For instance, QoT measurements depend on the actual routing and spectrum allocation of an optical connection; in consequence, real measurements can only be available after such optical connection is established, and might change due to the provisioning of neighboring connections. However, ML algorithms need to be ready to be deployed at connection set-up time and thus, special techniques are needed to train accurate ML algorithms before data for that specific network entity is available. Further, the inherent prediction ability of ML algorithms can be used during the lifetime of the network entity to elastically allocate resources to the optimality.

Synthetic data generation is one of the solutions that can be implemented for the identified challenges and can run in a sandbox domain. However, for the generated data to be reliable and accurate, they must be generated using techniques that rigorously reproduce the real scenario, thus creating a digital twin. Such a digital twin can be based on a combination of analytics and simulation models, which need to be tuned using the characteristics of the real entity, as well as with real measurements collected before or during operation.

In this context, some open-source projects, like GNPy, are considering the specific characteristics of the different optical devices that participate in the optical layer, like Reconfigurable Optical Add / Drop Multiplexers (ROADM), TRXs, and In-Line OAs, e.g., Erbium Doped Fiber Amplifier (EDFA). The GNPy library is being developed within the Telecom InfraProject [TIP] for physical layer -aware networking [Fi18]. The core of GNPy is the QoT estimator calculating the Generalized Signal to Noise Ratio (GSNR), considering both the ASE noise and NL Interference (NLI) accumulation; GSNR is the accepted parameter as performance meter for optical data transport, corresponding to the error vector magnitude (EVM) [Ch12]. For the NLI evaluation, the current version of GNPy is using the generalized Gaussian-noise model [Ca18]. In order to derive the GSNR, a series of parameters is provided as input to the GNPy, together with the network topology, which includes the characteristics of the ROADMs, fiber types, span length, and EDFAs gain, power, and Noise Figure (NF). GNPy can be used as a tool to estimate the expected QoT for a set of lightpaths for several purposes, from off-line and in-operation network planning [VeRu17] to performance measurements dataset generation for ML algorithm training purposes [Ve19.2].

For the packet layer, a digital twin can be based on the CURSA-SQ methodology [Ru18]. CURSA-SQ's includes a continuous G/G/1/k queue model with a first-in-first-out discipline based on the logistic function, which enables solving the model in near-real time.

To illustrate accurate data generation, Figure 2-6 presents two examples of digital twins for the packet (Figure 2-6a-b) and the optical layer (Figure 2-6c-d). For the packet layer, Figure 2-6a presents an example of a network with four nodes interconnecting four data centers (DC), where DC1-3 exchange data with DC4 (flows are also represented). Let us assume that traffic is monitored at the input interfaces, so a number of observation points have been activated. A digital twin is represented in Figure 2-6b based on the CURSA-SQ methodology. To accurately reproduce the real scenario, however, parameter tuning for the queues is required. To that end, the *dynamic configuration* module is in charge of defining the traffic to be generated and consumed by every DC, as well as the entities configuration, which evaluates the accuracy of the estimation by comparing it against the real traffic conditions measured from the observation points in the network.

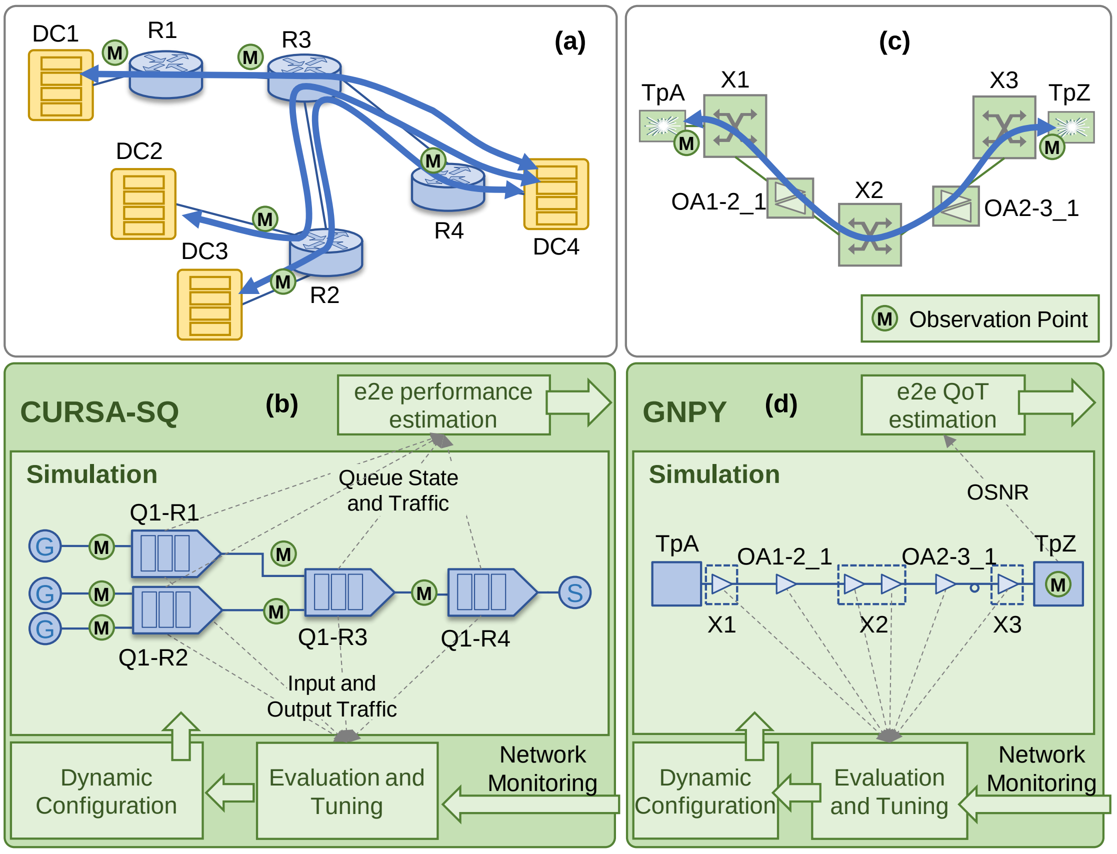

Figure 2-6 Examples of digital twins for the packet (a-b) and the optical (c-d) layers.

In the case of the optical layer, Figure 2-6c reproduces an example of optical connection established between two locations A and Z; optical transponders in the remote locations, cross-connects and intermediate amplifiers are represented. As for the optical layer, a digital twin is represented in Figure 2-6d, based on the GNPy tool [Fi18] to estimate the expected SNR of the optical connections. In this case, the dynamic configuration module finds the most likely value of modeling parameters based on the monitoring data received from the network.

Chapter 3

State-of-the-Art

In this chapter, we present a review of the state-of-the-art of the different goals defined for this Ph.D. thesis with the twofold objective of ensuring that these goals have not yet been covered in the literature and for serving as a starting point for this research work.

3.1 Optical Network Health Analysis

3.1.1 Failure Detection and Localization

Network performance monitoring is a key enabler for failure identification and localization, which can greatly bring down both, the repair time and operational cost of optical networks. Many research efforts have been dedicated to develop failure localization techniques for hard failures, i.e., unexpected events that suddenly interrupt the established connections. Nonetheless, although some works can be found in the literature focused on the identification and localization of soft failures, i.e., events that progressively degrade the QoT, this topic remains rather unexplored. Owing to the fact that soft failures might eventually evolve to hard failures, it is of paramount importance not only to detect them a priori before connections disruption, but also to localize their cause in order to take proper action, e.g., finding a restoration path. Such monitoring data can be used by data analytics applications, especially those based on ML [Ra18.1].

Recently, the authors in [APV17] proposed several solutions to monitor the performance of lightpaths at the transponders side to verify their proper operation, as well as to detect BER degradations. The authors studied several soft-failure causes affecting signal QoT, such as Filter Shift (FS) and Filter Tightening (FT), and proposed algorithms to detect and identify the most probable failure. Some of these failures happen in the optical switching intermediate nodes, so monitoring the signal solely at the egress node (or even ingress) does not allow their localization. Hence, monitoring techniques to evaluate QoT in-line are required.

As the abovementioned failures noticeably affect the optical spectrum of the lightpaths, Optical Spectrum Analyzers (OSA) can be used to monitor the spectrum along the transmission line aiming at detecting and localizing that type of failures. Practically speaking, the realization of such solutions become possible with the emergence of a new generation of compact cost-effective OSAs with sub-GHz resolution in the form of optical components [FINISAR] allowing real-time monitoring of the optical spectrum of the lightpaths.

Considering the optical spectrum of a lightpath, when a signal is properly configured, its central frequency should be around the center of the assigned frequency slot to avoid filtering effects, and it should be symmetrical with respect to its central frequency. The authors in [APV18], presented several descriptive features to characterize the optical spectrum of a lightpath. Such features were used to train a set of ML algorithms to detect and identify failures. The most common filtering related failures are FS and FT; the optical spectrum becomes asymmetrical in the case of FS, and its edges get noticeably rounded in the case of FT. These irregularities allow distinguishing optical spectra suffering from such failures from the properly configured ones.

Authors in [Sh19] extended the work in [APV18] and studied different feature-based approaches that use optical spectrum features for classification, as well as the residual-based approach, in which the received signal is pre-processed using a theoretically-calculated expected signal. Note that one single filter type was considered in [APV18] and [Sh19], which limits the deployment of ML approaches in real operator networks that usually consist of equipment from different vendors. The most straightforward solution to overcome this limitation is to have different models being trained upon various types of filters that might be available in the network. Nonetheless, it makes the training phase very complex and data-hungry. Yet, it will not be easy to comprehend the sequence of filters a priori and the responses of a slightly non-identical filters in the network might not be well detected, necessitating even more combination of models to have an appropriate generic model. The application of out-of-field model training and in-field adaptation [Ve19.2] leads to a robust, yet feasible, solution for networks with heterogeneous filtering; just one type of filter is used for ML training and adaptation of the optical spectrum acquired from OSA that have passed through several type of different filters is developed.

In fact, to the best of our knowledge, no works in the literature have focused on the analysis of the QoT degradation produced by soft-failures in the optical devices and fibers and the estimation of the evolution of the values of its working parameters that are causing the observed effects in the QoT. Therefore, our work will be focused on addressing the latter by implementing techniques to localize soft-failures and device parameters estimation and study their SNR measurement based on the value of working parameters.

3.1.2 Feasible Configuration of Optical Devices and Fibers

Several approximate non-linear fiber propagation models have been proposed over the years. Recent re-consideration and extension of earlier modeling efforts has led to the formalization of the so-called Gaussian-noise (GN) model. The evidence collected so far hints at the GN-model as being a relatively simple and, at the same time, sufficiently reliable tool for performance prediction of uncompensated coherent systems, characterized by a favorable accuracy versus complexity trade-off. Authors in [Po14] tried to gather the recent results regarding the GN-model definition, understanding, relations versus other models, validation, limitations, closed form solutions, approximations and, in general, its applications and implications in link analysis and optimization, also within a network environment.

Authors in [Po12] focused on the GN model which describes non-linear propagation in uncompensated coherent transmission systems. They reviewed similar models and validation efforts and then the main equations of GN model were presented. The features of equations and the main characteristics of the NLI noise spectra that the GN model produces were discussed. To speed up the numerical integration, they proposed a new formulation in hyperbolic coordinates. Also, for distributed-amplification scenarios, an extension of GN model was introduced. They studied about NLI noise accumulation vs distance and band-width and the concept of GN model for optimization and design of networks and system were discussed.

In conclusion, considering the previous works, it is obvious that the GN model appears as a useful tool for system and network analysis design and control and is suitable to focus on to further study in deep to propose methods to use the GN model as an accurate source.

3.1.3 Severity Estimation

Optical connections support virtual links in MPLS-over-optical multilayer networks and therefore, errors in the optical layer impact on the quality of the services deployed on such networks. Monitoring the performance of the physical layer allows verifying the proper operation of optical connections, as well as detecting BER degradations and anticipating connection disruption. Authors in [APV17] used linear extrapolation in three different time instants for max BER anticipation. Simulation results in this work showed that maximum BER violation was anticipated several days before the connection was disrupted, which allows planning a network reconfiguration to be per-formed on low activity hours.

Authors in [Sh18] used the prediction to anticipate a potential anomaly, when a signal's CF shifts and might impacting neighboring signals. They proposed an algorithm that periodically scans the whole C-band and compares the found signal against the list of lightpaths received from the network controller. By using this scan process, three different anomalies can be identified. The detection of any of these anomalies triggers a notification with critical severity level to the controller.

In compare to previous works' methods, we can use polynomial extrapolation in our estimation because it fits a nonlinear model to data and we can make better prediction in our research.

3.1.4 Experimental Validation

The key-operation to enabling an effective data transport abstraction in open optical line systems (OLS) is the capability to predict the QoT, that is given by the GSNR, including both the effects of the ASE noise and the nonlinear interference NLI accumulation. Among the two impairing effects, the estimation of the ASE noise is the most challenging task, because of the spectrally resolved working point of the EDFA depending on the spectral load, given the overall gain. While, the computation of the NLI is well addressed by mathematical models based on the knowledge of parameters and spectral load of fiber spans. So, the NLI prediction is mainly impaired by the uncertainties on insertion losses a spectral tilting. An accurate and spectrally resolved GSNR estimation enables to optimize the power control and to reliably and automatically deploy lightpaths with minimum margin, consequently maximizing the transmission capacity. Authors in [Cu19] addressed the potentialities of ML methods combined with analytic models for the NLI computation to improve the accuracy in the QoT estimation. They also analyzed an experimental data-set showing the main uncertainties and addressing the use of ML to predict their effect on the QoT estimation.

We can conclude that, although some previous works have proposed algorithms and different methods for failures detection and localization at the optical layer, many improvements can still be made, where finding the actual configuration of optical devices and fibers can be used to improve the performance of the network.

As summarized in Table 3-1, in this Ph.D. thesis we assume that modulation formats used in the metro segment are 16QAM and QPSK and devices that will be suffering from soft-failure are the TRX, WSS and Fiber; in the other side modulation format in the core segment will be limited to just QPSK and devices that will be suffering from soft-failure are the optical TRX, A/D WSS and Optical Amplifier. This advanced network performance analysis procedure supported by GNPy tool facilitates diagnosis and network maintenance.

Table 3-1: Study scenarios

Metro scenarios	**Core scenarios**
Modulation formats	
QPSK and QAM-16	QPSK
Degradations (Soft-failures)	
WSS, TRX, and Fiber	Optical Amplifier, TRX, and WSS

3.2 Reliable vLink Autonomous Operation

Over 38% of the total power consumption of a coherent optical transponder comes from subsystems that could be switched off in case a SC can be de-activated [Fl20]. The authors in [Fr17] show power increments of ~28% for an optical transponder when increasing the order of the QAM over QPSK and about the same ratio when increasing the symbol rate from 32 to 43 GBaud. Therefore, a proper dynamic configuration of the SCs in terms of MF and SR to adapt the capacity of the lightpath to the actual traffic can lead to non-negligible energy savings, since the power consumption of several subsystems, including those that are always active, depends on the actual configuration of the SCs.

Some works can be found in the literature exploiting the inherent capability of Elastic Optical Networks (EON) [EON16] to adapt lightpaths as a function of the actual traffic, and to create multiple parallel lightpaths to offer a combined capacity as seen from the virtual link (vlink) perspective in the packet layer (see e.g., [Kl13], [Pa14]). In this work, we target at extending EON capabilities by adopting dynamic capacity management of SC-operated lightpaths. To implement such dynamic configuration of the SCs, both the Tx and the Rx sides must be synchronized to properly encode and decode the optical signals of every SC. To that end, the SDN controller can be in charge of configuring each SC of every lightpath by programming both sides with the specific configuration. However, this would significantly increase the number of tasks to be performed within the centralized controller (i.e., analyzing measured traffic, finding optimal SC configuration, and re-tuning Tx and Rx when needed for every single lightpath) and, because it requires near real-time operation, it would introduce more complexity in the whole network.

However, a key issue remains to be addressed; i.e., how the lightpath can be managed to provide enough capacity to the packet layer without detrimental effects, like added delays or packet losses, and at the same time minimize energy consumption.

3.3 Autonomous Packet Flow Capacity Management

Several works have proposed the application of RL algorithms for autonomous network operation. In the context of optical networking, the authors in [Ch19.1] proposed the use of *Actor–Critic*-based algorithms running in the SDN controller for dynamic lightpath provisioning. They showed that changes in the traffic profile impact the obtained performance. The authors of [Ch19.2] extend their work from [Ch19.1] to multi-domain scenarios where multiple RL agents improve their learning by transferring knowledge. The authors of [Tr21] studied the application of several deep RL algorithms (including DQN) and reward functions to increase network availability in SDN-controlled wide area networks. Finally, the work in [Pa19] proposed an RL algorithm for autonomous bandwidth allocation in the context of multilayer optical networks. They proposed a centralized algorithm running in the SDN controller that supervises the network performance. When the network performance degrades, the centralized algorithm tunes parameters in the RL algorithms.

One of the key issues in the previous works is the time needed to learn optimal policies, as exploration entails low-reward decision making (i.e., far from optimal operation), as shown in [Ch19.1]. In view of this, the performance of RL methods is typically evaluated after some training phase, i.e., when reward achieves a stationary behavior. However, a subject that is poorly or not even considered in the literature is when RL algorithms need to operate before they are properly trained. Note that this happens in our case, as the actual characteristics of the traffic flow are unknown until it is provisioned. Moreover, it is not realistic to assume, in general, the same conditions during training and operation phases, due to mid/long-term traffic evolution, which makes it difficult to reproduce highly accurate operation conditions during training. To solve these issues, the authors of [Ve19.2] proposed a general learning lifecycle that included both offline training (e.g., in a sandbox domain [Ru20.1]) and online learning, in the context of supervised ML. The objective of that work was to accelerate autonomous operation by deploying accurate models that are firstly trained offline and fine-tuned while in operation, thus adapting pre-trained models to actual in-field operation conditions.

Although some previous works have proposed algorithms and different methods for autonomic PkC capacity management, they have not considered realistic network scenarios where RL approaches can be deployed without a major impact on the performance of the PkC until the optimal policies are learned.

3.4 Conclusions

In this chapter, we have reviewed the state-of-the-art of relevant works related to the goals of this thesis. Table 3-2 summarizes the study.

Table 3-2: State-of-the-art summary

Goals	References
G1 - Optical Network Health Analysis	**Failures detection and localization** [Ra18.2], [APV17], [FINISAR], [APV18], [Sh19], [Ve19.2]
	Feasible configuration of optical devices and fibers [Po14], [Po12]
	Severity Estimation [APV17], [Sh18]
	Experimental Validation [Cu19]
G2 - Reliable vLink Autonomous Operation	[Fl20], [Fr17], [EON16], [Kl13], [Pa14]
G3 - Autonomous Packet Flow Capacity Management	[Ch19.1], [Ch19.2], [Tr21], [Pa19], [Ve19.2], [Ru20.1]

In view of this study, although some previous works have presented proposals related to degradation detection and localization and autonomous operation, the challenges defined as objectives for this Ph.D. thesis remain still open. In the following chapters, we present the essence and contributions of this Ph.D. thesis for the defined objectives.

Chapter 4

Optical Network Health Analysis

In the previous chapters, we have reviewed the state-of-the-art and the background concepts needed to fully understand this work. In this chapter, we focus on analyzing the health of the optical network.

The performance of optical devices can degrade because of aging and external causes like, for example, temperature variations. Such degradation might start with a low impact on the QoT of the supported lightpaths (soft-failure). However, it can degenerate into a hard-failure if the device itself is not repaired or replaced, or if an external cause responsible for the degradation is not properly addressed. In this chapter, we propose comparing the QoT measured in the transponders with the one estimated using a QoT tool. Those deviations can be explained by changes in the value of input parameters of the QoT model representing the optical devices, like noise figure in optical amplifiers and reduced Optical SNR (OSNR) in the WSS. By applying reverse engineering, the value of those modeling parameters can be estimated as a function of the observed QoT of the lightpaths. Experiments reveal high accuracy estimation of modeling parameters, and results obtained by simulation show large anticipation of soft-failure detection and localization, as well as accurate identification of degradations before they have a major impact on the network.

4.1 Introduction

The massive application of the optical technology [EON16] in the core, metro, and access segments [Ve13], is a clear consequence of its high bandwidth, low latency, and high reliability, which enables the deployment of 5G and beyond. Because of the growing complexity of optical systems, it is critical to assess the QoT of optical connections (lightpath). This can be quantified in terms of Signal to Noise Ratio (SNR) and measured within Optical TRX.

The QoT is related to the linear and nonlinear (NL) optical noise, and it can be estimated based on a model describing the physics of propagation, e.g., the generalized Gaussian Noise (GN) model [Ca18]. Additionally, effects such as aging of optical devices might severely affect the QoT. Aging effects are usually considered by means of costly system margins [Po17]. Examples include: i) the degradation of OA, which can be quantified as increased NF; and ii) detuning of the lasers in the TRXs or frequency drift of the filters in WSSs, which can lead to misalignments. If those degradations (soft-failures) are not properly handled (e.g., by retuning, repairing, or replacing the related optical device), they can degenerate into hard-failures when the SNR reduces, and zero post- FEC error cannot be achieved (FEC limit); this could affect a large portion of network services. Therefore, it is of paramount importance not only to detect any QoT degradation, but also to identify the cause and localize the device causing the degradation.

Further, a considerable effort is being paid towards disaggregating the optical layer to enrich the offer of available solutions and to enable the deployment of solutions that better fit optical network operators' needs [Ve18.2]. Such disaggregation, however, tends to make network surveillance and maintenance more complex in general, due to the absence of vendors providing support of vertically integrated network equipment.

To support failure management, the control plane of the optical network needs to be enriched with MDA capabilities [Ve19.1], [Gi18]. Once monitoring data, notifications, and alarms have been collected from the data plane, data analytics algorithms (e.g., based on ML techniques [Ra18.1]) can analyze them to proactively detect the degradation, identify and localize the cause, and anticipate hard-failures before they occur. Once detected, identified, and localized, recommendations can be issued to the network controller so it can decide about rerouting and/or reconfiguring the network [Ve17], as well as notifying the management plane for maintenance. Note that ML-based approaches require training and validation datasets, which makes their practical application difficult due to key drawbacks, namely: *i*) limited data availability; *ii*) long duration of the training and validation phases until obtaining robust and reliable ML models (this could be accelerated by using simulation tools in sandbox domains [FGML19], [Ru20.1]); *iii*) poor adaptability in the event of physical layer changes; and iv) reduced exportability to other scenarios/ conditions different than those used for training.

The topic of failure management in optical networks (including anticipated detection, identification, and localization) has been extensively explored and several related works can be found in the literature, in particular using ML techniques (see the tutorial in [Mu19]). For soft-failure detection and identification, the authors in [APV17.1] proposed to analyze the evolution of the BER in the transponders and issue notifications when the BER increases; an algorithm running in the centralized network manager anticipates degradations and identifies the most probable cause of failure and its probability. The work in [Sh19] focused on detecting and identifying filter-related failures by analyzing the spectrum of optical signals at the receiver. An autoencoder-based solution to detect and identify soft-failures in optical links was proposed in [Va20], while in [Lu20] the authors proposed a convolutional neural network running in the TRXs that estimates the probabilities for four types of soft-failures with good performance for single failure scenarios. The work in [Zh20] presented a solution for failure prediction that scores the features related to failures based on their importance. The authors in [Pa18] proposed a classifier to predict the failure probability of optical links complemented with a heuristic for failure localization under the single link-failure assumption. Methods for localization of filter-related failures were proposed in [APV18] by analyzing the optical spectrum in intermediate locations. Finally, a method based on graph neural networks was proposed in [Li20] that analyzes the alarms received to identify the root alarm and localize the failure.

Apart from alarm correlation, several of these works centered on analyzing the QoT represented by the measured BER, spectrum, etc. for detecting failures, or correlating alarms for localization. In contrast, the status of optical devices was analyzed in [Ra18.2] through measures related to device parameters like optical power, gain, temperature, etc. to proactively detect and localize potential faults and determining the likely root-cause. This approach to failure detection, derived from the analysis of devices' parameters, is key to really identify and localize the failure itself.

However, it is not always possible to obtain the right value of those devices' parameters that can be related to the QoT, in particular in disaggregated scenarios. Note that any QoT model uses a set of input parameters to describe the specific characteristics of the different optical devices that participate in the optical layer, like WSSs as building blocks of ROADM, TRXs, and In-Line OAs, e.g., EDFA. The authors in [Se18], [Bo18] proposed ML methods for finding the right value of such QoT model's parameters aiming at improving the QoT estimation. Our approach applies reverse engineering from the real QoT values—collected periodically from the TRXs—to derive the evolution of the value of QoT model's parameters (referred to as modeling parameters in the rest of the chapter) that explain such QoT observations. We believe that, by analyzing such evolution, it is possible to anticipate more precisely future degradations, and enable failure localization.

This chapter proposes the MESARTHIM methodology that targets at: *i*) detecting and localizing the optical device responsible for the soft-failure; *ii*) identifying the modeling parameters that explain the observed effects in the QoT; and *iii*) estimating the evolution of the value of such parameters to find whether the soft-failure will degenerate into a hard-failure. This advanced network performance analysis procedure facilitates diagnosis and network maintenance. Furthermore, because the relation between monitored SNR and modeling parameters is not linear, the analysis carried out in the later space (i.e., modeling parameters) can accelerate soft-failure detection, identification, and localization.

The rest of the chapter is organized as follows. MESARTHIM methodology for soft-failure detection, identification, and localization, modeling parameter estimation and severity estimation. Section 4.2 details its building blocks. Network surveillance and soft-failure localization based on device modeling parameter estimation, which is a key part of the MESARTHIM methodology. Soft-failure localization and device working parameters estimation in disaggregated scenarios algorithms based on the analysis of the SNR and optical device modeling parameters are detailed in Section 6.2. Moreover, this section presents a procedure that combines the analysis of SNR values with the expected ones, obtained with the open source GNPy QoT tool [Fi18], to find the most likely value of modeling parameters. Procedures for identification and severity estimation, once a soft-failure has been detected and localized. Section 6.2 applies time series forecasting techniques to provide answers to critical questions, such as whether and when an SNR threshold will be violated for a given soft-failure.

The discussion is supported by the experiments and numerical results presented in Section 4.5.

4.2 The MESARTHIM methodology

Among the effects degrading the QoT within optical systems, in this chapter, we consider degradations arising from ROADMs and In-Line OAs, where a ROADM consists of WSSs and OAs. Both building blocks face aging and non-ideal conditions. For example, although OAs are considered robust devices, they also suffer time-varying effects like NF which might increase over time due to the aging of the amplifier building blocks. The NF is also frequency dependent and, as the allocation of the spectrum might become time-dependent. Therefore, the NF can be modeled as a time-frequency variation. The pump lasers of the EDFAs also present degradation, which can be adjusted thanks to internal control loops, but which still reduces the EDFA efficiency. For what concerns the WSSs, they might suffer temperature-dependent variations, which might lead to frequency shift over time; furthermore, individual channels can drift as well, and both effects can be highly detrimental in terms of QoT. In the context of this chapter, we consider gradual time-varying device degradations on OA and add/drop (A/D) WSSs in the ROADMs. Specifically, we consider that soft-failures can be explained by one of the following events in the modeling parameters: a) NF increase; b) maximum optical output power (P-max) decrease; and c) OSNR degradation caused by frequency drifts of the WSSs due to temperature fluctuation. Our proposed architecture for soft-failure analysis is based on that in Figure 1-1, where the QoT tool is based on GNPy.

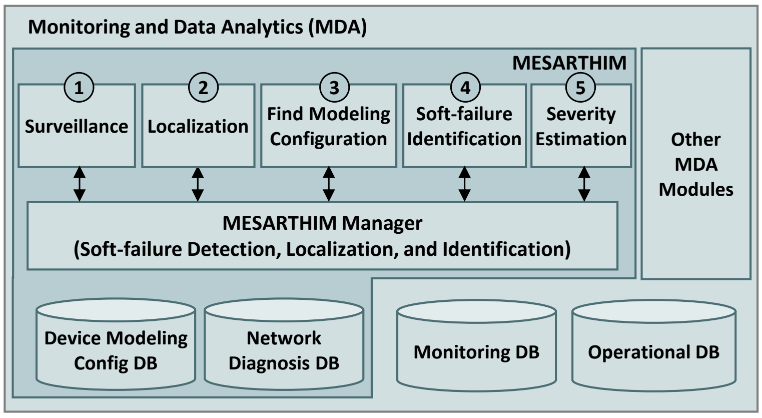
Monitoring and Data Analytics (MDA)
MESARTHIM
1
Surveillance
2
Localization
3
Find Modeling Configuration
4
Soft-failure Identification
5
Severity Estimation
Other MDA Modules
MESARTHIM Manager (Soft-failure Detection, Localization, and Identification)
Device Modeling Config DB
Network Diagnosis DB
Monitoring DB
Operational DB

Figure 4-1 Overview of the proposed MESARTHIM methodology

The MDA system stores a replica of the operational databases (DB) that are synchronized from the network controller. In addition, it collects measurements from the optical devices with a given periodicity and stores them in a Monitoring DB; in this chapter, we assume that the MDA collects SNR samples from the TRXs every 15 minutes. These measurements are used by MESARTHIM to: *i*) estimate those modeling parameters related to optical devices (resources); *ii*) analyze the evolution of the measured SNR and that of the modeling parameters to detect any degradation as soon as it appears; and *iii*) determine the severity of the degradation based on the foreseen impact on the performance of the lightpaths.

Figure 4-1 sketches the MESARTHIM methodology implemented in the MDA system. Specifically, the following building blocks can be identified: (1) the Surveillance block that analyzes the SNR measurements and the value of modeling parameters to detect any meaningful degradation (e.g., by threshold crossing); (2) the Localization block that localizes the soft-failure; (3) the Find Modeling Configuration block that finds the most likely value of the modeling parameters of a given resource, so it results into SNR values of the lightpaths being supported by such resources similar to those that have been actually measured; (4) the soft-failure Identification block that, assuming a resource has been localized as the source of the soft-failure, finds what is the modeling parameter responsible for such failure; and (5) the Severity Estimation block that estimates whether and when the soft-failure will degenerate into a hard-failure. In addition, two internal repositories are used: *i*) the Device Modeling Config DB with the evolution of the value of modeling parameters along time for every resource; and *ii*) the Network Diagnosis DB that stores historical data for analysis purposes. The MESARTHIM manager coordinates those blocks to achieve intelligent QoT analysis, as well as manages the interface with the QoT tool. The main procedures for the different blocks of MESARTHIM are detailed next.

4.3 Surveillance and Localization

In this section, we describe two different approaches for the surveillance block, named SNR-wise that analyzes the evolution of the SNR, and Modeling-wise that analyzes the evolution of the value of modeling parameters. Resources affected by a soft-failure procedure are localized. Additionally, the main procedure for the Find Modeling Configuration block is presented. Table 4-1 introduces the used notation. We assume that surveillance is carried out periodically, e.g., after at least one new SNR measurement has been collected for every lightpath in the network. Both algorithms return the resources with the found likely modeling configuration, each with a subset of lightpaths, indicating that some soft-failure has been detected.

Table 4-1: Notation

G	Graph representing the network topology.
P	Set of all lightpaths
P'	Subset of lightpaths (P'⊆P)
R	Set of optical devices, index r.
C	Set of clusters of lightpaths with found same behavior ({<behavior, P'>})
SR	Set of resources suspicious. Each element identifies the resource r and the lightpaths that it supports (SR = {<r, P'>}).
SF	Set of Soft-Failures. (SF = {<r, P'>})

4.3.1 SNR-wise Surveillance

This approach focuses on the analysis of SNR measurements and compares them to the SNR estimated by the QoT tool for every lightpath, to detect any meaningful deviation (exceeding a differential threshold). The lightpaths that exceed the differential threshold are considered degraded and are further analyzed in terms of the behavior of the measured SNR evolution to find a correlation among them; behavior is the result of stationarity analysis [Sh05] of the SNR evolution. Non-stationary patterns (e.g., trend, periodicity), if found, are quantified (e.g., a period interval in case of seasonality) to compose the behavior. For illustrative purposes, Figure 4-2 shows three examples of behavior: a) stationary (typical for lightpaths that do not exceed the differential SNR threshold); b) gradual decay; and c) cyclic. In the case of finding groups of lightpaths with similar behavior, common underlying resources are analyzed to localize the responsible for such degradation. It is worth highlighting that grouping lightpaths with similar behavior enables localizing multiple soft-failures. In such a case, the likely configuration parameters are estimated using the Find Modeling Configuration block with all lightpaths supported by that resource.

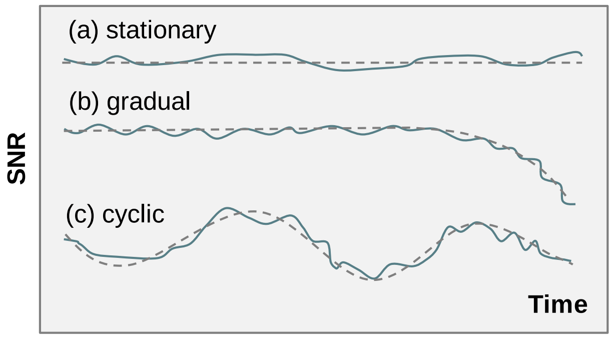

Figure 4-2 Three examples of behavior.

Algorithm 4-1 describes the procedure used to find the behavior of the evolution in time of a time series data. The algorithm receives an object *x*, which includes: *i*) the time series to be analyzed (e.g., the SNR of a path p); *ii*) a window size *w* used for smoothing purposes; and *iii*) a threshold *thr* used to detect a significant non-stationary behavior.

Algorithm 4-1. Find Behavior Procedure

```
INPUT: x                                OUTPUT: hasBehavior
1:   Y ← x.<time series>      # snr OR evol
2:   Ỹ ← nonOverlappingMovingAverage(Y, x.w)
3:   if max(Ỹ) - min(Ỹ) < x.thr then return False
4:   if isMonotonic(Ỹ) then
5:       trendline ← computeFittestTrendline(Ỹ)
6:       x.behaviour ← <"gradual", trendline>
7:   else
8:       period ← findPeriodicity(Ỹ)
9:       if period then x.behaviour ← <"cyclic", period>
10:      else x.behaviour ← <"other", ∅>
11:  return True
```

The data series (Y) is smoothed (Ỹ) by computing a moving average in non-overlapped windows of size w (lines 1-2 in Algorithm 4-1). Then, the difference between maximum and minimum in Ỹ is computed and compared with the threshold; if it is lower than the threshold, no behavior is returned (line 3). Otherwise, the algorithm carries out an analysis to characterize the type of behavior by clearly distinguishing between gradual degradation (gradual) and cyclic fluctuation (cyclic), as well as any other undefined evolution (e.g., random peaks). Specifically, if Ỹ presents an incremental or decremental monotonic evolution, the fittest trendline (in terms of Pearson correlation coefficient) among linear, polynomial, exponential, and logarithmic trends is computed and returned as a parameter of the identified gradual degradation (lines 4-6). Otherwise, the periodicity of Ỹ is computed based on the results of automated periodogram power spectral density analysis [Sh05]. In case that a significant period is found, cyclic fluctuation with that period is returned (lines 8-9), whereas other behavior is returned if neither gradual nor cyclic behavior is found (line 10).

Algorithm 4-2 details the pseudocode of the SNR-wise Surveillance algorithm; it receives as input the network graph *G*, the list *P* of lightpaths currently established in the network, the number T of historical monitoring samples to be considered, and the current time (current_t).

Algorithm 4-2 SNR-Wise Surveillance Algorithm

```
INPUT: G, P, T, current_t                OUTPUT: SR
1:   P' ← ∅
2:   for p in P do
3:   if getMonitoringData(p, current_t) < SNR_threshold(p) then
4:       P' ← P' ∪ {p}
5:   if P' = ∅ then return ∅
6:   C = {<behavior, P'>} ← ∅
7:   for each p in P' do
8:       p.snr ← getMonitoringData(p, T)
9:       hasBehavior ← findBehavior(p)
10:      if hasBehavior then addByBehaviorSimilarity(C, p)
11:  if C = ∅ then return ∅ else SR ← ∅
12:  for each c in C do
13:      R = {<resource, P'>} ← FindCommonResources(G, c.P')
14:      SR ← SR ∪ R
15:      for each r in R do
16:          r.evol ← ∅
17:          for each t in T do findLikelyModelingConfig (r, t)
18:  return SR
```

The algorithm first retrieves and examines the last monitoring data available for every lightpath looking for those with degraded SNR (lines 1-5 in Algorithm 4-2). In case some SNR degradation is found, SNR-wise Surveillance proceeds with an in-depth SNR analysis carried out in two steps. During the first step, the set of clusters C, capturing the behavior observed in the lightpaths, is found (lines 6-10); for this analysis, the last T monitoring samples are considered. Note that by considering the evolution of lightpaths' SNR, spurious measurements in one lightpath can be detected and ignored. In the case that, at least, one set of lightpaths presents a similar behavior, e.g., decay or periodicity (as in Figure 4-2), the algorithm continues with the second step. The common resources supporting the lightpaths in each cluster c are computed and added to the set SR of resources that are suspicious of being affected by a soft-failure (lines 12-14). Moreover, for each common resource, a likely evolution of the input parameters is found (lines 15-17); the estimated configuration is stored in the Device Modeling Config DB for further analysis. The resources with the found likely configuration, each with a subset of lightpaths, are eventually returned (line 18).

4.3.2 Modeling-wise Surveillance

This surveillance approach analyses the evolution of the value of modeling parameters of the resources. In this case, the SNR measurements of all the lightpaths in the network supported by a resource are used to estimate the most likely modeling configuration of such resource using the Find Modeling Config block. The found modeling configuration is stored and its evolution is analyzed to detect any meaningful degradation, e.g., a significant trend and/or variation.

Algorithm 4-3 Modeling-Wise Surveillance Algorithm

```
INPUT: G, P, T, current_t                 OUTPUT: SR
1:   SR ← ∅
2:   R = {<resource, P'>} ← GroupPathsByResources(G, P)
3:   for each r in R do
4:       for each p in r.P do
5:           p.snr ← getMonitoringData(p, current_t)
6:       findLikelyModelingConfig(r, current_t)
7:       r.evol ← configDB.SELECT(r, T)
8:       hasBehavior ← findBehavior(r)
9:       if hasBehavior then SR ← SR ∪ {r}
10:  return SR
```

Algorithm 4-3 details the pseudocode of the Modeling-wise Surveillance algorithm; it first initializes the SR data structure (line 1 in Algorithm 4-3) and creates the set of resources with the lightpaths that each one supports (line 2). Next, for every single resource, the algorithm uses the last SNR measurements to find the current value of the parameters modeling the resource, which are stored in the Device Modeling Config DB by the Find Modeling Configuration block (lines 3-6). The behavior of the modeling parameters evolution is analyzed (by calling Algorithm 4-1) and, if a non-stationary pattern is found, the resource is added to the SR set (lines 7-9). It is worth noting that this analysis could detect soft-failures that have not yet had a relevant impact on the lightpaths (i.e., the SNR degradation threshold has not been exceeded yet), as parameters and SNR are not linearly related.

4.3.3 Soft-Failure Localization

In case that the surveillance phase has identified a set of suspicious resources, Algorithm 4-4 localizes the soft-failures. The algorithm first removes the suspicious resources that explain the very same set of lightpaths (lines 1-6 in Algorithm 4-4), as localization is not yet possible in those cases. Next, the resources that explain the SNR of complete subsets of lightpaths are localized and classified as independent soft-failures, *iSF* (lines 6-10). The rest of the suspicious resources are related to soft-failures that affect common subsets of lightpaths, so a given lightpath can be affected by more than one soft-failure.

Algorithm 4-4 Soft-Failure Localization Algorithm

```
INPUT: $SR$                              OUTPUT: $iSF, mSF$
1:    for each $r$ in $SR$ do
2:        $Rr \leftarrow \emptyset$
3:        for each $r'$ in $SR \mid r \neq r'$ do
4:            if $r.P = r'.P$ then $Rr \leftarrow Rr \cup \{r, r'\}$
5:        $SR \leftarrow SR - Rr$
6:    $iSF \leftarrow \emptyset$
7:    for each $r$ in $SR$ do
8:        if $r.P \cap r'.P = \emptyset\ \forall r'\ SR \mid r \neq r'$ then
9:            $iSF \leftarrow iSF \cup \{r\}$
10:           $SR \leftarrow SR - \{r\}$
11:   return $iSF, SR$
```

4.3.4 Finding the Most Likely Modeling Configuration

The above surveillance approaches use the FindModeling Configuration block, which estimates the most likely modeling configuration of a given resource r. Given the ranges of feasible configuration values $\mathbb{V}$ of r, the configuration estimation problem consists in finding the most likely values v, by minimizing the error (computed as mean squared error -MSE) between the measured (S) and the estimated ($\hat{S}$) SNR for the set of lightpaths being supported by r, P(r), i.e.:

$$\min_{v \in \mathbb{V}} MSE\left(S(P(r)), \hat{S}(P(r)|v)\right) \tag{4-1}$$

The SNR estimation $\hat{S}(\cdot)$ is obtained by calling the QoT tool and thus, the optimization problem in (4-1) cannot be solved by traditional methods like Steepest Descent, which are based on computing the gradient of the function to be minimized. In view of that, the findLikelyModelingConfig() procedure uses the modelingConfigSearch() one (Algorithm 4-5) to solve the optimization problem in (4-1). The algorithm interrogates the QoT tool with different values of the parameters and the configuration entailing the lowest error with respect to the SNR values measured is returned. The procedure assumes that: *i*) the function is convex in $\mathbb{V}$, i.e., there is just one minimum that is the global minimum (tests supporting this assumption will be carried out); and *ii*) there is just one of the modeling parameters of r with a value different than the initially found. The procedure fixes the value(s) of the parameter(s) and requests the QoT tool to compute, with such configuration, the SNR values of the lightpaths being supported by r. By computing the mse(·) function, the procedure determines if such configuration is likely enough or if more queries to the QoT tool are needed.

As calls to the QoT tool are time consuming, modelingConfigSearch() targets at minimizing them; instead of using the brute force and request the estimation of the SNR for the whole range of possible values, the procedure uses the projection of two points to determine the next value of the parameters to be used for the estimation. As parameters typically evolve smoothly in time when devices are affected by a soft-failure, it also stores the last configuration(s) in the Device Modeling Config DB; every time it is called, it uses such configurations as starting points for the search aiming at finding the optimal solution fast.

Algorithm 4-5 Modeling Config Search

```
INPUT: $P$, $r$, $v_{min}$, $v_{max}$                OUTPUT: $<v, m>$
1:   $<v, m> \leftarrow configDB$.getMin(); numIters $\leftarrow$ 0
2:   while $m > epsilon$ AND numIters++ < MaxIters do
3:       $<v_l, m_l>, <v_r, m_r> \leftarrow configDB$.getNeigbours($v$)
4:       $v_a \leftarrow$ intersect($v, m, v_l, m_l, v_{min}, v_{max}$)
5:       $v_b \leftarrow$ intersect($v, m, v_r, m_r, v_{min}, v_{max}$)
6:       if $v_a = v_l$ then $v_a \leftarrow (v + v_l) / 2$
7:       if $v_b = v_r$ then $v_b \leftarrow (v + v_r) / 2$
8:       $m_a \leftarrow configDB$.getConfig($v_a$)
9:       if $m_a$ = None then
10:          $m_a \leftarrow$ MSE($P.SNR$, QTool($P, r, v_a$))
11:          $configDB$.addConfig($<v_a, m_a>$)
12:      $m_b \leftarrow configDB$.getConfig($v_b$)
13:      if $m_b$ = None then
14:          $m_b \leftarrow$ MSE($P.SNR$, QTool($P, r, v_b$))
15:          $configDB$.addConfig($<v_b, m_b>$)
16:      $<v, m> \leftarrow configDB$.getMin()
17:  return $<v, m>$
```

4.4 Soft-Failure Identification and Severity Estimation

Let us now focus on the Soft-Failure Identification and the Severity Estimation blocks, which are assumed to be executed as soon as degradation is detected and localized (via SNR and/or device configuration analysis). These blocks make MESARTHIM able to generate notifications to the network controller containing not only the list of degraded lightpaths, but also their expected evolution and the estimated time for the soft-failure to degrade into a hard-failure.

Let us imagine that the surveillance and localization analysis in Section 4.3 detected some degradation at time t and therefore, non-empty ISR and/or MSF sets were found. In addition, let us define state as the combination of the estimated modeling configuration of the resources that are involved, and the SNR experienced by the supported lightpaths. With the aim of an accurate diagnosis, it is interesting not only to analyze the current state but also to predict its future evolution. It is for this very reason that historical data (within a pre-defined time window) are gathered from monitoring and device config DBs and stored in the Network Diagnosis DB. The evolution of each parameter (lightpaths' SNR and device modeling config parameters) is analyzed individually using time series forecasting techniques. By using different techniques with different parametrization, several expected evolutions can be obtained as a practical way to generate different likely projections for parameter degradation.

For illustrative purposes, let us analyze an example of the evolution of three parameters selected from a hypothetical state: the SNR of a given lightpath affected by an SNR degradation, as well as the NF and P-max parameters modeling an OA traversed by that lightpath. Figure 4-3 presents three time-evolutions of the OA modeling parameters and SNR, and their analysis at current time t. At this time, the failure has been correctly localized in the selected OA; however, the cause of the degradation (either NF or P-max) is still unclear. This is the reason behind performing the estimation and evolution analysis for all modeling parameters; such analysis is carried out following forecasting techniques. Three curves representing the upper (f_u), centered (f_c), and lower (f_l) projected possible evolutions are depicted for each parameter. Based on such projections, monitored data are evaluated and an indicator (φ) is computed and used to discard modeling parameters while identifying the one that is the most likely to be the real cause of the observed performance degradation. Hence, the indicator provides large values when the modeling parameter is far from the expected behavior of an affected parameter. The obtained indicator is accumulated with the values obtained in the previous computations, and identification is positive when the parameter with the lowest accumulated indicator is far from all the rest of the parameters with a significantly higher accumulated one. This evidence can be easily observed by setting up a threshold allowing the discrimination of low and high accumulated indicator modeling parameters.

Once the Soft-Failure Identification block has found enough evidence of the modeling parameter explaining the soft-failure, the Severity Estimation block uses the centered projection of the evolution of such modeling parameter to estimate the likely evolution of the SNR for the affected lightpaths (i.e., those being supported by the localized resource). Analyzing such evolution, it is easy to check whether any lightpath would exceed a given threshold. For instance, the minimum SNR defined by its modulation format and bit rate. The next subsections detail these two MESARTHIM blocks.

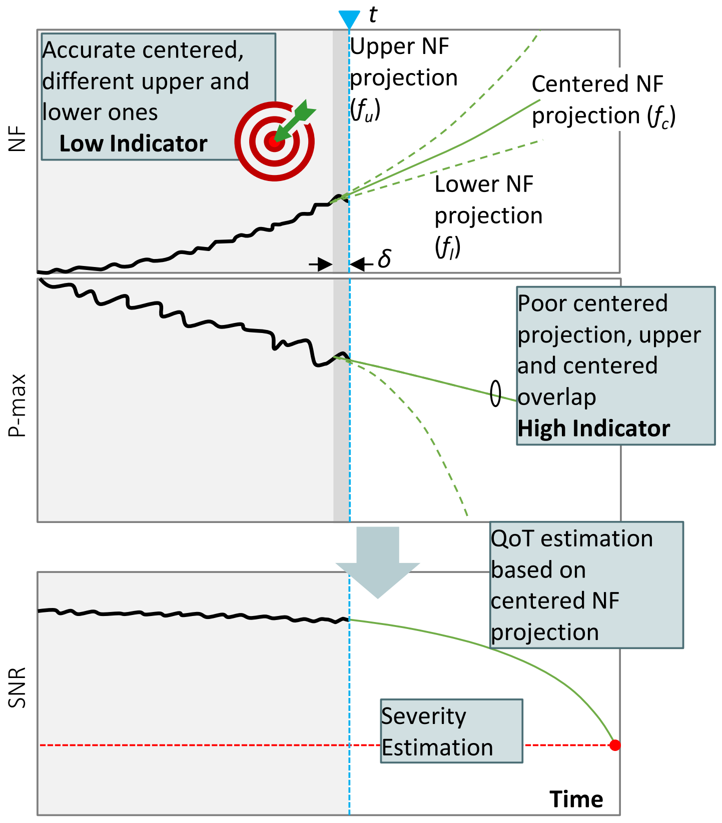
t
NF
Accurate centered, different upper and lower ones
Low Indicator
Upper NF projection (f_u)
Centered NF projection (f_c)
Lower NF projection (f_l)
δ
P-max
Poor centered projection, upper and centered overlap
High Indicator
QoT estimation based on centered NF projection
SNR
Severity Estimation
Time

Figure 4-3. Example of identification and severity estimation at time t.

4.4.1 Soft-failure Identification

Algorithm 4-6 is used to identify the most likely modeling parameter(s) explaining the observed performance degradation; it receives as input the resource responsible for the soft-failure and the number T of historical monitoring samples, and, if sufficient evidence is found, it returns the modeling parameter identified as a potential failure.

The algorithm starts by retrieving the modeling parameters v that characterize the state of the resource, as well as the evolution of each modeling parameter in the last T measurements (lines 1-2 in Algorithm 4-6). Then, each parameter i in v is evaluated independently to compute a score indicating how likely is that such parameter is responsible for the resource failure. Specifically, the time series of the parameter i is selected and split into two portions: one with the first T-δ data points (Y_{fit}) used for fitting and a second one (Y_{eval}), with the last δ measurements, used for evaluation and indicator computation (lines 3-6) (dark grey area in Figure 4-3). Using the Y_{fit} segment, a set of time-dependent functions F, where the parameter value is modeled as a function of time, is obtained by applying Holt-Winters exponentially-based modeling and polynomial fitting in a wide range of degrees (e.g., from 1 to 7) [30] (line 7). The set F contains all functions with similar goodness-of-fit, i.e., +/- 5% of variation in terms of Pearson correlation coefficient. Moreover, functions are evaluated in the time interval of Y to verify that trend is always monotonic; otherwise, the function is discarded. Then, three of those functions are selected to be the likely projections illustrated in Figure 4-3 (line 8). This selection contains: *i)* f_l (lower) and f_u (upper), with the functions with the lowest and highest value at the current time, respectively; and *ii)* f_c (centered), with the function with the smallest number of coefficients providing maximum Pearson correlation coefficient (+/- 5%), which is assumed to be the most likely parameter evolution.

Algorithm 4-6 Soft Failure Identification

```
INPUT: r, T                         OUTPUT: param
 1: v ← getModelingParameters(r)
 2: r.evol ← configDB.SELECT(r, T)
 3: for each i in v do
 4:     Y ← getTimeSeries(r.evol, i)
 5:     $Y_{fit}$ ← Y[1..$T$-$\delta$]
 6:     $Y_{eval}$ ← Y[$T$-$\delta$+1..$T$]
 7:     F ← fitTimeDependentFunctions($Y_{fit}$, $\delta$)
 8:     $F^*$=<$f_l$, $f_c$, $f_u$>←selectLikelyEvolution(F,T)
 9:     r.φ[i]← φ($F^*$,$Y_{eval}$) (Eq. (4-2))
10: v* ←selectHighIndicatorParameters(r)
11: for each i in v* do
12:     r.accumφ[i]+=r.φ[i]
13:     if r.accumφ[i]>thr then v← v \ i
14: if |v| = 1 then return v.getFirst()
15: return ∅
```

After obtaining the likely projections, they are compared with the trendline (computed using the same methodology of f_c) in Y_{eval}. This comparison is carried out using an additive multi-factorial indicator (φ) that combines several Boolean and continuous variables according to Eq. (4-2), where xi represents a variable and bi the weighting coefficient for that variable.

$$\varphi = \sum_{i=1..n} b_i \cdot x_i \tag{4-2}$$

Table 4-2 briefly describes the considered variables, sorted in the descendent degree of importance. Two Boolean functions are used: x_1 returns True if there is no evidence of degradation in the parameter, whereas x_4 checks if any of the upper and lower projections is the same function as the centered one. In addition, two continuous variables are defined: x_2 accounts for the relative Mean Square Error (rMSE) of the data in the evaluation portion with respect to the centered projection, whereas x_3

returns the minimum rMSE of the data with one of the projections. Note that if measurements in the evaluation portion follow a trend showing a parameter degradation similar to the projections (preferably, the centered one), the indicator remains low; otherwise, the indicator increases indicating that the observed behavior differs from the expected one and therefore, the likelihood of the parameter not to be the cause of the failure increases.

Table 4-2 Indicator function components

i	**Description (x_i)**
1	[boolean] Projections f_l, f_c, f_u do not show parameter degradation
2	[continuous] rMSE(Y_{eval}, f_c)
3	[continuous] min(rMSE(Y_{eval}, f_i)) | $i = \{l,c,u\}$
4	[boolean] $f_l = f_c$ OR $f_u = f_c$

Once the indicator is computed for all modeling parameters characterizing the state of the resource, the selection of parameters, whose indicator is significantly higher than the rest, is conducted (line 10). Thus, considering φ_{min} as the minimum indicator value of a parameter, the limit $\varphi_{min}+\Delta\varphi$ is defined as the reasonable limit for parameters with low indicator, being all parameters above $\varphi_{min}+\Delta\varphi$ selected as those with high indicator. For the resultant set of parameters (if not empty), the cumulative indicator is updated by adding the current one (lines 11-12). Finally, the cumulative indicator is compared with an identification threshold *thr* and, if exceeded, the parameter is removed from the candidate parameter set (line 13). The identification is considered positive when just one parameter remains as a candidate and it is eventually returned (line 14). Otherwise, the algorithm returns no identification (line 15). It is worth noting that the value of *thr* needs to be high enough to clearly identify the parameter without false positives.

4.4.2 Severity Estimation

Once a modeling parameter has been identified as the cause of the observed degradation, the severity estimation algorithm is executed. This method uses the projection of the modeling parameters to estimate when some affected lightpath will cross the FEC limit.

Although the severity estimation could be based on the projected evolution of the modeling parameters, defining a threshold for each one is not easy as different lightpaths are impacted differently by its degradation.

Algorithm 4-7 details the pseudocode; it receives as input the resource responsible for the soft-failure, the list of lightpaths supported by such device, the number T of historical monitoring samples, and the identified modeling parameter, and it returns the estimated time that the soft-failure will cause a major impact on, at least, one of the lightpaths. The algorithm first retrieves the last T configuration values from the Device Modeling Config DB, which are used to compute the centered projection fc for the considered input parameter on a given time window (lines 1-2 in Algorithm 4-7). The projection fc is used as the input parameter to estimate the SNR for the list of lightpaths; in case that the estimated QoT for any of the lightpaths falls behind the minimum SNR, the algorithm returns the estimated time of this event to happen (lines 3-6); otherwise, it returns a large value that exceeds the considered time window (line 7).

Algorithm 4-7 Severity Estimation

```
INPUT: r, P, T, param                OUTPUT: estimatedTime
1:  r.evol ← modelingConfigDB.SELECT(r, T)
2:  $f_c$←getCenteredProjection(r.evol[param],timeWindow)
3:  for t in [1, timeWindow] do
4:      SNR ← $\hat{S}(P \mid f_c(t))$
5:      for each p in P do
6:          if SNR[p] < p.minSNR then return t
7:  return INF
```

4.5 Results

4.5.1 Experimental assessment

Being the basis of the MESARTHIM methodology, the Find Modeling Configuration has been evaluated experimentally in the testbed depicted in Figure 4-4. Two commercial coherent transponders (labeled TRX-1 and TRX-2), with optical line interface at 100G (32-GBd Quadrature Phase-Shift Keying -QPSK), have been connected using an optical multi-span link. The pair of transponders has been equipped with a specifically designed driver enabling both the configuration and the real-time monitoring of the SNR; the generated signal is filtered by a WSS Wave Shaper device. The optical link consists of 4 spans, each realized by an 80 km single-mode-fiber spool, for a total distance of 320 km. Five EDFAs have been used to compensate for the power attenuation; all being the single stage with gain in the range 15-25 dB. OA1 was configured with a constant 17.5 dB gain to compensate for the filter insertion losses and the other OAs with a constant gain of 16 dB to compensate entirely for the fiber losses within the span.

Two different experiments were carried out. In the first, we reproduced the effect of a filter detuning. We configured the TRXs at 193.9 THz and the WSS with a bandwidth of 50 GHz, collecting the estimated SNR at TRX-2. Then, we reconfigured the WSS filter, reducing the bandwidth with steps of 2 GHz, until the operational status of TRX-2 card was down. GNPy was used as a tool to estimate the expected

QoT for the lightpath. In order to estimate the QoT, together with the scenario that includes fiber types and span length, modeling parameters of the WSS, OAs and the TRXs are provided as input to GNPy; it estimates the QoT using the generalized GN model [Ca18], which considers both the ASE noise and NLI accumulation.

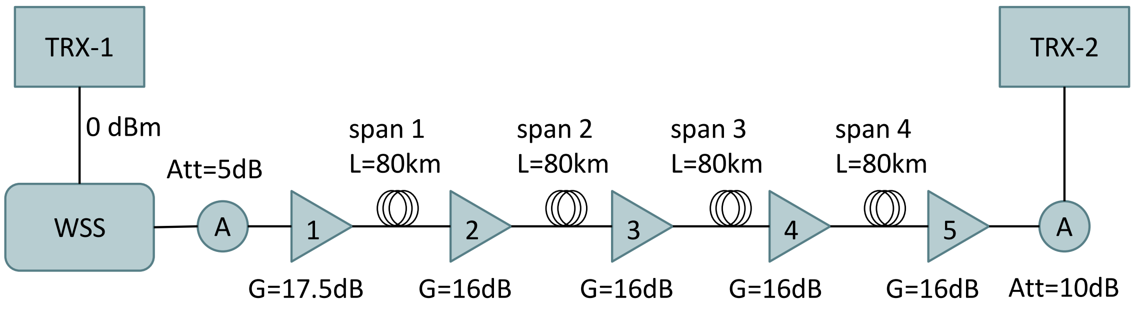

Figure 4-4 Experimental testbed

Assuming that the device responsible for the SNR measured in TRX-2 is unknown, we run the Find Modeling Configuration block of MESARTHIM to estimate the most likely modeling configuration of the WSS and one of the OAs in the optical link. Figure 4-5 presents the results obtained when the observed SNR is explained by a reduction in the OSNR of the A/D WSS (Figure 4-5a) and by an increased value of the NF in one of the OAs (Figure 4-5b). We observe that changes in both modeling parameters could explain the evolution of the observed SNR in the lightpath with minimal error, being the resulting values of the modeling parameters within a feasible range. Note that with just one lightpath in this experiment, it is not possible to make any localization, as any of the devices could be responsible for the observed reduction in the SNR.

In the second experiment, we slightly changed the multi-span link scenario with respect to that in Figure 4-4, by adding 5 dB attenuators before spans 2-4 emulating an additional 25 km in each span. Therefore, the gain of OAs 3-5 had to increase to 21 dB to compensate for the increased losses that also affected the NF of our amplifiers (which is inversely proportional to the configured gain). The experiment was carried out in three steps, where one span was modified at a time. For each step, we continuously collected the estimated SNR at TRX-2, detecting the variation of the transmission metrics during the testbed evolution. Figure 4-6 presents the results from the Find Modeling Configuration block when the length of the spans 2-4 was increased to an equivalent of 105 km and consequently, the gain of OAs 3-5. At each step, the module was able to explain the increment in the SNR of the lightpath by a reduction in the NF of the related OA. For illustrative purposes, the estimated SNR of the lightpath that would be obtained by keeping the NF constant is also represented in Figure 4-6. These two experiments assess the high accuracy of the Modeling Config Search for estimating the modeling parameters of the devices.

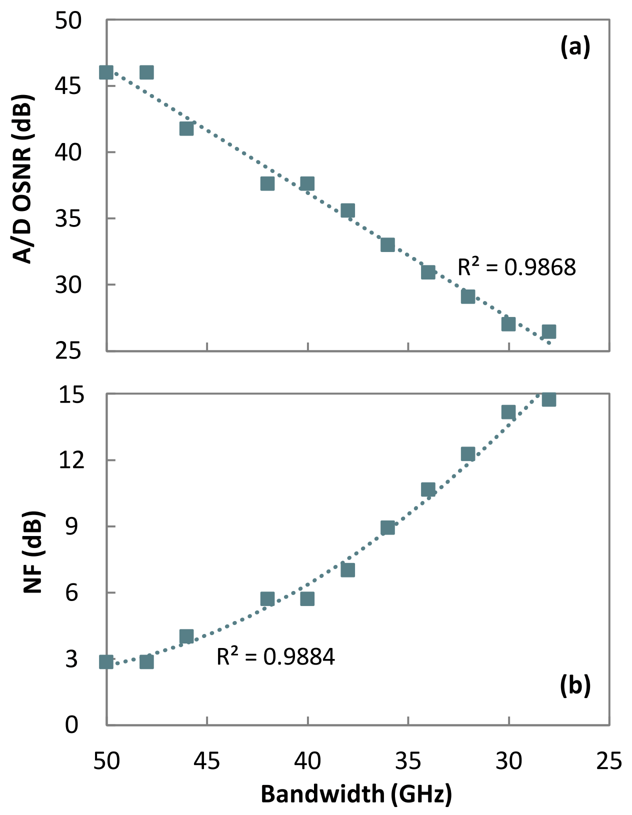

Figure 4-5 Modeling parameter value vs. bandwidth for A/D WSS OSNR (a) and OA NF (b)

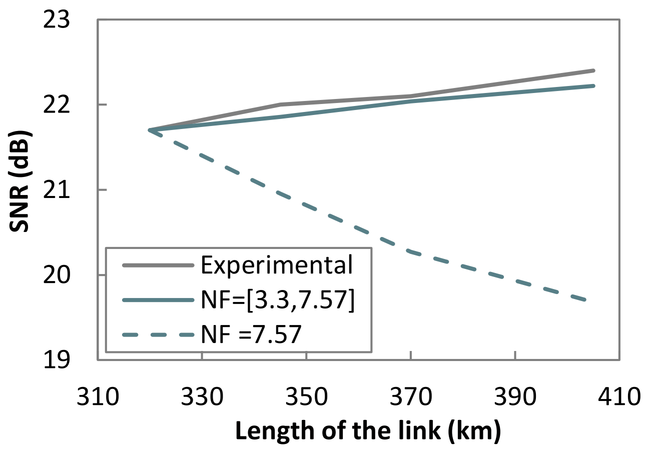

Figure 4-6 SNR vs. link length

The next subsections evaluate the MESARTHIM methodology through simulation.

4.5.2 Simulation environment

For the simulation, we selected a German-like network topology with 17 nodes and 26 bidirectional links (see Figure 4-7). 136 bidirectional lightpaths, representing all the origin-destination pairs, were established through the shortest route in terms of hops. Figure 4-8 plots the number of lightpaths that every link in the network is supporting (which is particularly important for failure localization). For the sake of simplicity in the analysis of the results, we assume that all signals use the QPSK modulation format.

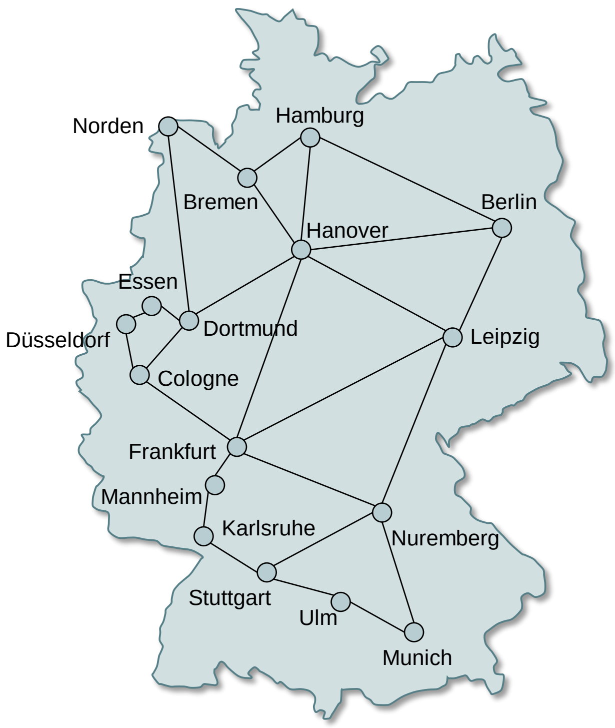

Figure 4-7 Optical network topology considered in this chapter.

The optical data plane was simulated by a GNPy instance. We generated SNR measurements for every lightpath by varying every modeling parameter of every intermediate OAs and A/D WSSs in the ROADMs in the network, independently. With these measurements, a set of realistic types of failures (use cases) affecting optical devices were reproduced by forcing the modeling parameters of the selected devices (NF and P-max in the OAs and OSNR in the WSSs) to vary over time. From the different variations that might happen, we focus on gradual variations, i.e., those soft-failures that can eventually degenerate into hard-failures. Among all possible gradual degradations, we focus on the exponential increase (NF) and logarithmic decay (P- max and OSNR), since both types of degradations accelerate in time and hence, it is crucial to anticipate their detection and localization as much as possible. Finally, variability to the SNR samples was added in the form of random noise.

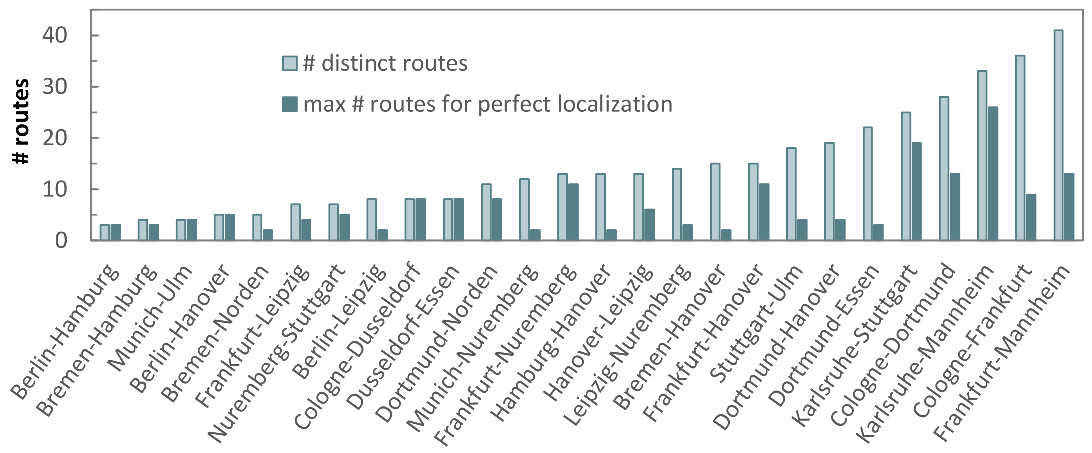

Figure 4-8 Number of distinct routes per link and max number of routes for localization.

The resulting samples were stored in the simulated control plane and fed the module implementing the MESARTHIM methodology. In the case of the SNR- wise Surveillance algorithm, the SNR_threshold (line 3 in Algorithm 4-2) was set to the expected SNR for each given lightpath minus a fixed value that exceeds the random variations introduced by the monitoring generator.

The next subsections present the obtained results for the different procedures of the MESARTHIM methodology based on this simulation setup.

4.5.3 Surveillance and Device Configuration Estimation

Let us first illustrate the convergence of the Modeling Config Search algorithm with an example entailing two sets of lightpaths. We are interested in finding the most likely modeling config for the OSNR of an A/D WSS and for the NF of an OA (each supporting one of the sets of lightpaths), given its monitored SNR. Figure 4-9 plots the MSE as a function of the configuration value, as well as those values explored by the algorithm for the two optical devices. The inset tables specify the MSE values, where the configuration that gives the minimum MSE is finally selected. From these results, as well as from those in the experimental assessment, we conclude that the algorithm converges in the whole range of the true soft-failure origin, regardless of the selected QoT parameter.

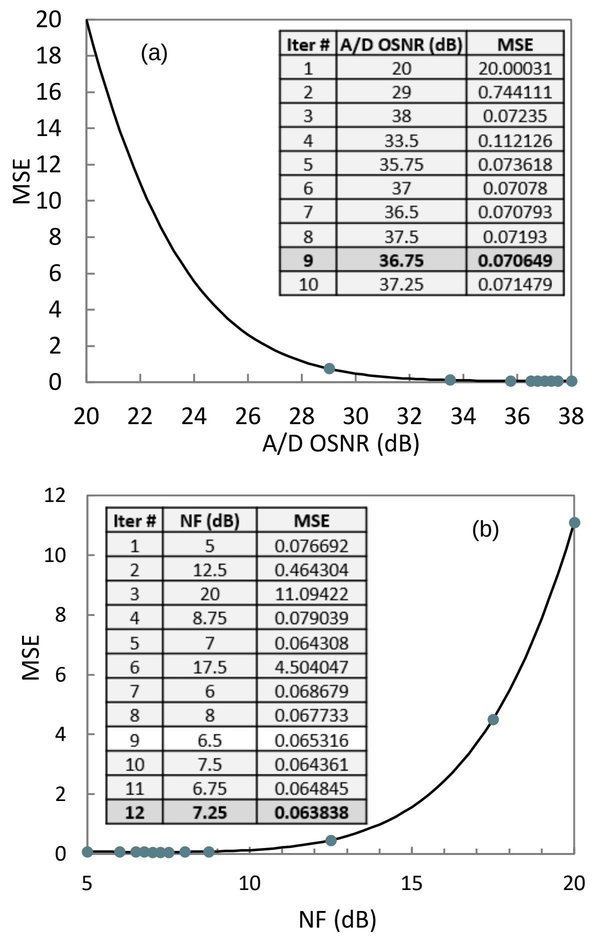

Iter #	A/D OSNR (dB)	MSE
1	20	20.00031
2	29	0.744111
3	38	0.07235
4	33.5	0.112126
5	35.75	0.073618
6	37	0.07078
7	36.5	0.070793
8	37.5	0.07193
9	**36.75**	**0.070649**
10	37.25	0.071479

Iter #	NF (dB)	MSE
1	5	0.076692
2	12.5	0.464304
3	20	11.09422
4	8.75	0.079039
5	7	0.064308
6	17.5	4.504047
7	6	0.068679
8	8	0.067733
9	6.5	0.065316
10	7.5	0.064361
11	6.75	0.064845
12	**7.25**	**0.063838**

Figure 4-9 Modeling Config Search

We now focus on the evolution of the SNR over time for the defined use cases. The graphs in the upper row in Figure 4-10 (P-max gradual), Figure 4-11 (NF-gradual), and Figure 4-12 (A/D WSS gradual) present such evolution, where, for the sake of clarity, we plot only one sample of the affected lightpath. Note that only the lightpaths affected by the failure will experience an evolution in their SNR, whereas the rest of the lightpaths will show no variation over time other than a random one plus some uncorrelated spurious measurements introduced by the monitoring generator. The time in the graphs is normalized, as the time-scales for the considered soft-failures are different, ranging from days to months or even years. The evolution of the modeling parameters is shown in the bottom-row graphs, where the actually programmed value and the interval of values [max, min] estimated by the Find Configuration block is plotted.

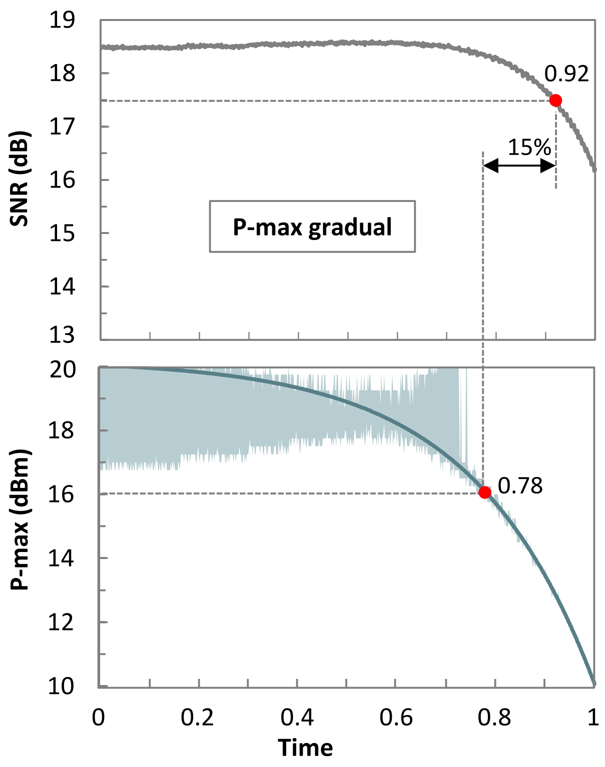

Figure 4-10 Evolution of monitored SNR and estimation of modeling parameters.

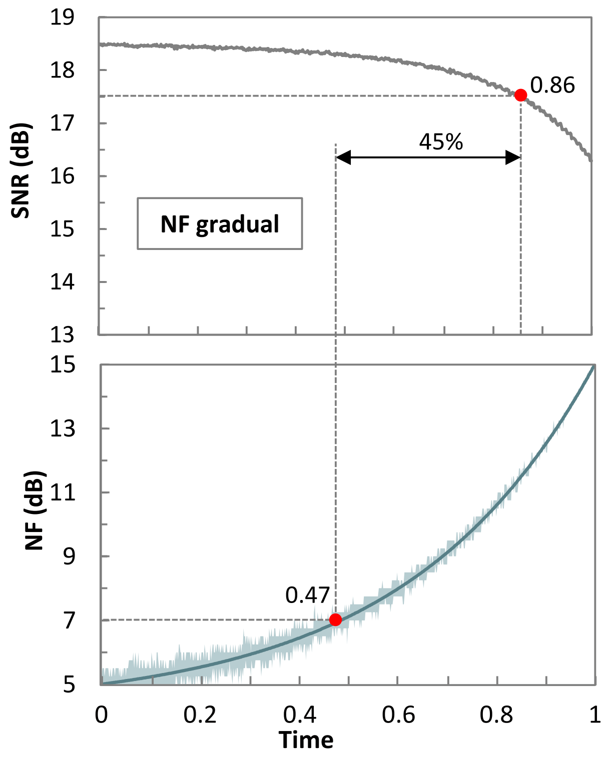

Figure 4-11 Evolution of monitored SNR and estimation of modeling parameters.

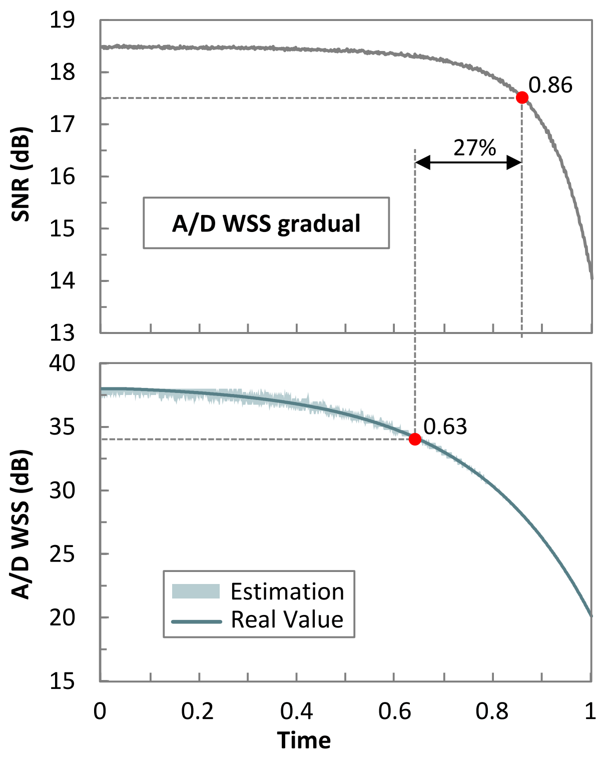

Figure 4-12 Evolution of monitored SNR and estimation of modeling parameters.

We observe that the range of possible values of the modeling parameters is tighter when the value of the parameter deviates from its nominal one. In addition, the range of possible values for the modeling parameters is different for the different parameters, being the P-max of the OAs the one with the largest range. This might have a clear impact if the detection of the soft-failure is performed by tracking the evolution of that parameter. Figure 4-13 complements the previous study by plotting the maximum and average error in the estimation of the modeling parameters as a function of the magnitude of the degradation. We observe in Figure 4-13a that both maximum and average P-max estimation errors are high for low degradation magnitudes (15.6% and 7.8%, respectively). In contrast, the average error for NF and A/D WSS (Figure 4-13b.c) are remarkably low and almost constant for the degradation magnitudes studied. Figure 4-13 also confirms the observation regarding the error in the estimation of the value of the modeling parameters greatly reduces with the magnitude of the degradation, which is a very promising result and it can be exploited for soft-failure localization and identification.

Some conclusions can be drawn from the results obtained so far: 1) the proposed method for estimating the value of modeling parameters of the devices has shown remarkable accuracy in the experimental tests, which has been confirmed by simulation for all failure use cases; 2) in general, the estimation interval is tighter when the impact of the value of the parameter on the observed SNR is higher; 3) in the specific case of the maximum power of the OAs, the range of values that result in the SNR values observed is large when the observed SNR remains around the nominal value. However, when SNR degrades with evident trend, the correlation between P-max and SNR becomes larger.

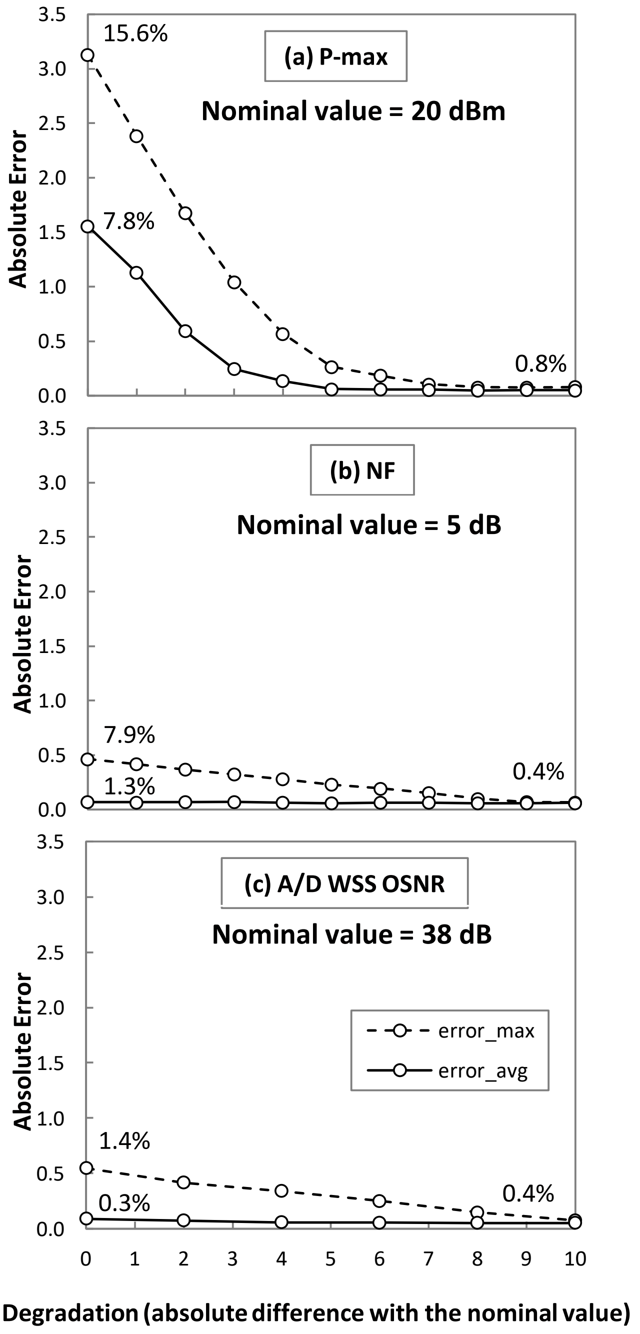

Figure 4-13 Absolute and relative modeling parameter estimation error.

To help developing intuition about the differences that can be expected by analyzing the SNR of the lightpaths and the value of the modeling parameters of optical devices, Figure 4-10, Figure 4-11, and Figure 4-12 compare the time to detect a degradation by analyzing the measured SNR and the value of the modeling parameters. For the sake of simplicity, let us assume that degradation detection is performed by threshold crossing; the threshold was set to 1 dB below the nominal SNR value for the lightpaths, not below a minimum SNR resulting in a pre-FEC BER over $4 \cdot 10^{-3}$ for QPSK signals. The thresholds related to modeling parameters were defined as a percentage of the variation range given by the nominal value and the extreme value. Values are selected to reduce detecting false degradations: *i*) for P-max it was set to 40% in the interval between the nominal value (20 dBm) and the extreme value (10 dBm) due to the large range of variation observed; *ii*) for NF of the OAs, the percentage was set to 20% in the interval between the nominal (5 dB) and the extreme value (15 dB); and *iii*) for the OSNR of the A/D WSSs, the percentage was set also to 20% in the interval between the nominal (38 dB) and the extreme value (20 dB).

With these values, the detection of the degradation in the case of the SNR of the lightpath happened at normalized times 0.92, 0.86, and 0.86 for the P-max, NF, and A/D WSS OSNR gradual soft-failure use cases, respectively. This contrasts with the detection at times 0.78, 0.47, and 0.63 when the analysis was in the value of the P-max, NF, and OSNR of the A/D WSSs, respectively, which results in anticipation between 15% and 45%. Note that such anticipation is enabled by the different evolution of modeling parameters and their non-linear impact on the SNR of the lightpaths.

4.5.4 Soft-Failure Localization

The above discussion considered the time for the detection only. Note that soft-failure location (Algorithm 4-4 in Section 4.3.2) requires several lightpaths to find the common resources in the network topology. When the evolution of the monitored SNR changes suddenly, SNR-wise surveillance (Algorithm 4-2) collects enough lightpaths to easily localize the failure; however, under a gradual degradation, the lightpaths exceeding the threshold might be not enough for the localization.

Figure 4-8 includes a study of the maximum number of distinct routes that need to be considered to unambiguously identify every link as responsible for a soft-failure, considering that longer lightpaths will be more affected by device degradations. For the study, we selected all the links in the network, together with an incremental number of lightpaths selected by their total length, and fed Algorithm 4-4 for the (multiple) soft-failure localization (i.e., 26 soft-failures were localized with a single execution of Algorithm 4-4). For the localization, not only the number of lightpaths is important, but also their routes. We repeated the experiments with the lightpaths sorted in inverse order, i.e., assuming that shorter lightpaths would exceed the (relative) threshold first. The results showed that all soft-failures could be perfectly localized when the resources of the two shortest lightpaths were analyzed.

With the above in mind, let us now show how the SNR-wise surveillance and localization evolves over time. Table 4-3 presents the results from two different failures. The first failure was in an OA in the link Frankfurt-Mannheim (supporting 41 distinct lightpaths), and the second in the A/D WSS in the Dusseldorf ROADM (supporting 16 distinct lightpaths). For each failure, each row shows the detection time when the measured SNR of some new lightpaths is below the threshold (bear in mind that the threshold is relative to the expected SNR for that specific lightpath). However, the localization of the soft-failure is not successful until just one resource (assuming that it is responsible for the failure) can be identified. Such identification happens at normalized times 0.93 and 0.91 for the failures in the OA and the A/D WSS, respectively. Note that the number of lightpaths needed to localize the soft-failure, although small, adds some extra time that could be of paramount importance for the impact on the network.

Table 4-3 Examples of Soft-Failure Localization

Failure in OA in link Frankfurt-Mannheim		
Time	**Degraded paths**	**Common Resources**
0.86	1	2 TRXs, 2 A/Ds, 1 Link
0.90	2	2 Links
0.93	4	1 Link (Failure in Frankfurt-Mannheim)
Failure in A/D WSS Dusseldorf		
0.86	1	2 TRXs, 2 A/Ds, 1 Link
0.91	2	1 A/D WSS (Failure in Dusseldorf)

In contrast, soft-failure localization under the Modeling-wise approach considers all the lightpaths supported by such resource, as it analyzes the estimated evolution of the modeling parameters by resource. In consequence, Algorithm 4-4 under the Modeling-wise approach can localize the cause of degradations in their very early stages (between 31% and 49% with respect to the SNR-wise approach).

As a final remark, it should be noted that even though the Modeling-wise approach considers all the lightpaths supporting a given resource, unambiguous localization might still not be possible if few lightpaths with distinct routes are established. Figure 4-8 shows that, for some links in the considered scenario, unambiguous localization of a soft-failure is only possible when all supported lightpaths are analyzed. Therefore, in case that not all these paths are established, the localization procedure (Algorithm 4-4) would be unable to localize the failure. E.g., let us consider the soft-failure in the link Frankfurt-Mannheim in Table 4-3 and imagine that only one lightpath is supported by such link. Then, a degradation in that lightpath can be explained by degradation in more than one resource. This highlights the need for additional procedures to be applied for those scenarios which result in ambiguous localization.

4.5.5 Identification and Severity Estimation

Once the degradation has been localized, let us focus on the identification of the modeling parameter responsible for such degradation. We assume that the device explaining the observed degradation is an OA. According to the notation in Section 4.4.1, identification performance is clearly dependent on the configuration of all coefficients related to indicator φ. Several configurations were tested to find the one giving the desired importance to every component, ensuring that parameters with a high indicator are correctly selected, while guaranteeing no false positives. Such configuration *is* $<b1, b2, b3, b4, \Delta\varphi, thr> = <20, 10, 2, 1, 5, 30>$, which will be used hereafter.

Figure 4-14 shows the obtained results for a gradual degradation caused by NF, whereas Figure 4-15 shows the results for a gradual degradation caused by P-max. In both cases, Figure 4-14a and Figure 4-15a plot the evolution of the accumulative indicator with time, and the decision threshold *thr*. Both indicators remain clearly under the threshold until time around 0.32, where enough evidence of the cause of the degradation is found. Note that the time of such identification represents 32% of anticipation compared to the earliest time obtained for degradation detection (at time 0.47) using a threshold on the evolution of the input parameter and 64% compared to the earliest detection time using a threshold on the evolution of the SNR. Figure 4-14b-c and Figure 4-15b-c show the computed projections for the two modeling parameters under study and for both failures; note that such figures are similar to Figure 4-3. The projections are plotted for a long window (around 0.25 time units) for clarity purposes, although the value used for fitting and evaluation was $\delta = 0.03$ normalized time units.

In the case that the failure is a consequence of the NF degradation (Figure 4-14b-c), we observe that the centered projection fc for the NF parameter is highly accurate and clearly between the upper and lower ones, which results in the minimum indicator parameter. On the contrary, P-max indicates an evident but less accurate projection and moreover, f_c overlaps with f_u, which increases its indicator above 5 units from the one of NF. As a consequence of this, P-max is selected as a parameter with a high indicator, so its accumulative indicator increased. Conversely, in Figure 4-15b-c the minimum indicator is that of P-max, where there is an evident degradation for f_l. Note that this indicator is much lower than that computed for NF, where no degradation is observed, thus exceeding by far the indicator limit. In conclusion, we see how the proposed methodology allows discriminating the actual failing parameter and perform a fine failure identification.

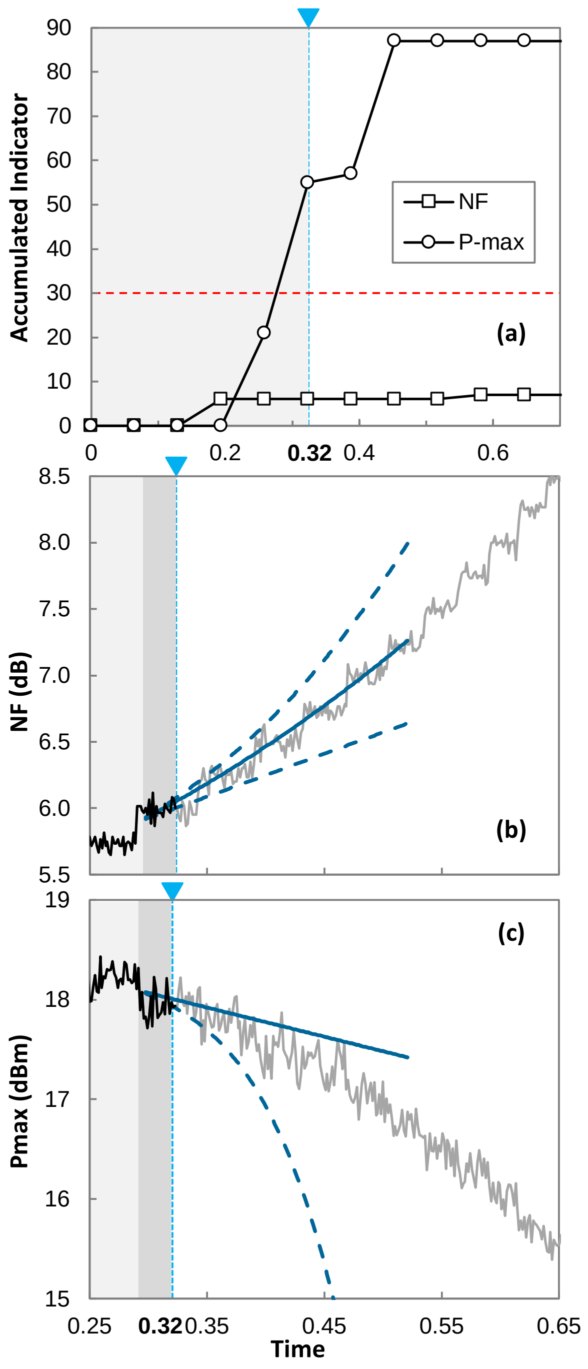

Figure 4-14 NF Gradual Soft-Failure Identification.

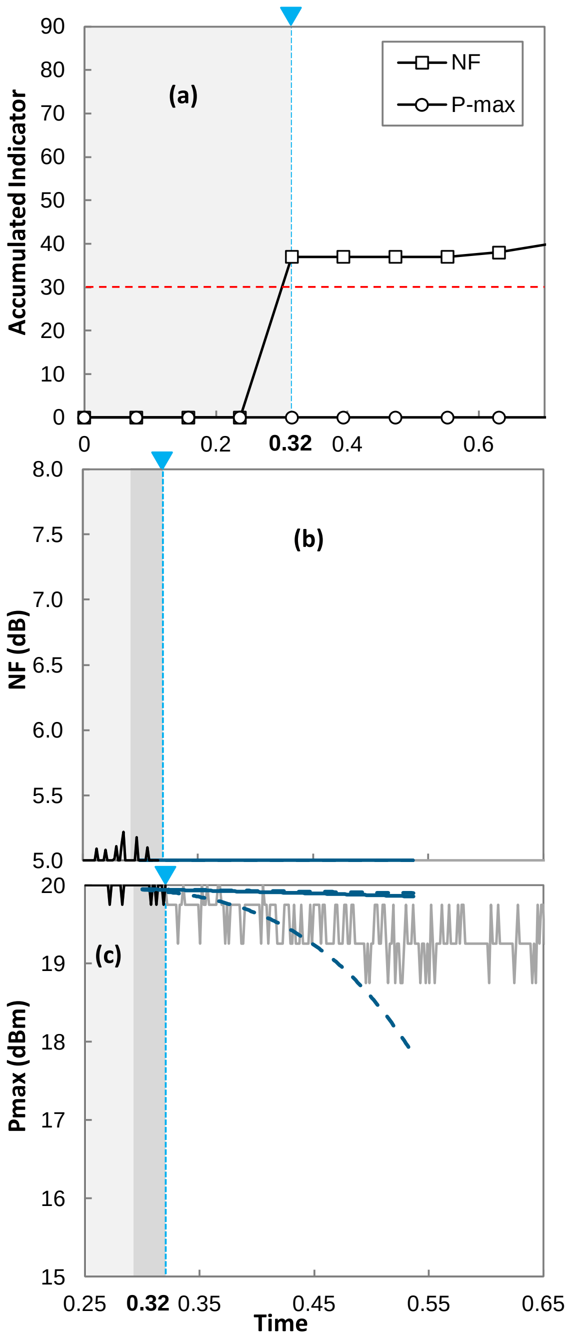

Figure 4-15 P-max Gradual Soft-Failure Identification.

We can take advantage of the identification method to implement an alternative localization method that can be applied when not enough lightpaths with distinct routes are established in the network. This allows the unambiguous localization of a soft-failure, as motivated at the end of Section 4.5.4. In this case, we assume that only lightpaths between the two end ROADMs of the link Frankfurt-Mannheim are established and have considered soft-failures in one of the supporting devices (OA, TRX or A/D WSS), in line with Table 4-3. In this case, we execute Algorithm 4-6 considering a single *virtual* resource that abstracts the supporting optical device types. The algorithm returns the most probable modeling parameter among those of OA, TRX and A/D WSS, which helps to reduce the number of devices to be analyzed manually.

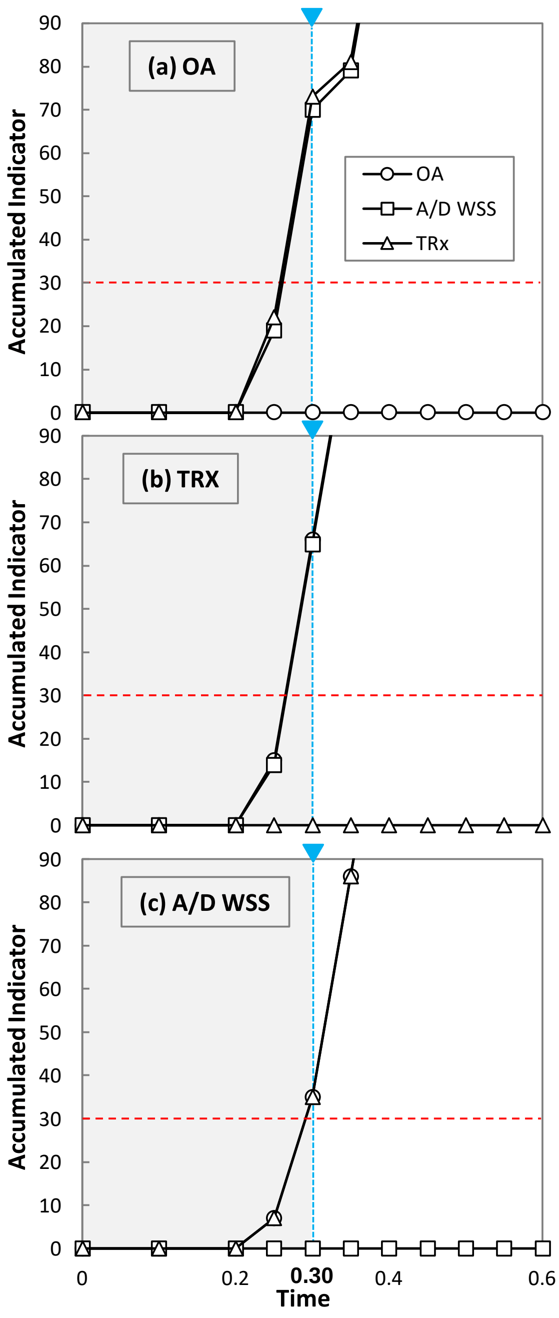

Figure 4-16 Localization by identifying the Soft-Failure.

Figure 4-16 shows the performance of the identification procedure for soft-failure localization. Three scenarios are considered for the real cause of the soft-failure: *i*) gradual NF degradation in an OA (Figure 4-16a), *ii*) gradual OSNR degradation in an A/D WSS (Figure 4-16b), and *iii*) gradual OSNR degradation in a TRX (Figure 4-16c). We observe that the accumulated score clearly increases for the two types of devices that are not the real cause of the failure for all the analyzed scenarios. This happens at time 0.3 in all the cases.

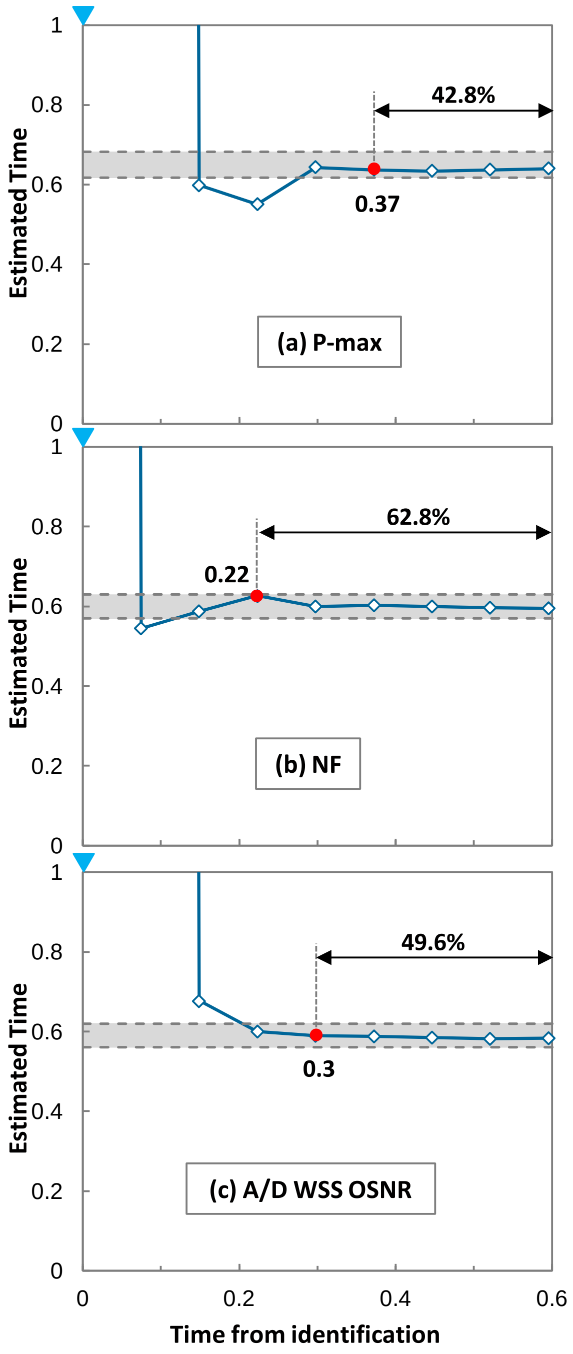

Figure 4-17 Severity Estimation.

Finally, Figure 4-17 presents the obtained results for severity estimation for gradual degradation of P-max, NF and A/D WSS OSNR as a function of the time. The plots show the evolution of the estimated time with the real-time, where the area in grey color highlights the real-time when the soft-failure degenerates into a hard-failure ±5%. We observe that the estimated time takes a large value when the estimation does not observe a major impact in the selected *timeWindow* for any of the affected lightpaths, and rapidly converges to the real degeneration time. In fact, assuming that the severity is accurately estimated after two consecutive executions returning estimated times close enough one to the other, anticipation over 42% to the degeneration time are obtained, which leave enough time to plan the adequate maintenance operations.

4.6 Concluding Remarks

QoT estimation is typically carried out during the provisioning phase and in-operation planning to ensure that computed lightpaths will provide zero post-FEC errors, assuming some values for the QoT model input parameters related to the optical devices in the network. In this chapter, QoT estimation was used for the reverse process, i.e., given the real measured QoT of a set of lightpaths, we were interested in estimating the value of the modeling parameters of the optical devices.

Because of the non-linear relation between lightpaths QoT and the value of the modeling parameters, the ability to estimate the value of such parameters opens the opportunity to analyze its evolution, which can be as a result of, e.g., aging, temperature variations, etc. The proposed MESARTHIM methodology combines analysis of the evolution of the monitoring QoT and their transformation into the estimated modeling parameters space, not only for the degradation detection, but also for its localization, identification, and severity estimation.

After the experimental assessment of the method for estimating the modeling parameters of the devices, the MESARTHIM methodology was evaluated through simulation. The methodology demonstrated remarkable anticipation in failure detection and localization by analyzing the estimation of the value of the modeling parameters of the devices. A simple example showed the reason behind such potentials in the different evolution of the modeling parameters and the lightpaths SNR. In addition, accurate cause identification based on the analysis of the projected evolution of the modeling parameters was demonstrated, which enabled the estimation of the severity in terms of the time when the soft-failure degrades into a hard-failure. Such severity estimation allows planning maintenance, as it largely anticipates degradation.

Table 4-4 summarizes the main characteristics with pros and cons of the MESARTHIM methodology.

Table 4-4 Summary of the MESARTHIM Methodology

Method	Degradation Detection and Failure Localization	Cause Identification and Severity Estimation
Analysis in the lightpaths' SNR space	• SNR-wise surveillance finds common resources in sets of affected lightpaths by analyzing its SNR. • Analyzes all lightpaths. For failure localization, the algorithm needs that several lightpaths to be affected.	• No cause can be identified. • QoT can be estimated based on the projected evolution of the SNR.
Analysis in the devices' modeling parameters space	• Modeling-wise surveillance analyzes the value of the modeling parameters for all network devices. • The algorithm detects degradations and localizes their sources very ahead in time.	• Cause identification based on the projected evolution of the modeling parameter of the device where the failure is localized. • Severity estimation difficult to estimate by analyzing the evolution of the input parameters.

Chapter 5

Towards Autonomous vLink Capacity Management

The massive deployment of 5G and beyond will require high capacity and low latency connectivity services, so network operators will have either to overprovision capacity in their transport networks or to upgrade the optical network controllers to make decisions nearly in real time; both solutions entail high capital and operational expenditures. A different approach could be to move the decision making toward the nodes and subsystems, so they can adapt dynamically the capacity to the actual needs and thus reduce operational costs in terms of energy consumption. To achieve this, several technological challenges need to be addressed. In this chapter, we focus on the autonomous operation of DSCM systems, which enable the transmission of multiple and independent subcarriers (SC). Herein, we present several solutions enabling the autonomous DSCM operation, including: *i*) SC quality of transmission estimation; *ii*) autonomous SC operation at the transmitter side and blind SC configuration recognition at the receiver side. We provide useful guidelines for the application of autonomous SC management supported by the extensive results presented.

5.1 Introduction

In this chapter, we propose a decentralized approach where the intelligence is distributed [APV17.2]; the Tx decides autonomously the SC configurations, i.e., the SC's MF and SR, and the Rx can detect and recognize such configurations. Nevertheless, the role of the SDN controller is of paramount importance as it solves the routing and spectrum allocation (RSA) [Ve12] for the request, thus providing a lightpath in the optical network topology that satisfies not only the needed capacity but also the required QoT for every SC. Note that individual SCs are impaired differently when they cross WSSs, which are part of ROADM. To this end, software tools like the open source GNPy [Fe20], can be used but need to be upgraded to properly consider the filter penalties.

The remainder of the chapter is organized as follows. Section 5.2 introduces the proposed solution for autonomous SC operation, where an intent, with the operational objective to allocate enough capacity, is in charge of autonomously making decisions to configure and activate or deactivate SCs at the Tx side. Section 5.3 focuses on lightpath provisioning and includes an estimation of per-SC QoT, which is later used to solve the RSA with SC (RSA-SC) configuration problem. Section 5.3 proposes algorithms to manage the SC at the Tx and Rx sides; the Transponder Agent at the Tx side is in charge of managing the capacity of the lightpath by properly configuring the different SCs to minimize energy consumption, whereas the agent at the Rx side needs to recognize the configuration of each SC. Section 5.3.2 is devoted to our intent-based solution and the approach is proposed to anticipate future traffic conditions thus minimizing or totally eliminating undesirable effects at the packet layer. This solution uses a short-term traffic forecast. Section 5.3.2 is devoted to our intent-based solution and our approach is proposed to anticipate future traffic conditions thus minimizing or totally eliminating undesirable effects at the packet layer. This solution uses a short-term traffic forecast. The discussion is supported by extensive illustrative results in Section 5.4, including exhaustive simulations over realistic scenarios. Finally, Section 5.5 draws the main conclusions of our work.

5.2 Autonomous Capacity Management

As previously stated, we propose the autonomous operation of the vlinks performed locally at their end nodes and being able to recognize in one end the decisions made at the remote end. This is particularly important at the optical layer, as the Rx optical transponder of the lightpath supporting the vlink needs to realize the actual configuration of the signal that was transmitted. From the packet layer perspective, it is also desirable to devise solutions that: *i*) do not introduce delays and traffic losses; and *ii*) minimize the changes in the capacity of the vlink to facilitate the management of such capacity at the packet nodes.

Figure 5-2 presents the key elements in the control and data planes and overviews the envisioned workflow of vlinks. At the set-up time, the SDN controller receives a request to create a vlink between two end nodes with a given maximum capacity. The SDN controller computes the best route of the underlying lightpath and estimates the QoT. Based on such estimation, the SDN controller determines the number of SCs and a configuration map with the set of feasible configurations for each SC s in terms of pairs <*MFs, SRs*> that can be used; this would allow the autonomous SC operation and will support the given maximum capacity (step 1 in Figure 5-2). Then, the SDN controller establishes the lightpath by allocating the needed optical spectrum along the path connecting Tx and Rx, and sends the configuration map to the vlink intent in charge of the autonomous vlink operation (step 2). The SDN then relies on the vlink intent to manage the capacity of the vlink as a function of the input traffic (step 3). An illustrative example of such capacity management is displayed in the inset in Figure 5-2, where the capacity of the vlink (orange line) increases and decreases to serve the input traffic (blue area). The vlink intent communicates the desired capacity of the vlink to the Transponder Agent, which activates or deactivates SCs in the underlying optical signal. Such decision making is performed within the Tx and consequently, a mechanism is needed for the Rx to detect and configure SCs' MF and SR, as well as to detect the absence of a SC (step 4). Finally, notifications are sent to the SDN controller informing about changes in the vlink and the optical signal (step 5).

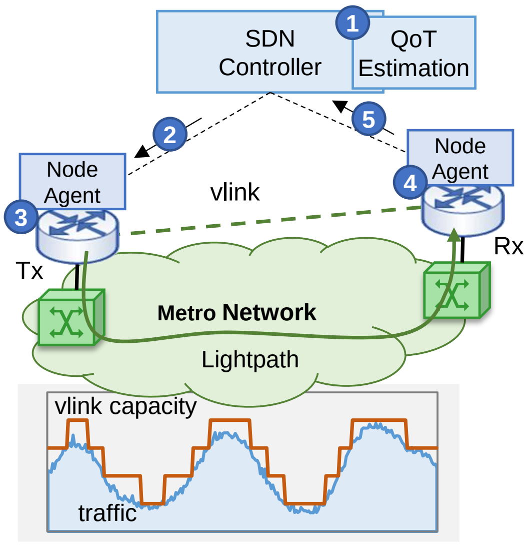

Figure 5-1 Vlink workflow overview.

Figure 5-2 presents an example of the evolution over time of the input traffic and the active configuration of the optical signal, as decided by the Tx, to meet the capacity requirements of the vlink intent. Once the connection is set up by the SDN controller at time t0, the vlink intent observes the amount of input traffic and makes decisions consequently. For instance, based on required capacity, the transponder agent within the Tx configures the first 8 GBaud QPSK SC (SC1) at t0, which entails that the connection capacity is 25 Gb/s, considering a FEC overhead of 20%. Based on periodical capacity updates, received from the vlink intent, the Tx increases connection's capacity to 50 Gb/s at t1 by activating SC4 with the same configuration as for SC1. The capacity is increased to 100 Gb/s at time t2 by activating SC2 configured as 11 GBaud 8QAM. If the input traffic would continue increasing, the last SC (SC3) would be activated, e.g., with an 11 GBaud 16QAM configuration to increase capacity up to 170 Gb/s. On the contrary, if the capacity requirements would decrease (as in t3), one or more SCs could be turned off, thus saving energy.

Note that the decisions made in the SC configuration can limit the maximum capacity of the vlink. For instance, if all SCs can be configured with QPSK, 8QAM or 16QAM MFs and 8 or 11 GBaud, the maximum capacity of the vlink would lie in the range [100-280] Gb/s depending on the selected configuration. Therefore, assuming that SCs cannot be reconfigured (i.e., to change the configuration of a SC, the SC needs to be deactivated and then activated again with a different configuration, which would cause packet losses if the SC is supporting traffic), such decision-making process need to be intelligently carried out to maximize the potential capacity of the connection without traffic disruption, while saving as much energy as possible. For instance, in view of the evolution of the traffic at t1, the vlink intent could have requested a capacity of 75 Gb/s, so that the Tx would have configured SC2 as a 11 GBaud 16QAM signal and then, deactivated SC4, thus resulting in the same performance but with lower total energy and configuration changes. In addition, note that not all SCs can support all different configurations, as this depends on the expected SNR at the receiver. For example, a cascade of filters will affect the “external” SCs more severely than the inner ones, thus limiting the MF order of the former to just QPSK. This introduces additional complexity in the decision-making process.

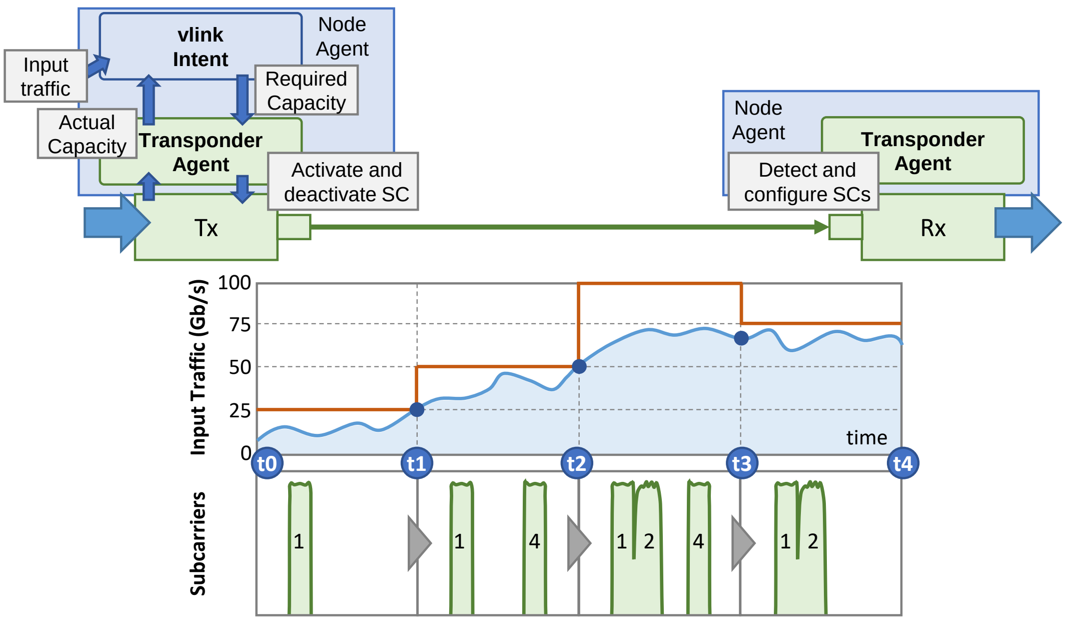

Figure 5-2 Intent-based autonomous vlink operation to allocate capacity for the input traffic.

The modules that make possible the envisioned autonomous vlink operation are presented next.

5.3 Capacity Management

When the lightpath is established, the actual capacity that is provided by the connection can be managed by activating and configuring each SC independently as a function of the traffic to be conveyed. In this section, we first present the procedures for the Tx to select the configuration of the optical connection, including which SCs are active and their configuration to provide the needed capacity. Then, we propose a solution to predict the traffic evolution. We assume that the SC definition contains a SC configuration map with all possible options, from those allowed by the transponder, that do not exceed the maximum configuration received from the controller.

5.3.1 Transponder Agent

We propose two different policies for the autonomous management of the optical connection at the transponder agent:

- the *maxSC* connection management policy, which allocates the SC with maximum possible capacity, thus potentially minimizing the changes in the connection's configuration;
- the *adaptive* connection management policy, which allocates the minimum capacity to satisfy the input traffic needs, targeting at minimizing the excess of capacity with respect to the actual traffic with the goal of eventually minimizing the total energy consumption.

Both algorithms return one single SC change in the connection configuration. Therefore, they must be executed within an outer loop until they cannot perform more changes (i.e., returning *<s=∅, config=∅>*).

The pseudocode for *maxSC* connection management policy is presented in Algorithm 5-1. The algorithm receives as input the state of the connection in terms of the configuration of the SCs, the map of feasible configurations for each SC, and the target capacity for the connection. It returns the SC to be activated/deactivated, if any, and its target configuration. The algorithm computes the difference of capacity between the current and the requested ones (line 1). In case the capacity of the connection needs to be increased, the SC providing the largest capacity among those not yet active is selected (lines 2-3). On the other hand, the capacity of the connection is reduced by selecting the active SC with the lowest capacity, whose deactivation leaves enough capacity in the connection (lines 4-6). Finally, the selected SC, if any, and the target configuration are returned (line 7).

This policy enables minimizing the number of configurations to be supported thus potentially reducing the cost of the transponders. It selects the SC with the largest capacity among the non-active ones; this minimizes the number of changes in the capacity of the connection, which facilitates its management at the packet layer. Nonetheless, this policy might lead to large energy consumption due to the overprovisioning, since the selection of the SC to be activated does not depend on the actual capacity needs.

Algorithm 5-1 maxSC Capacity Management

```
Input: conn, configMap, targetCapacity
Output: s, config
1:  diffCap ← targetCapacity - conn.capacity
2:  if diffCap > 0 then
3:     <s, config> ← argmax{s.getMaxConfig(configMap)
                          ∀ s ∈ conn | NOT s.isActive()}
4:  return <s, config>
5:  config ← ∅
6:  s ← argmin{s.capacity ∀ s ∈ conn | s.isActive() AND s.capacity < -diffCap}
7:  return <s, config>
```

Algorithm 5-2 presents the adaptive connection management policy, which targets at minimizing the energy consumption by configuring the connection capacity as close as possible to the actual needs.

Algorithm 5-2 Adaptive Capacity Management

```
Input: conn, configMap, targetCapacity
Output: s, config
1:   diffCap ← targetCapacity - conn.capacity
2:   if diffCap > 0 then
3:      activeSC ← argmax{sc.upgradability ∀ s ∈ SC |
           sc.upgradability = sc.getMaxConfig(configMap) - diffCap}
        if activeSC ≠ ∅ then
4:         <s, config> ← findNonActiveSC(conn, configMap,
5:                          activeSC.capacity + diffCap)
           if s ≠ ∅ then return <s, config >
6:      <s, config> ← findNonActiveSC (conn, configMap, diffCap)
7:      if s ≠ ∅ then return <s, config >
8:      <s, config> ← argmax{s.getMaxConfig(configMap)
9:                          ∀ s ∈ conn | NOT s.isActive()}
10:     return <s, config >
11:  config ← ∅
12:  s ← argmax{s.capacity ∀ s ∈ conn |
              s.isActive() AND c.capacity < -diffCap}
13:  if s = ∅ AND conn.numActiveSCs = 1 then
14:     <s, config> ← findNonActiveSC (conn, configMap, targetCapacity)
15:  return <s, config >
```

In case that an increment of capacity is requested, the algorithm identifies the active SC with the largest potential capacity increase (lines 2-3 in Algorithm 5-2), so another SC can be activated supporting the requested capacity plus the identified active SC (lines 4-6). In that case, a consecutive execution of the algorithm will find that the first SC can be deactivated. If any active SC is identified, a non-active SC needs to be activated, which is configured to support the requested increment of capacity (lines 7-8). In case that the increment of capacity cannot be supported by just one single SC, the non-active SC with the maximum capacity is returned (lines 9-10). In the case of reducing capacity, a target SC is identified, so the total capacity of the connection still supports the requested one (lines 11-12). If no SC can be deactivated and there is just one single SC activated, the algorithm tries to activate one SC so all target capacity can be served (lines 13-14). Again, a consecutive execution of the algorithm will find that the first SC can be deactivated, so just one single SC will remain active.

The algorithm for the *adaptive* connection management policy calls the findNonActiveSC() function. This identifies the non-active SC providing the minimum overprovisioning (line 1 in Algorithm 5-3) and among them, the one that will be closer to its maximum capacity (line 2). The configuration that better fits the required capacity is returned, except if there is just one single non-active SC, where the maximum configuration is returned (lines 4-6).

Algorithm 5-3 FindNonACtiveSC() Function

```
Input: conn, configMap, capacity
Output: s, config
1:  SC={s} ← argmin{s.overProvision ∀ s ∈ conn |
        NOT s.isActive() AND s.overProvision =
        s.getMinConfig(configMap, capacity) - capacity}
2:  <s, config> ← argmin{s.upgradability ∀ s ∈ SC |
3:      s.upgradability = s.getMaxConfig(configMap) -
        s.getMinConfig(configMap, capacity)}
4:  if s ≠ ∅ AND conn.numNonActiveSCs = 1 then
5:      return <s, s.getMaxConfig(configMap)>
6:  return <s, config>
```

5.3.2 Virtual Link Intent-Based Capacity Management

The capacity management algorithms, introduced in the previous section, require measuring the input traffic to determine the capacity that needs to be ensured. However, such monitoring reflects the capacity that was needed at the time the measurement was performed, so in case that the target capacity exceeded the one of the optical connections, some traffic might need to be queued waiting for more capacity to be available; this is at the cost of introducing delay or even traffic losses in case the queue capacity is exceeded. In addition, this approach is purely reactive, as if the traffic volume reduces, the capacity of the connection reduces as well, which can derive into capacity oscillations making difficult for the packet nodes managing it. Therefore, it is desirable to devise solutions that not only reduce the energy consumption by managing the configuration of the SCs, but also predict: *i*) how to configure the SCs before the capacity is *exhausted* to avoid introducing delays and traffic losses; and *ii*) how to reduce the changes in the vlink capacity. To this end, we propose a capacity management to be carried out at the vlink level and keep the capacity management at the transponders as a back-up in case the prediction fails and the current capacity is exhausted, so that the measured traffic volume is always ensured provided that is under the maximum capacity to be guaranteed.

A solution is to use *short-term* traffic forecasts, instead of the actual measured traffic, to predict future capacity needs. This short-term *prediction* can be obtained by projecting forward the last monitored traffic samples, i.e., interpolating traffic in the last w measurements and extrapolating for next δ time units [Is02]. Although this approach can help to anticipate potential capacity exhaustion by allocating capacity in advance, when the traffic volume decreases, the reduction of capacity can lead to undesired capacity fluctuations and to increase queuing.

5.4 Illustrative Results

In this section, we first introduce the power model used for comparing the proposed SC management solutions, and then we study the performance of different SC configurations and the QoT estimation, with the aim of finding the operational limits of DSCM for autonomous capacity management. Next, we analyze the performance of the capacity management performed at the transponder or by the vlink intent.

5.4.1 Power Model

The results in the following subsections present power savings that have been computed assuming a power model aiming to abstract the actual realization of a DSCM transponder. The power model is based on the conclusions from [Fl20] and [Fr17] that can be summarized as follows: *i*) the power consumption of a transponder is related to its actual configuration in terms of MF and SR, and *ii*) the architecture of a DSCM transponder contains subsystems that are always active independently of the number and configuration of active SCs (e.g., DAC / ADC), and others that can be switched off in case a SC is not active.

With the above considerations, the power consumption of a DSCM transponder can be modeled as Eq. (5-1), where P_{base} is the minimum power consumption and $\beta(\cdot)$ is a multiplier that depends on the actual configuration of the SCs. Eq. (5-2) defines $\beta(\cdot)$ as the summation of two components, those coming from *always active* subsystems and those from subsystems that are associated to a particular SC and thus, can be switched off if that SC is not active. The ratio $R(\cdot)$, defined in Eq. (5-3), computes the proportion of power from subsystems in each group, and $\alpha(\cdot)$ computes the incremental power as a function of the MF and SR configured in a given SC, being 0 if the SC is not active. Then, from Eq. (5-2), the power consumption of *always active* subsystems starts from a minimum one given by the minimum configuration supported (e.g., <QPSK,8>) and increases depending on the actual configuration, whereas that of the subsystems associated to a particular SC can be 0 if that particular SC is not active.

$$P = P_{base} * \sum_{SC} \beta(MF_{SC}, SR_{SC}) \tag{5-1}$$

$$\beta(MF_{SC}, SR_{SC}) = R(always\ on) * max(\alpha_{min}, \alpha(MF_{SC}, SR_{SC})) + R(per\ SC) * \alpha(MF_{SC}, SR_{SC}) \tag{5-2}$$

$$R(\cdot) = \frac{P_{base}(\cdot)}{P_{base}} \tag{5-3}$$

In this chapter, we assume: *R(always on)* = 62%, and the values of *α(·)* in Table 5-1. This leads to energy savings in the range [56.6%-46.8%] when only one SC is active.

5.4.2 Transponder Agent Capacity Management

From the viewpoint of the pure optical layer, all the configurations studied can be used, especially for 50 and 62 GHz slot widths. However, transponders not supporting all such configurations might be more cost effective. With this in mind, we now focus on the capacity management and study whether reducing the number of configurations available would be also convenient from the packet layer perspective. In this subsection, we consider that the transponder agent at the Tx side adapts the configuration of the optical connection to provide enough capacity for the input traffic, by running the algorithms in Section 5.3.1.

For this analysis, we define three configuration sets for the transponders (see Table 5-1): *i*) *all*: transponders implement all possible configurations; *ii*) *selected*: transponders implement some configurations with the maximum diversity in capacity and lightpath scenarios; and *iii*) *16QAM*: transponders implement only 16QAM for all SRs. The normalized power consumption and capacity (assuming 20% FEC overhead) of every configuration are detailed in Table 5-1. Besides the power related to the SCs, another 15% of the maximum configuration supported by the transponder for each SC (active or not) needs to be accounted.

Two different policies have been carefully selected to concentrate numerical evaluation under relevant conditions: *i*) the *maxSC* with only the *16QAM* configuration set; and *ii*) the *adaptive* connection management with the three configuration sets. Two traffic profiles lasting for 2.5 days are used to compare the aforementioned policies, namely *High Traffic* and *Low Traffic*. In the *High Traffic* profile, the traffic varies from 20 to 240 Gb/s, whereas in the *Low Traffic* case it is limited to 60 Gb/s. The traffic profiles have been especially tailored to induce many configuration changes, as they contain traffic variations around the values of the capacity of the SC configurations, as well as sudden trend changes that might cause poor performance at the packet layer.

Table 5-1 Configurations, Power, and Sets

Config. (<MF, SR>)	**α(<MF, SR>)**	**Capacity [Gb/s]**	**Config. Set**		
			all	**sel**	**16QAM**
QPSK, 8	1.00	25.6	x	x	
QPSK, 11	1.29	38.4	x		
8QAM, 8	1.14	35.2	x	x	
8QAM, 11	1.47	51.2	x		
16QAM, 8	1.28	52.8	x	x	x
16QAM, 11	1.65	70.4	x	x	x

A simulation environment based on CURSA-SQ was used to study the impact of the vlink capacity management of the packet layer. The results in Figure 5-3 have been obtained for a connection with a configuration map where the external SC can be configured with any MF but only with 8 GBaud, whereas the internal ones could be configured with all possible configurations supported by the transponder.

Figure 5-3 shows the input traffic and the allocated capacity (upper row), and the active capacity per SC (lower row) for the two profiles and for all four combinations of policies and configuration sets. In the case of the *High Traffic* profile, we observe that although all four combinations manage the capacity of the connection as a function of the input traffic, the *maxSC* policy needs a lower number of changes at the cost of a larger capacity overprovisioning and energy consumption (Figure 5-3a). On the opposite, the *adaptive* policy adapts the capacity almost perfectly (Figure 5-3b-d) independently of the configuration set, at the cost of a larger number of changes. We also observe that the reactive nature of the algorithms might result in capacity exhaustion as some SCs are not configured to their maximum capacity (Figure 5-3d).

This is more evident for the *Low Traffic* profile, where although all different combinations keep active just one single SC simultaneously, the *adaptive* policy performs many changes targeting a perfect adaptation of the capacity of the connection to the input traffic to minimize overprovisioning; the *maxSC* policy keeps the SC configuration constant at the cost of a larger overprovisioning. Table 5-2 summarizes the results, where we observe that all combinations result in virtually the same energy consumption and reach energy savings higher than 28% under the *High Traffic* profile and 47% under the *Low Traffic* one.

Although in general, the different combinations achieve a noticeable capacity adaptation and large energy savings, two main disadvantages can be observed from this solution: *i*) it is purely reactive, so the capacity is allocated or released as a function of the current input traffic, without considering any requirement (e.g., time) to properly configure the connection, and consequently induces packet loss and added delay as a result of the time packets spent in the vlink queue; and *ii*) it does not consider the traffic evolution, so it produces unnecessary fluctuations in the configuration of the connections.

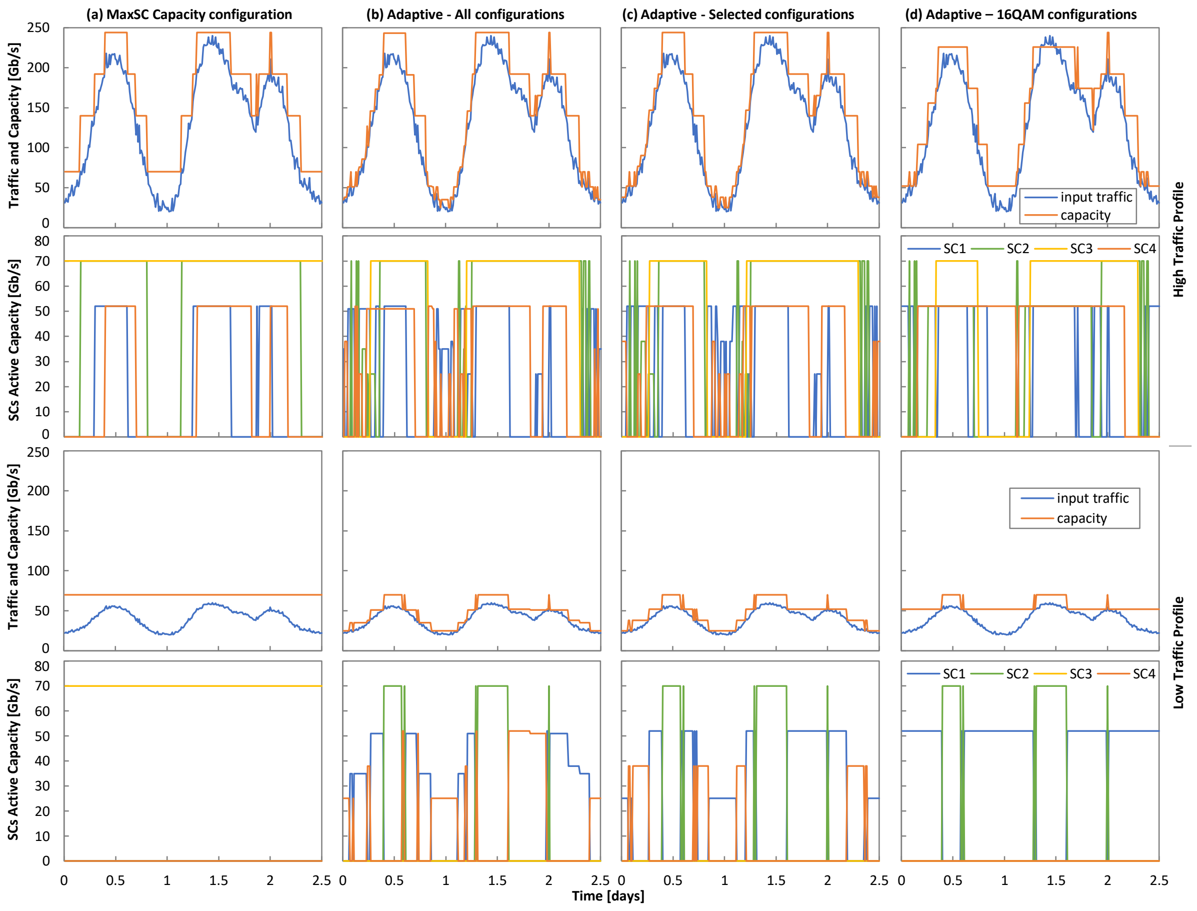

Figure 5-3 Optical connection managed by the Transponder Agent. Total and SCs capacity vs time for two traffic profiles.

Table 5-2 Summary of Results for Optical Connection Configuration Managed by the Transponder Agent

	High Traffic Profile			
	maxSC	**adapt-all**	**adapt-sel**	**adapt-16Q**
#Changes per day	8.8	51.2	51.2	23.2
Energy savings [%]	28	30	31	32
Packet Loss [MB]	**4.8**	**14.9**	**11.4**	**14.9**
Queue (max) [MB]	**16**	**16**	**16**	**16**
Queue (avg) [MB]	**0.3**	**1.4**	**1.4**	**1**

	Low Traffic Profile			
	maxSC	adapt-all	adapt-sel	adapt-16Q
#Changes per day	0	68	82.4	44
Energy savings [%]	47	51	53	51
Packet Loss [MB]	0	0	0	0
Queue (max) [MB]	0	**9**	**8**	**8**
Queue (avg) [MB]	0	**1.2**	**1**	**0.7**

5.4.3 Intent-based vlink operation

Let us now consider the architecture depicted in Figure 5-3, where the vlink intent takes the role of client to manage the capacity of the vlink and the Transponder Agent serves such capacity by properly managing the configuration of the SCs. In view of the results obtained in the last subsection, for this study we consider the two policies with only the 16QAM configuration set for the transponders.

For the predictive solution, we exhaustively explored configurations of δ and w ranging between 1 and 20 minutes. The obtained results for the configuration with best performance (6 and 10 min for δ and w, respectively) are presented in Table 5-3. We observe that no packet loss has been produced and the time in the vlink queue has been drastically reduced by using a short-term prediction of the evolution of the traffic. Such queue is produced as a result of the no perfect accuracy of the prediction, which produces some capacity exhaustion, and thus the capacity of the vlink is increased automatically by the transponder agent. Besides, we observe a slight reduction in the number of configuration changes and on the energy savings, that are now over 26% and 45% for the *High* and *Low Traffic* profiles, respectively.

Table 5-3 Summary of Results for Optical Connection Configuration Managed by vlink Intent

	High Traffic Profile		Low Traffic Profile	
	maxSC	adapt-16Q	maxSC	adapt-16Q
#Changes per day	7.2	18.8	1.6	20.8
Energy savings [%]	26	28	45	49
Packet Loss [MB]	0	0	0	0
Queue (max) [MB]	**4.5**	**10.3**	0	**5**
Queue (avg) [MB]	0	**0.2**	0	**0.1**
Cap. Exhaust. per day	1	5	0	4

5.5 Concluding Remarks

The autonomous operation of SCs has been presented in this chapter from a holistic perspective, with the objective to reduce energy consumption at the optical layer, motivated by the fact that SCs can be configured independently with the desired MF and SR. This, together with the possibility to switch off parts of the transponder directly related to each of the SC and the fact that the power consumption of a transponder is related to its actual configuration in terms of MF and SR, opened an opportunity to save energy by activating only those SCs which are needed to support the upper layer packet traffic.

The need to perform a per-SC QoT estimation was introduced, which considering the path and the specific SC configuration. Such QoT estimation can be used to define the SC configuration map that will be used afterwards for the autonomous capacity management.

The autonomous capacity management problem was faced following an incremental approach. First, the algorithms in the transponder agent were built with the objective to provide the required capacity for the lightpath and reduce energy consumption by activating SCs when their capacity is needed, while not adding detrimental effect neither for the packet traffic (packet loss and time spent in the vlink queue) nor for the packet nodes (excessive changes in the capacity of the vlink). At the Tx side, two policies for capacity management were discussed and the required algorithms designed. Specifically, the *maxSC* targeting at minimizing the changes in the SC configuration and the *adaptive* focuses on minimizing the energy consumption by adjusting the capacity of the lightpath to the input traffic as much as possible.

The capacity management implemented in the transponder agent is purely reactive, which would impact on the operation and performance of the packet layer. To solve that, an intent-based solution was proposed to manage the vlink capacity at the packet layer, where such capacity is actually used. The intent-based solution targets to ensure the packet layer performance indicators, like packet loss, time in queue, and configuration changes, while relying on the transponder agent for the SC configuration management targeting at minimizing energy consumption. A solution based on short-term prediction was developed.

Table IX summarizes the main lessons learnt in this work, which we believe that might help telecom operators and system vendors to introduce autonomous SC management in their networks and portfolios.

Table 5-4 Main Lessons Learnt

Features	**Main observations**
Set of supported SC configurations	Having a large variety of SC configurations might increase the cost of the transponders unnecessarily, as they do not show additional energy savings and their use might result in variations in the capacity of the vlink, which might add additional complexity at the packet layer.
Capacity management at the Tx side	Algorithms that try to tightly adapt the capacity of the vlink to the current or near future input traffic, did not show large energy savings. Increments in capacity of one SC configured to the maximum capacity resulted in effective alternatives, which also simplifies the algorithms. Capacity management uniquely at the optical layer, resulted in poor performance at the packet layer.

Chapter 6

Autonomous Packet Flow Capacity Management

One of the solutions that might bring cost savings to network operators is the dynamic capacity management of large packet flows, especially in the context of packet over optical networks. However, managing packet flows requires meeting strict performance (e.g., delay, packet loss, and capacity overprovisioning) and therefore, is of paramount importance to develop solutions that guarantee them. Machine Learning, particularly Reinforcement Learning, seems to be an enabler for autonomicity as a result of its inherent capacity to learn from experience. However, precisely because of that, RL methods might not be able to provide the required performance when managing the capacity of packet flows, until they learn the optimal policy. In view of that, we propose a management lifecycle with three phases: 1) a self-tuned threshold-based approach operating just after the packet flow is set up and until enough data on the traffic characteristics are available; 2) an RL operation based on models pre-trained with a generic traffic profile; and 3) an RL operation with models trained for real traffic.

Exhaustive simulation results confirm the poor performance of RL algorithms until the optimal policy is learnt and when traffic characteristics change over time, which prevents deploying such methods in operators' networks. In contrast, the proposed lifecycle outperforms benchmarking approaches, achieving noticeable performance from the beginning of operation while showing robustness against traffic changes.

6.1 Introduction

Control loops can be put into practice based on policies that specify the action to be taken under some circumstance (policy-based management), e.g., allocate the capacity of a packet flow so that the ratio traffic volume over capacity is under 80%. In packet flows, this ratio is related to the average delay that the packets in the flow will experience because of queuing, and thus to the SLA in the case that the packet flow is related to some customer connection. Although such policies can be modified, they are purely reactive. Under high traffic variations, they might entail either poor QoS (e.g., high delay or even traffic loss) and SLA breaches or poor resource utilization, which in both cases represent large costs for network operators. Note that policy-based management does not define the desired performance and thus, agents implementing those policies are unable to learn the best actions to be taken. Although many ML techniques could be potentially applied for the autonomous capacity operation of traffic flows, in this chapter, we rely on RL and consider several methods of different complexity and analyze their performance, in particular: (*i*) Q-learning; (*ii*) D3QN, and (*iii*) TD3 (see [Fu18]).

With the deployment of network slicing [Ve18.1] and the support to time-sensitive applications [Ve20], the flow capacity autonomous operation (hereafter referred to as CRUX) focuses on answering a major problem that network operators are facing nowadays: how to allocate the right capacity to every traffic flow, so as to provide the desired QoS (e.g., by preventing traffic loss and ensuring a given maximum average delay), while minimizing overprovisioning (i.e., *capacity–traffic*).

In this chapter, we apply the main lessons learnt from the previous chapter to IBN agents based on RL. We assume that a packet flow (alternatively, referred as traffic flow or simply flow) conveying traffic with unknown characteristics is established and the allocated capacity needs to be set to ensure the required QoS (from the set-up time), while minimizing resource utilization. To this end, a policy-based management is used at the set-up time to start operating the capacity of the flow; meanwhile, traffic measurements are collected to characterize the traffic. Note that policy-based operation can be highly re-liable, as it is based on specific rules that can be defined and understood by human operators. However, such an operation usually obtains poor resource utilization. Therefore, it would be useful to substitute policy-based operation by an RL model as soon as possible. To that end, pre-trained generally applicable models for the partly observed traffic characteristics are loaded and the RL algorithm starts operating. A per-flow algorithm supervises the performance of the RL algorithm and tunes model parameters to ensure the re-quired QoS. Once enough traffic measurements are available, offline training is carried out in a sandbox domain to produce a specific model well-suited for that particular traffic flow, which then substitutes the generic one. Since the traffic characteristics can change over time, analysis must be continuously performed to detect them and change the operating model when needed. By iterating that cycle, the proposed RL agent will be able to adapt to traffic changes that would otherwise degrade performance.

The rest of the chapter is organized as follows. The pros and cons of applying RL to real network operation is highlighted in Section 6.2, which include poor performance during the initial set-up and during changes in the traffic flow. The CRUX problem and the pro-posed approach are as follows: it targets operating a traffic flow and ensuring the required QoS from set-up time without previous knowledge of the traffic characteristics. The motivation behind the different phases of operation and the proposed lifecycle is presented, where pre-trained models and offline–online RL cycles aim at solving the identified is-sues. The CRUX problem is formally defined in Section 6.3. Several RL approaches can be used to solve CRUX, and each one requires different settings of states and actions. A methodological approach is provided to model the problem with different RL algorithms, and how the QoS targets are related to parameters in the reward function. Section 6.4 presents the algorithms that analyze the traffic characteristics, supervise the performance, and make decisions regarding the model and parameters to be used for operation. The discussion is supported by the results presented in Section 6.5. Finally, Section 6.6 concludes this chapter.

6.2 The Flow Capacity Autonomous Operation (CRUX) Problem

6.2.1 Flow Capacity Autonomous Operation

Let us start by analyzing the result of the autonomous capacity operation of a traffic *flow*. Similar to the transponder agent defined in Chapter 5, a *flow manager* might collect monitoring data from the network and expose some interface, so a flow intent based on RL can take an action. For illustrative purposes, Figure 6-1 shows a typical RL framework, where the learning agent is separated into two different blocks, the *learner* and the *agent*.

Let us assume that the monitoring data include the byte count since the last monitoring sample (amount of traffic) and the actual capacity allocated to the flow. The actions to be taken are related to the actual capacity allocated to the flow, which can be increased or decreased as needed with some *granularity* to meet the required QoS. For instance, a customer connection can manage the capacity of the flow with granularity 1 Gb/s by configuring some packet node, whereas in a virtual link supported by the optical layer, the capacity can be increased/decreased by establishing or tearing down parallel lightpaths, each with a capacity of 100 s Gb/s. It seems clear that the time to change the capacity is also different, ranging from seconds to minutes. The RL algorithm should then decide the capacity to be allocated to the flow to absorb *variation* in the traffic from one monitoring sample to the next, plus the time to increase the allocated capacity, with the objective to avoid any traffic loss and ensure some additional QoS metric. Then, the *traffic variation* becomes a major feature for a flow, together with the *traffic pattern*, i.e., the evolution of the mean traffic with time.

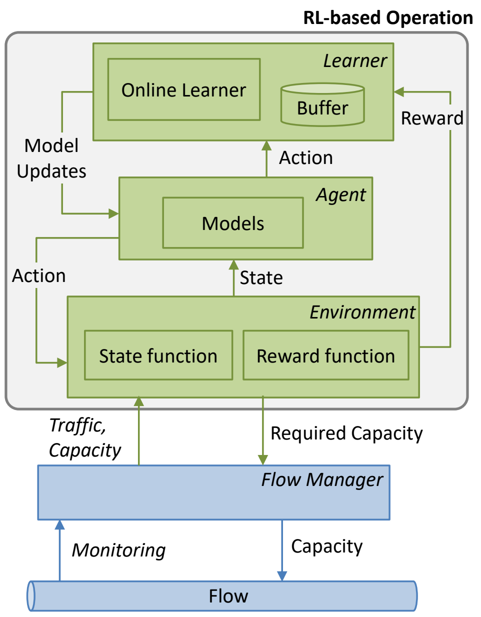

Figure 6-1 Flow capacity autonomous operation. RL framework with learner, agent, and environment.

This approach can provide excellent performance once the policies that avoid traffic losses meet the desired QoS, and minimize overprovisioning are learned; however, online learning of such policies requires time. In addition, there are several issues that can impact the aforementioned online learning performance, e.g., (1) changes in traffic variability might produce loss before new policies are learned; (2) smooth model fine tuning could not be enough to mitigate persistent errors in taking some specific actions; and (3) online learning tends to forget valuable learning in the long run, thus reducing the model's accuracy [SuBa18].

Figure 6-2a represents a possible evolution of the traffic variation (the traffic pattern is omitted here for simplicity) and the obtained performance—overprovisioning, traffic loss, and some other QoS metric. The path supporting the flow is established at time t_0 and the desired QoS is specified, so the RL algorithm needs time to learn the traffic variation (and the traffic pattern); meanwhile (until *ta* in Figure 6-2a), poor performance, including traffic loss, can be expected. Once a good model is obtained, it is expected that an RL algorithm can provide the target performance. However, a steep change in the variation of the traffic (times t_1 to t_2) can impact the performance until the new variation is learned. Nonetheless, it might happen that the performance does not converge to the desire level even after learning the new traffic variation.

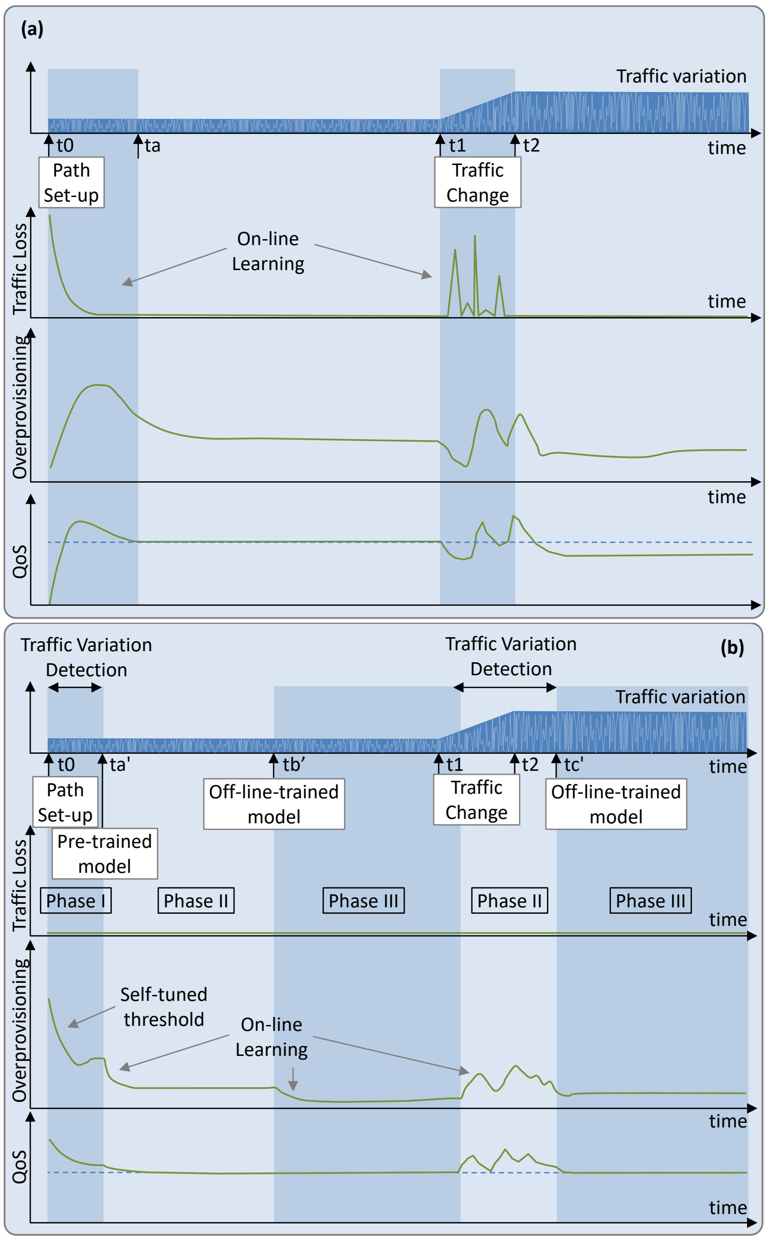

Figure 6-2 Operation lifecycle. (a) Online learning RL operation. (b) Offline training with online fine tuning RL operation.

It seems clear that the above behavior is unacceptable for network operators, as it would provide poor performance and might incur penalties due to SLA breaches. Specifically, it seems of paramount importance to start the operation with already trained models. To that end, an initial model can be trained offline using a network simulator in a sandbox domain. Once in operation, the model will be improved by the online learner. However, there are traffic characteristics, e.g., traffic pattern, that are observed after a long period of time, e.g., several days. Therefore, some alternatives are needed to operate the flow during that initial time.

Our solutions go beyond training offline and propose implementing offline–online learning cycles to deal with large changes in traffic flow, i.e., to provide guaranteed performance during the whole lifetime of the traffic flow (Figure 6-2b). Specifically, (*i*) a policy-based management implemented as a self-tuned *threshold-based* algorithm is in charge of managing the flow capacity during the time immediately after the path is set up (*Phase I*: time interval [t_0, *ta'*], where *ta'*-t_0 should be short, e.g., 1 h). That algorithm tunes a threshold for the flow capacity and accurately determines the traffic variation. This approach enables dynamic flow capacity allocation by fixing the right values for the threshold that minimize overprovisioning. However, avoiding traffic loss and guaranteeing that the required QoS is met is not a straightforward task, as it depends on the variance in the traffic flow—defined as the difference between maximum and minimum amount of traffic during some period. Therefore, during this period, the threshold is set conservatively to avoid *underprovisioning* (i.e., traffic exceeds capacity, and some traffic is loss) at the expense of large overprovisioning. (*ii*) Once the variation of the traffic has been determined, a pre-trained *generic model* can be used for flow operation (*Phase II*: time interval [*ta'*, *tb'*]). The model is general as it has been pre-trained assuming a given traffic pattern, e.g., sinusoidal with daily periodicity, but supporting the measured traffic variation. Once in operation, the pre-trained model starts to fine tune with the observed samples. (*iii*) Once enough measurements are available to determine the characteristics of the flow, including the traffic pattern, a specific model can be trained in a sandbox domain by using a simulator set to operate at time *tb'* (*Phase III*). That model should improve the performance or be easier to operate than the pre-trained one. (*iv*) Assuming that the traffic pattern does not change, any change in the traffic variation that cannot be absorbed by the current model can trigger returning to Phase II for more intensive parameter tuning for the new traffic variation, while a new specific model is trained and is set to operate at time *tc'* (Phase II-Phase III cycle).

6.2.2 Proposed Architecture

This work extends the basic RL-based flow capacity operation (Figure 6-1) and proposes a scheme based on (Figure 6-3): (*i*) analyzing the traffic to obtain meaningful traffic characteristics; (*ii*) making decisions regarding the allocated capacity when no model is in operation (Phase I); (*iii*) selecting pre-trained models that fit with the observed traffic characteristics; (*iv*) training new models in a sandbox domain (*offline learning*), where real traffic measurements are used to generate traffic in a simulation environment and the QoS can be realistically estimated; a replica of the RL algorithm in operation is used here for training new models; and (*v*) once accurate models are obtained, they are used for flow operation and will be progressively fine-tuned online. As in Figure 6-1, a *Flow Manager* collects monitoring data from the forwarding plane and enforces flow capacity.

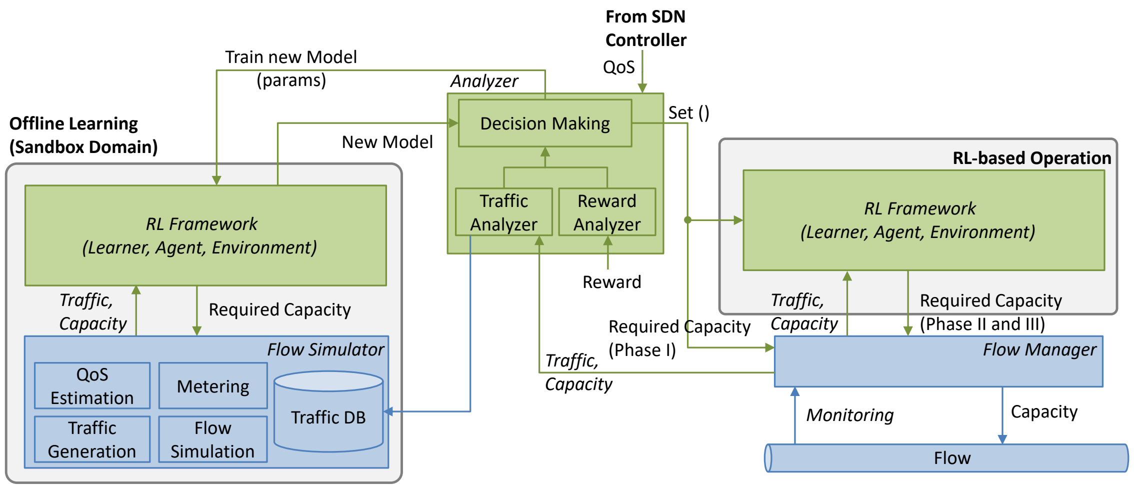

Figure 6-3 Extended architecture for flow capacity autonomous operation with offline learning.

The models include some parameters that need to be tuned as a function of the traffic, to provide the desired performance while meeting the required QoS. Such parameter tuning can be carried out during offline learning, as well as during online operation to deal with small traffic changes. Based on the analysis of the traffic and the reward, the Analyzer block decides when to tune parameters and when to update the model with an offline learned one (labeled *Set*() in Figure 6-3) to meet the given QoS. Note that both parameter tuning and the offline–online cycle can be completed several times during the operation to improve the learned models, which will also enable adaptability to changes.

The next section details the RL approaches used to solve the autonomous flow capacity management problem, CRUX.

6.3 CRUX Problem Definition and RL Methodology

This section formally defines the CRUX problem, and introduces the main parameters and variables used hereafter. Next, it introduces the methodology to solve the problem using RL, and finally defines the different RL approaches under study. The used notation is summarized in Table 6-1, where parameters and variables are defined.

Table 6-1: Notation

Capacity and QoS Params for the Flow	
z_{max}	Maximum capacity (Gb/s)
d_{max}	Target maximum delay (s)

l^*	Optimal load (unleashing d_{max}) ∊ [0, 100]%
qa	QoS Assurance (%)
	Traffic and Capacity
$x_{max}(t)$	Maximum traffic at time t (Gb/s)
$x_{var}(t)$	Traffic variation at time t (Gb/s)
$z(t)$	Capacity allocated at time t (Gb/s)
$o(t)$	Capacity slack/surplus at time t (Gb/s)
$y(t)$	Overprovisioning margin (Gb/s)
ρ	Traffic variance multiplier
b	Granularity of capacity allocation (Gb/s)
$w(t)$	Traffic loss margin (Gb/s)
	Autonomous Capacity Allocation
$a(t)$	Action time t (b/s)
n_a	Number of discrete actions
$s(t)$	State at time t
n_s	Number of discrete states
$r(t)$	Reward at time t
k	Threshold-based scaling factor
β_i	Reward function coefficients (≥0)

6.3.1 Problem Definition and Basic Modeling

Let us consider that the autonomous flow capacity management problem is solved periodically, when a new set of measurements, statistics, and parameters for the traffic flow x are collected and computed. Along this section and the following, we adopt the *informational representation* of time, where t represents a point in time that refers to the time interval [t - 1, t) [Po11]. Specifically, $x(t)$ represents the traffic measurements collected in [t - 1, t), and statistics, such as the maximum ($x_{max}(t)$) and variation ($x_{var}(t)$), summarize traffic dynamicity during that time interval. Additionally, decisions made at time t, e.g., the capacity to be allocated ($z(t)$), consider data that arrived up to time t.

The main objective of the CRUX problem is to find the optimal (minimum) capacity $z(t)$ at time t that satisfies a desired QoS. In this work, we assume that that the QoS is defined by a desirable maximum end-to-end delay d_{max}; this also entails that packet loss is not tolerated during flow operation.

Without loss of generality, we assume that the delay can be modeled as a function of the traffic volume, the allocated capacity for the flow, the *load* (ratio traffic/capacity), and other components such as the transmission delay (*load–delay* models). Such load–delay models can be obtained during the commissioning testing phase using, e.g., active monitoring techniques [Ru20.1]. Once the model is available, a target load l^* unleashing the target maximum delay d_{max} can be selected. Figure 6-4 illustrates an example of a load–delay model, where d_{max} has been selected to a value where queueing delay becomes the predominant delay component, e.g., for $l^* = 80\%$.

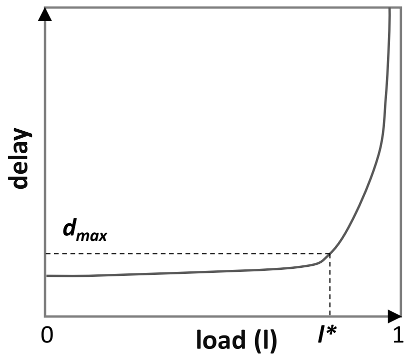

Figure 6-4 Delay model example.

A policy (threshold)-based approach can be used to make decisions from the currently available monitoring data, as defined in Eq. (6-1), where k is a constant factor that is related to the traffic dynamicity and variability; k needs to be tuned to guarantee the required QoS. However, finding the proper value of k is not a straightforward task: if the value of k is high, QoS is ensured at the cost of high overprovisioning, whereas if the value of k is low, QoS requirements might be not met. In addition, decisions are reactive, so altogether, *sub-optimal solutions* are usually obtained.

$$z(t) = k \cdot x_{max}(t)/l^* \tag{6-1}$$

The optimal capacity allocation to the CRUX problem requires knowledge of the expected traffic to allocate the capacity of the flow at time t - 1 to the value that fits the expected maximum load for the period [t - 1, t) (proactive decision making):

$$z^*(t-1) = x_{max}(t)/l^* \tag{6-2}$$

In the case that the capacity allocation is not optimal, some capacity slack/surplus (o) will exist, which can be formally computed at time (t) as follows:

$$o(t) = z(t-1) - x_{max}(t)/l^* \tag{6-3}$$

Figure 6-5 sketches an example of a traffic flow $x(t)$ for which some capacity allocation $z(t)$ is required. In the figure, the optimal capacity $z^*(t)$ that should be allocated at time t_{i-1} is shown. The different colors provide a visual representation of the values of $o(t)$. In particular, two different sub-optimal capacity allocations can be distinguished (see labels in Figure 6-6a): (*i*) if $z(t) > z^*(t)$ (i.e., $o(t) > 0$), QoS requirements are met at the expense of an excess of overprovisioning; (*ii*) if $z(t) < z^*(t)$ (i.e., $o(t) < 0$), QoS requirements are violated.

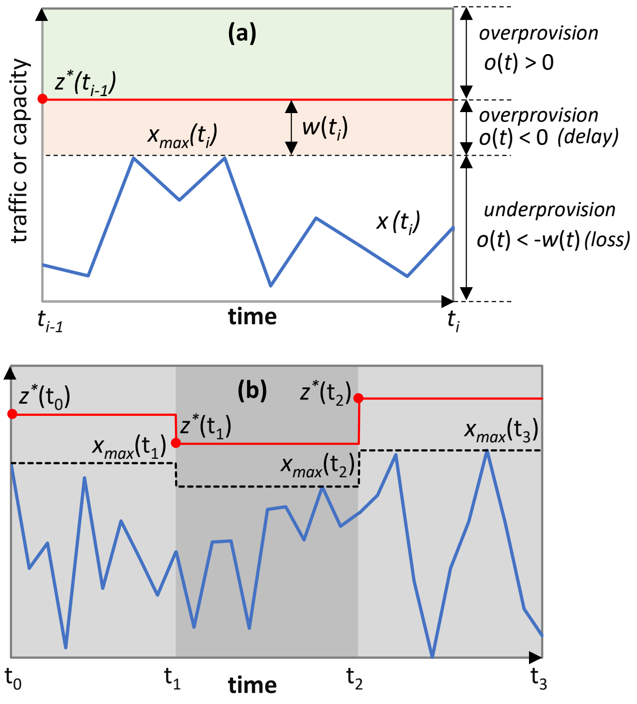

Figure 6-5 Capacity allocation definition (a) and evolution (b).

The width $w(t)$ of the high delay area is formally defined as a function of the maximum traffic in Eq. (6-4). Therefore, traffic loss appears if $o(t) \leq -w(t)$.

$$w(t) = x_{max}(t) * \frac{1 - l^*}{l^*} \tag{6-4}$$

It is worth noting that the quality of a solution taken at time t - 1 can only be evaluated at time t, which motivates the use of RL to learn the optimal policy that allocates the minimum value of $z(t)$ to meet the QoS requirements. The details of the RL-based methodology are presented in next subsections.

6.3.2 Generic RL-Based Methodology

Figure 6-6 illustrates the RL workflow, where the main three elements involved are represented, namely: (*i*) the learner in charge of learning the optimal policy; (*ii*) the agent in charge of taking actions to adjust the capacity allocated to the flow; (*iii*) the environment adaptation module in charge of implementing and evaluating the actions taken; and (*iv*) the flow manager, which enforces the capacity and collects traffic measurements. Three time periods are specified, from t_0 to t_2; let us assume that some initial policy model has been set in the agent before operation starts at time t_0, when the agent applies the first action $a(t_0)$.

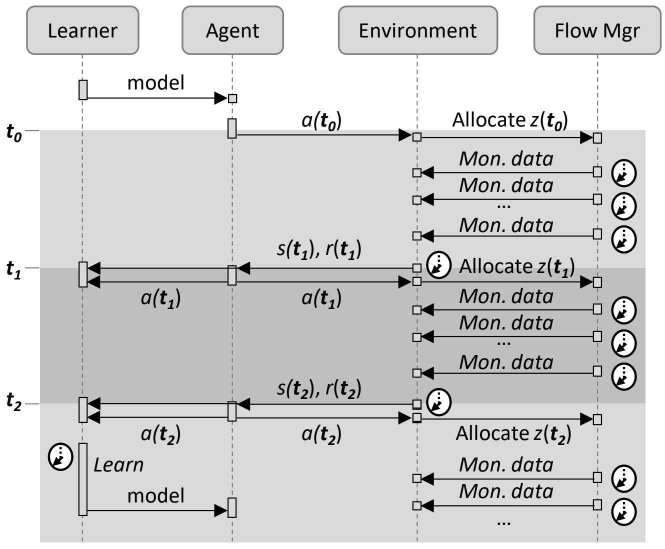

Figure 6-6 General RL workflow.

For the sake of simplification and to reduce complexity, action $a(t)$ is defined in Eq. (6-5) as the differential capacity with regard to the current one. Actions are processed by the environment, which computes the new capacity $z(t)$ to be allocated.

$$a(t) = z(t) - z(t-1) \tag{6-5}$$

The flow manager periodically sends traffic monitoring data to the environment, which processes them at the end of every time interval to compute state $s(t_i)$ and reward $r(t_i)$. Upon receiving the state, the agent finds the action $a(t_i)$ to be taken with the current policy. In addition, the learning process uses state, reward, and action to improve the model, which is updated in the next time interval. The state function $s(t)$ is defined in terms of $o(t)$ normalized by a parameter $y(t)$ (Eq. (6-6)), which is conveniently set up using parameter ρ to absorb the traffic variation observed in the flow (Eq. (6-7)).

$$s(t) = o(t)/y(t) \tag{6-6}$$

$$y(t) = \rho \cdot x_{var}(t) \tag{6-7}$$

As for the reward $r(t)$, the objective is to minimize overprovisioning, without providing high delay. To ensure that, the higher delay must be obtained by producing some overprovisioning. To that end, we have defined a piece-wise function with four different regions in the range of $o(t)$, representing the sub-optimal cases. Such division allows for individual modes of operation that correspond to an adequate reward in each case. The reward function $r(t)$ is formally expressed in Eq. (6-8) and illustrated in Figure 6-7. The first and second components of $r(t)$ penalize traffic loss and high delay, respectively. Both components are linear functions of $o(t)$, where coefficients β_1 and β_2 can be tuned to penalize traffic loss and high delay. The third component gives the maximum reward, which is slightly shifted to the positive values of *o*(*t*) to reduce the risk of QoS violation. This segment is concave quadratic with regard to the relation *o*(*t*)/*y*(*t*), with the maximum value weighted by coefficient β_3. Finally, overprovisioning above *y*(*t*) is linearly penalized by coefficient β_4.

$$r(t) = \begin{cases} \beta_1 \cdot \big(o(t) - w(t)\big) + \beta_2 \cdot w(t), & o(t) < -w(t) \\ \beta_2 \cdot o(t), & -w(t) \le o(t) < 0 \\ \beta_3 \cdot \left(1 - \frac{o(t)}{y(t)}\right) \cdot \frac{o(t)}{y(t)}, & 0 \le o(t) < y(t) \\ -\beta_4 \cdot (o(t) - y(t)), & o(t) \ge y(t) \end{cases} \tag{6-8}$$

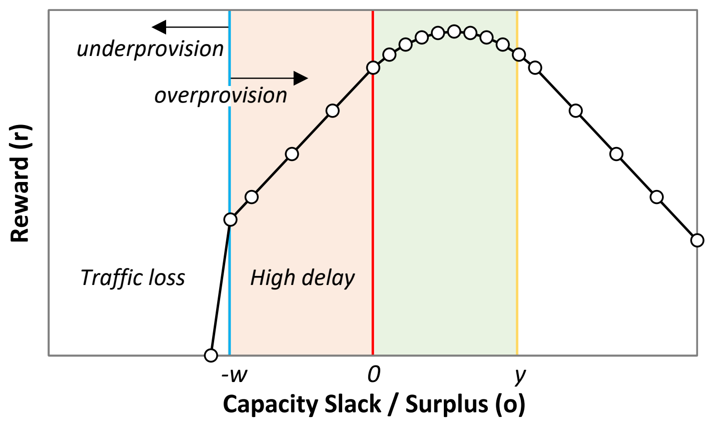

Figure 6-7 Reward function vs. capacity slack/surplus.

6.3.3 Specific Adaption of RL Approaches

As introduced in Section 6.2.1, three RL methods are considered to solve the CRUX problem, namely: (*i*) Q-learning, (*ii*) D3QN, and (*iii*) TD3.

For each method, the main adaptation of the generic problem definition is to discretize state and action spaces. Q-learning requires discretizing the continuous state function *s*(*t*) in Eq. (6-6) into a number of discrete states (n_s). Such discrete state function *s'*(*t*) can be formally expressed as Eq. (6-9). Discrete states 0 and n_s - 1 indicate underprovisioning and overprovisioning above margin *y*(*t*), respectively, whereas the rest states n_s - 2 are used to evenly discretize the overprovisioning below margin *y*(*t*).

$$s'(t) = \begin{cases} 0, & s(t) < 0 \\ \lceil (n_s - 2) \cdot s(t) \rceil, & s(t) \in [0,1] \\ n_s - 1, & s(t) > 1 \end{cases} \tag{6-9}$$

In addition, Q-learning and all DQN variants require a discrete space of n_a actions. Let us define *a'*(*t*) as the set of discrete actions, where a discrete action is defined by an integer number of units of capacity *b* to update (add or subtract) the current capacity. The discrete set of actions that depend on both $n_a \in 2 * \mathbb{N} - 1$ (natural odd number) and *b* can be formally defined as:

$$a'(t) \in \left\{ b \cdot i, i \in \left[-\frac{n_a - 1}{2}, \frac{n_a - 1}{2} \right] \right\} \tag{6-10}$$

Table 6-2 summarizes the main characteristics and parameters to be configured for each method.

Table 6-2: Summary of RL approaches

Approach	**State Space**	**Action Space**	**Parameters**
Q-learning	Discrete Equation (6-9)	Discrete Equation (6-10)	n_s, n_a, b
D3QN	Continuous Equation (6-6)	Discrete Equation (6-10)	n_a, b, DNN config, Replay buffer
TD3	Continuous Equation (6-6)	Continuous Equation (6-10)	Actor/critic DNN config Replay buffer

6.4 Cycles for Robust RL

This section is devoted to the details of the operation lifecycle presented in Figure 6-2b. Let us assume that when a new path for a flow is set up, an instance of every element in the architecture in Figure 6-3 is instantiated. The characteristics of the instances depend on the flow requirements, e.g., pre-trained generic models loaded in the *Offline Learning* block are those that were trained with similar QoS requirements (d_{max} and q_a) to those of the current flow. When the operation starts, no *online RL* models exist and the maximum capacity for the flow z_{max} is allocated. All the algorithms presented next run in the *Analyze*r block (see Figure 6-3), which makes decisions and orchestrates the rest of the blocks based on some analysis results.

Algorithm 6-1: Analyzer Initialization

```
INPUT: offlineLearn, onlineRL, flowMgr
OUTPUT: -
1: store(offlineLearn, onlineRL, flowMgr)
2: initialize DB
3: params ← [<l*, z_max, k, eps>,          // Phase I
           <qa, cfl, Δρ>,                 // Phase II
           <var_l, var_h, r_l, m>]        // Phase III
4: phase ← PhaseI
```

Algorithm 6-1 shows the Analyzer initialization that receives the pointers to external modules that interact with the *Analyzer*, i.e., *offline learner, online RL*, and *flow* *manager*, and stores them (line 1 in Algorithm 6-1), and initializes the main variables used by the rest of the procedures. In particular, *DB* contains the needed traffic-related data for the analysis carried out at every phase (line 2), *params* is a vector with the parameters that characterize flow's requirements and some configuration and that are used during the different phases (line 3), and *phase* records the current phase, which is initialized to Phase I (line 4).

Before describing the algorithms for the different phases, let us present a specific procedure for traffic variance analysis. Algorithm 6-2 is applied to the set of observed traffic-related measurements, stored in *DB*, with the objective of characterizing and quantifying the fluctuation of the traffic around its observed average. After retrieving data time series contained in *DB*, the average pattern on the given traffic time series X is computed (lines 1–2 in Algorithm 6-2). Note that the result of this operation produces time series X_{avg}, with the smoothed average that better fits X. Without loss of generality, we assume that a combination of regression techniques including polynomial fitting, spline cubic regression, and sum-of-sin regression is applied, returning the best result in terms of accuracy and model complexity [Ma21]. The relative residuals are computed (line 3) and the difference between maximum and minimum of these residuals (*var*) is considered as the traffic *variance* measurement (line 4). This value together with the previous *var* measurements stored in *DB* (time series Y) are used to compute the derivative *drv* of *var* in time, i.e., the first-order difference [Br16] (lines 5). The last value in *drv* denotes the current derivative, which is later used for the identification of the traffic variance (line 6). In addition, a variance *score* is computed as the maximum absolute derivative value normalized by the observed variance (line 7). The score approaches 1 if the traffic fluctuates around its maximum range between two consecutive time measurements. This score will be used later for generic model tuning purposes. The computed variance results are eventually returned (line 8).

Algorithm 6-2: varianceAnalysis()

```
INPUT: DB
OUTPUT: V
 1: $<X, Y> \leftarrow <DB.\text{traffic}, DB.\text{var}>$
 2: $X_{avg} \leftarrow \text{computeAveragePattern}(X)$
 3: $X_{res} \leftarrow (X — X_{avg}) \odot X^{-1}$
 4: $var \leftarrow \max(X_{res}) — \min(X_{res})$
 5: $Y.\text{append}(var)$
 6: $drv \leftarrow \text{computeDerivative}(Y)$
 7: $score \leftarrow \max(|drv|)/var$
 8: return $<\text{var} = var, \text{curdrv} = drv[-1], \text{score} = score>$
```

Algorithm 6-3 specifies the main procedure running in the Analyzer block and it is called periodically every time *t*. First, new traffic monitoring data are gathered from the flow manager (line 1 in Algorithm 6-3). Then, the specific procedure for each phase is called with the current time and the collected data, and the phase changes only when the called procedure returns *True* (lines 2-10); *DB* is initialized every time phase changes (line 11).

Algorithm 6-3: Main Analyzer Procedure

```
INPUT: $t$
OUTPUT: -
 1: $x(t)$ ← flowMgr.getMonitoringData($t$)
 2: if phase = PhaseI then
 3:     changePhase ← thresholdBased($t$, $x(t)$)
 4:     if changePhase then phase ← PhaseII
 5: else if phase = PhaseII then
 6:     changePhase ← modelSelectionAndTuning($t$, $x(t)$)
 7:     if changePhase then phase ← PhaseIII
 8: else // phase = PhaseIII
 9:     changePhase ← specificModel($t$, $x(t)$)
10:     if changePhase then phase ← PhaseII
11: if changePhase then initialize DB
```

Algorithm 6-4 defines the operation of the *Analyzer* block during Phase I. Recall that during this phase, flow capacity allocation is managed following a threshold-based procedure, defined by Eq. (6-1). First of all, *DB* is updated with the new monitoring data and the variance analysis described in Algorithm 6-2 is executed, storing the result in variable V (lines 1–2 in Algorithm 6-4). Then, the absolute value of the current derivative is compared with a small epsilon value (param *eps*) to decide whether enough traffic data have been already analyzed to estimate variance with high accuracy (line 3). If so, a generic pre-trained model f_0 for the computed variance is retrieved from the *offline learner* and factor ρ_0 is scaled with the ratio of scores between the generic model and the observed traffic (lines 4–5); the scaled factor increases (decreases) if the computed score is higher (lower) than the score of the generic model. The rationale behind such factor correction is to achieve a more robust and conservative operation of the generic model under the actual traffic variance behavior. Then, the *online RL* module is updated with new model f_0 and scaled factor ρ_1 and Phase I ends (lines 6–7).

In case the current derivative is still high, the threshold-based capacity allocation procedure continues. Here, factor k in Eq. (6-1) is adapted from its input value as soon as more traffic data are available and traffic variance is better estimated. With the estimated variance and target load l^*, factor $k(t)$ is computed. Then, k is updated in two different ways: (*i*) reducing by half between k and $k(t)$ if k is larger than needed; or (*ii*) replaced by $k(t)$ if is k is lower than needed (lines 8–10). The flow manager is requested to modify the flow capacity to the computed $z(t)$, which is bounded by the maximum capacity z_{max} (line 11) and Phase I continues (line 12).

Algorithm 6-4: thresholdBased() (Phase I)

```
INPUT: $t$, $x(t)$
OUTPUT: changePhase
 1: DB.traffic.append($x(t)$)
 2: $V$ ←varianceAnalysis(DB)
 3: if | V.curdrv | < eps then
 4:       <$f_0$, $\rho_0$, $sc_0$>← offlineLearn.getGenericModel(V.var)
 5:       $\rho_1$←$\rho_0$·($sc_0$ / V.score)
 6:       onlineRL.setModel($f_0$, $\rho_1$)
 7:       return True
 8: DB.var.append(V.var)
 9: $k(t)$←max(1, V.var / (1-$l^*$))
10: if $k(t)>k$ then $k$←$k(t)$ else $k$←$k$ - ($k$(t)-$k$)/2
11: flowMgr.setupCapacity(max($k$ · max($x$)/$l^*$, $z_{max}$))
12: return False
```

Algorithm 6-5: ModelSelectionAndTuning() (Phase II)

```
INPUT: $t$, $x(t)$
OUTPUT: changePhase
 1: offlrn.updateTrafficDB($x(t)$)
 2: if offlineLearn.newModelAvailable() then
 3:    <$f$, $\rho$>← offlineLearn.getModel()
 4:    onlineRL.setModel($f$, $\rho$)
 5:    return True
 6: $x_{max}(t)$=max($x$)
 7: $z(t$-1)← flowMgr.getCurrentCapacity($t$)
 8: $o(t)$←computeSlackSurplus($x_{max}(t)$, $z(t$-1)) // Eq. (6-3)
 9: if $o(t)<0$ then DB.QA.append(0)
10: else DB.QA.append(1)
11: $p_{obs}$←avg(DB.QA)
12: pval_l←BinomialTest1("$p_{obs}<qa$")
13: pval_g←BinomialTest2("$p_{obs}>qa$")
14: if min(pval_g, pval_l)>cfl then
15:    DB.QA←∅
16:    if pval_l<cfl then onlineRL.tuneParam('$\rho$', $\Delta\rho$)
17:    else onlineRL.tuneParam('$\rho$', -$\Delta\rho$)
18: return False
```

Algorithm 6-5 details the procedure during Phase II. Traffic data collected from the *flow manager* are sent to the *offline learner* block for updating a historical traffic database used to train RL models offline in the sandbox (line 1 in Algorithm 6-5). The offline model training procedure runs in parallel in the sandbox domain. When enough traffic measurements are collected and processed and an accurate and robust offline-trained RL model is available, it is sent to the *online RL* block to be used for flow capacity operation; this ends Phase II (lines 2–5). Otherwise, Phase II continues, aiming to identify whether the RL model currently in operation needs some parameter tuning (in addition to model updates that the RL algorithm performs during operation). In particular, this procedure aims to supervise the degree of QoS assurance (as compared with the target value, *qa*) obtained by the current model and modifying factor ρ when needed to achieve the target performance. Note that low overprovisioning is the secondary objective and therefore, QoS assurance analysis requires computing whether the current capacity violated maximum delay ($o(t) < 0$) or not ($o(t) \geq 0$). The result is stored in *DB* (lines 6–10). Next, two different one-sample proportion binomial hypothesis tests [Ca02] are conducted to detect whether the observed degree of QoS assurance is significantly below (test 1) or above (test 2) the target value *qa* (lines 11–13). In the case that some of the hypotheses can be confirmed (on the contrary, it is assumed that QoS assurance is in the target), ρ needs to be tuned. If hypothesis test 1 is confirmed, some extra capacity allocation is needed, which is achieved by increasing ρ with a given step size $\Delta\rho$. On the contrary, if hypothesis test 2 is confirmed, allocated capacity can be reduced, so ρ is decreased by the same step size.

Algorithm 6-6: specificModel() (Phase III)

```
INPUT: $t$, $x(t)$
OUTPUT: changePhase
1:  $rw(t) \leftarrow$ onlineRL.getReward($t$)
2:  DB.traffic.append($x(t)$)
3:  DB.reward.append($r(t)$)
4:  if |DB.traffic| > $m$ then DB.traffic.pop(0)
5:  if |DB.reward| > $m$ then DB.reward.pop(0)
6:  $V \leftarrow$ varianceAnalysis(DB)
7:  return V.var NOT IN [var_l, var_h] OR $rw(t) <$ rw_l
```

Finally, Algorithm 6-6 describes the procedure running in the Analyzer during Phase III. This algorithm analyzes the last m traffic measurements and the reward obtained by the *online RL* (lines 1–6 in Algorithm 6-6). The objective of this analysis is to check whether both the current traffic and reward follow the expected behavior (line 7). Let us assume that an extended estimation of the working variance with range [*var_l*, *var_h*] is found during the offline training phase—with a minimum and maximum variance that the RL model can support without losing either robustness or desired performance. Bear in mind that operating a traffic flow with more variance than what is supported by the model can lead to poor QoS assurance and even traffic loss. On the contrary, a traffic flow with less variance can produce large overprovisioning, which the *online RL* can hardly decrease with its fine adaption configuration. In fact, *online RL* continuously adapts the model to smooth traffic changes with controlled reward fluctuations, so that a minimum reward (*rw_l*) can be considered as the reasonable limit of a normal RL operation. Therefore, Phase II is triggered back when traffic variance leaves the working range of the RL model or the observed reward goes below that limit; otherwise, Phase III continues.

6.5 Illustrative Results

For the ongoing evaluation, a Python-based simulator reproducing the modules described in Figure 6-3 was implemented. Realistic traffic flow behavior was accurately emulated using a simulator based on CURSA-SQ [Ru18]. CURSA-SQ combines statistically based traffic flow generation and continuous G/G/1/k queue model based on the logistic function; multiple queuing systems can be numerically analyzed and related statistics, such as traffic magnitude, queuing delay, and packet loss, be computed. CURSA-SQ was validated with the experimental measurements in [Ru20.1] and was used to successfully reproduce realistic packet scenarios [Ve20.2], [Be20]. In the context of this work, CURSA-SQ is used as: (*i*) a lightweight network simulator to emulate a flow manager and the forwarding plane; and (*ii*) a flow simulator running in the ML sandbox domain for offline RL training purposes. It is worth highlighting that both CURSA-SQ instances have been independently configured and managed in order to reproduce the actual separation between the physical network and the sandbox domain.

Traffic was randomly generated according to different *traffic configurations*. Each traffic configuration is the combination of traffic pattern and variance. Two different daily patterns were considered: a simple *sinusoidal* pattern for offline training purposes, and a *realistic* pattern to emulate the real traffic in the forwarding plane. In both cases, traffic fluctuates between 5 Gb/s (valley) and 40 Gb/s (peak) throughout the day. Regarding variance, it is defined as a percentage of the mean, so the magnitude of traffic oscillations changes in time (heteroscedasticity). For the sake of a wider analysis, we considered five different variance values: 1%, 3%, 6%, 12%, and 25%.

RL algorithms running in the RL-based operation and offline learning modules have been implemented in Python3 using libraries such as *pytorch*. A general epsilon decay strategy was implemented in all the RL methods for balancing between exploration and exploitation [SuBa18], with decay factor equal to 0.00125. Moreover, a discount factor equal to 0.95 was set up. Q-learning was configured with $n_s = 14$ states and $n_a = 3$ actions, as well as capacity allocation granularity $b = 1$ Gb/s. In the case of D3QN and TD3, every DNN consisted of two hidden layers with 100 neurons each implementing the Rectified Linear Unit activation function. All DNNs were trained by means of the Adam replacement optimizer with learning rate equal to 0.001 and maximum replay buffer equal to 1e6 samples.

Finally, the capacity and QoS parameters for the flow under study are maximum capacity $z_{max} = 100$ Gb/s, optimal load $l^* = 80\%$, and QoS assurance $qa = 99\%$.

In the next two subsections, we first focus on comparing the different RL methods for the scenario where the pure online learning RL-based operation is performed (see Figure 6-2a). Next, we evaluate the offline leaning + online RL-based operation (Figure 6-2b), including the three proposed phases.

6.5.1 Online RL-Based Operation

Let us first analyze the reliability of the RL operation under real traffic; we focus specifically on the traffic loss. For this study, low (1%) and high (25%) variances were considered. Figure 6-8 plots the traffic loss as a function of time from the path set-up time. We observe extremely poor performance (high loss) at the beginning of operation, as it was anticipated in Figure 6-2a. Interestingly, we observe that the simplest Q-learning method provides the fastest convergence time to achieve zero loss, although it needs more than one day to achieve zero loss operation when traffic variance is high. Note that D3QN is the most sensitive to traffic configuration (zero loss operation time increases three times from low to high variance). TD3 is the method with the slowest convergence (around 4 days).

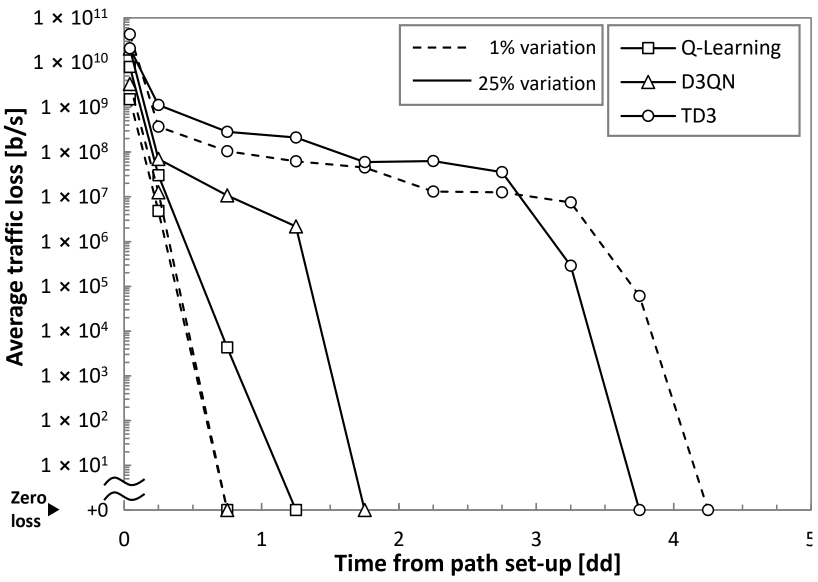

Figure 6-8. Achieving zero loss operation

As all the RL methods have achieved zero loss operation, the rest of the results analyze the performance after 5 days of operation. As an illustrative example of the RL-based operation, Figure 6-9 shows one day of real traffic x(t) and variance from low to high, as well as the capacity *z*(*t*) allocated using Q-learning; optimal *ρ* for each variance is configured. The optimal capacity allocation (*o*(*t*) = 0) and the margin for overprovisioning *y*(*t*) are also plotted. We observe that the allocated capacity is close to the optimal one, absorbing fluctuations with enough margin to meet the target QoS.

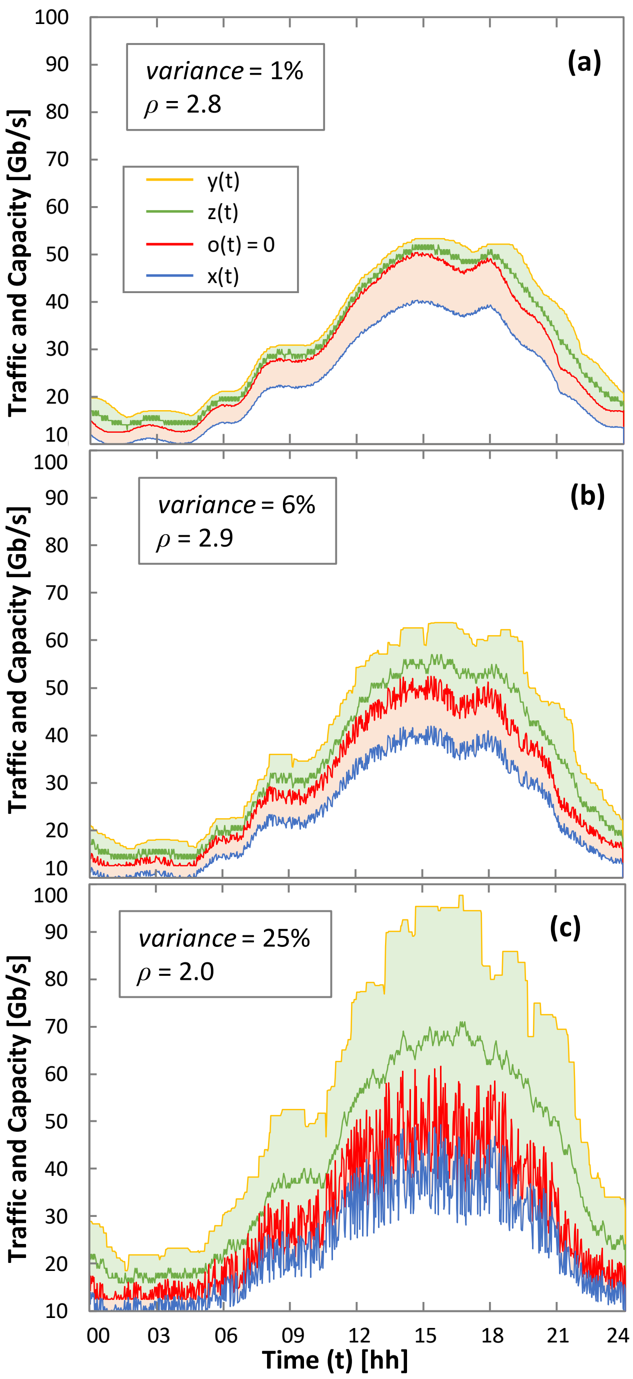

Figure 6-9. Q-Learning operation. Traffic and allocated capacity for low (a), moderated (b), and high (c) traffic variance.

Let us now analyze the impact of the margin multiplier ρ to achieve the desired QoS. Figure 6-10 shows the obtained QoS assurance as a function of ρ. For the sake of a comprehensive study, all traffic configurations for sinusoidal (Figure 6-10a-c) and real (Figure 6-10d-f) traffic patterns have been analyzed. The minimum ρ value has been set to 1. The ρ values for which the target QoS of 99% is achieved are highlighted with a round marker. We observe in the results that ρ depends not only on the traffic characteristics, but also on the RL method.

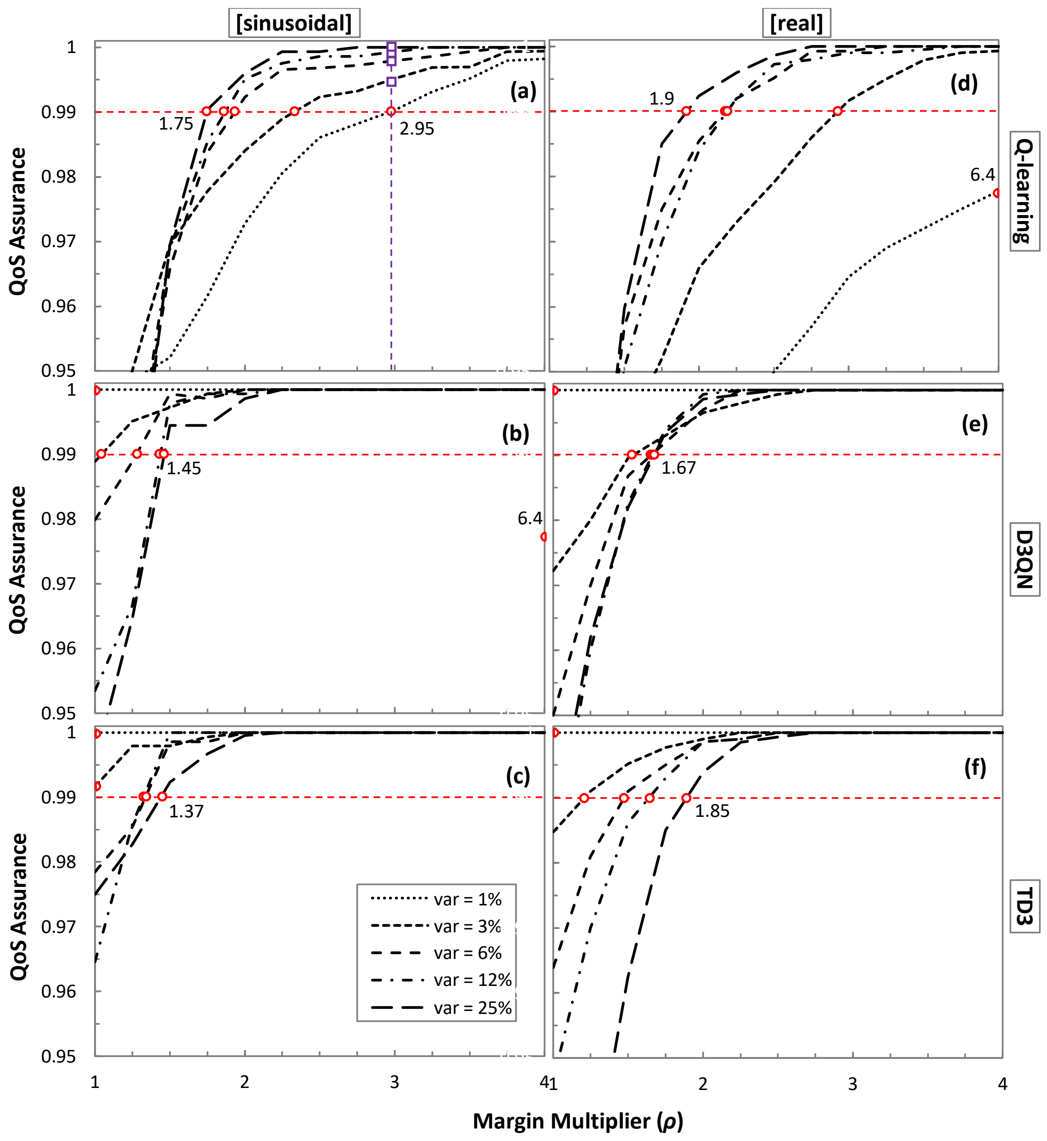

Figure 6-10 QoS as a function of ρ models trained with a sinusoidal traffic pattern (a–c) and real traffic (d–f).

Interestingly, Q-learning needs the widest range of values for all traffic configurations, requiring a smaller ρ as soon as variation increases. It is worth noting that the large range of values ([1.9, 6.4]) makes it more difficult to adjust ρ for different traffic configurations. Conversely, D3QN and TD3 show a smaller ρ range and opposite behavior as ρ increases with the traffic variance.

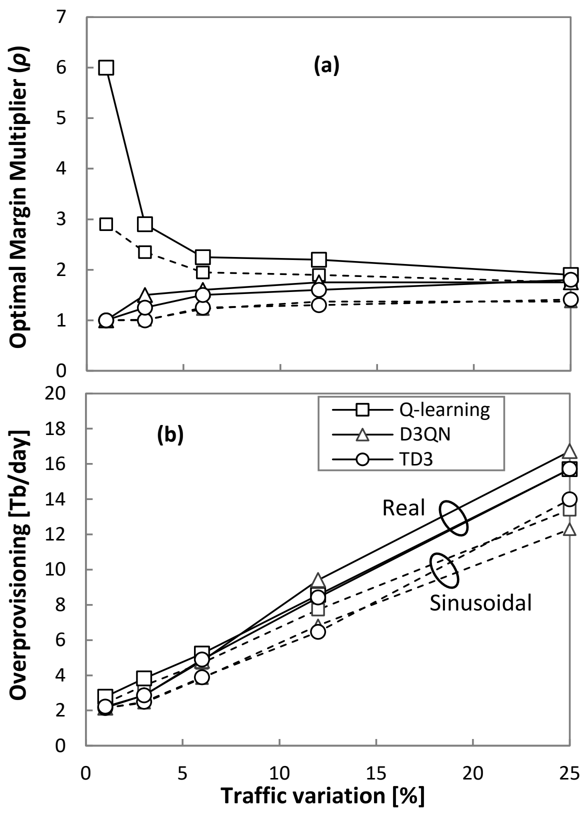

Figure 6-11. Optimal margin multiplier (a) and overprovisioning (b).

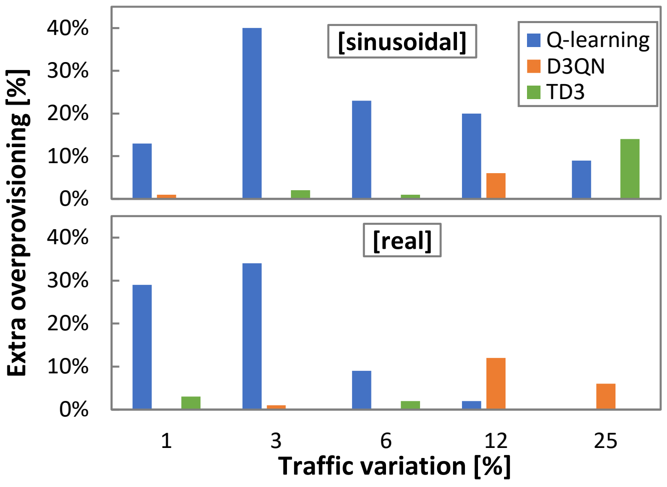

Figure 6-12 Relative extra overprovisioning.

The detailed evolution of the optimal ρ with respect to the traffic variation is plotted in Figure 6-11a, and Figure 6-11b shows the total overprovisioning introduced by every RL method operating with the optimal ρ. We observe that overprovisioning increases with traffic variation, with a slightly different trend depending on the traffic pattern (sinusoidal and real). Moreover, every RL method introduces different amounts of overprovisioning as shown in Figure 6-12, where the relative overprovisioning per RL method with respect to the minimum one for every traffic configuration is represented. Q-learning is the method that requires larger overprovisioning in general terms, whereas D3QN and TD3 show better performance. Interestingly, the differences are proportionally larger when traffic variation is small.

Let us analyze the effect in terms of extra-overprovisioning when ρ is fixed to a constant value, high enough to assure reliable QoS performance in online RL operation under traffics with a wide range of characteristics. The squared purple markers in Figure 6-10a indicate the QoS that could be achieved under different traffic characteristics for the largest ρ. Table 6-3 summarizes the relative and absolute increment of overprovisioning (computed in total Tb per day of operation) produced with the most conservative ρ configuration for all traffic configurations and RL methods. When the fixed ρ happens to be the optimal one for the traffic and RL method, no additional overprovisioning is set up (values in boldface); otherwise, additional overprovisioning is introduced. Q-learning is the method that adds the largest extra overprovisioning (exceeding 200% and 30 Tb/day). In any case, it is worth highlighting that achieving optimal performance in terms of QoS assurance while achieving efficient capacity allocation requires some method to find the optimal ρ for the traffic characteristics.

Table 6-3: Additional overprovisioning when fixing ρ

Traffic Pattern	**Traffic Variance**	**Q-Learning**		**D3QN**		**TD3**	
		%	**Tb/day**	**%**	**Tb/Day**	**%**	**Tb/Day**
Sinusoidal	1%	0.00%	0	0.88%	0.02	2.49%	0.05
	3%	19.18%	0.67	6.04%	0.16	20.67%	0.51
	6%	38.71%	1.85	5.21%	0.21	15.38%	0.63
	12%	44.15%	3.56	0.00%	0.00	4.01%	0.32
	25%	60.40%	8.29	0.00%	0.00	0.00%	0.00
Real	1%	0.00%	0	0.05%	0.00	4.95%	0.11
	3%	106.68%	3.94	9.52%	0.28	0.39%	0.01
	6%	192.50%	9.52	12.72%	0.60	2.90%	0.14
	12%	200.69%	18.37	0.00%	0.00	0.00%	0.00
	25%	219.35%	34.46	0.00%	0.00	0.00%	0.00

To conclude this section, we can highlight (*i*) that the CRUX problem proposed in Section 6.2 can be tackled using RL; under different traffic characteristics and RL methods, the target QoS is assured with reduced overprovisioning; (*ii*) online RL operation leads to traffic loss at the beginning of flow capacity operation; this fact prevents us from using RL until online learning has come up with a robust and reliable model to guarantee autonomous flow operation; and (*iii*) the comparison of the RL methods shows interesting differences among them. While Q-learning learns fast, it also produces larger overprovisioning. D3QN and TD3 need more time to ensure zero loss and adjust QoS at the benefit of reducing overprovisioning.

6.5.2 Offline Leaning + Online RL-Based Operation

Let us now focus on evaluating the operational approach detailed in Section 6.4 (Figure 6-2b), which consists of three phases. Before emulating flow operation, we generated synthetic data for all the traffic variances following the sinusoidal traffic pattern and used them to pre-train generic models independently for each traffic configuration and RL method. We ran every offline RL training for 14,400 episodes to guarantee QoS assurance with minimum overprovisioning.

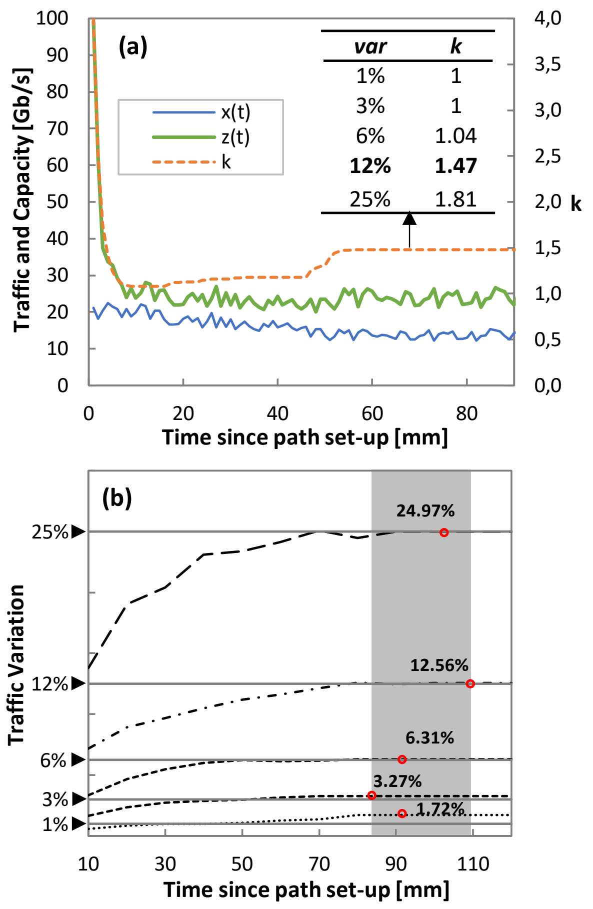

Figure 6-13. Phase I: Self-tuned threshold (a) and traffic variance analysis (b).

Starting with the analysis of Phase I, Figure 6-13a shows an illustrative example of the evolution of the capacity during the operation of the threshold-based algorithm (Algorithm 6-4) for the real traffic pattern and variation 12%. Actual traffic $x(t)$, allocated capacity $z(t)$, and the evolution of the self-tuned k parameter are also shown. Note that k quickly evolves from its initial value (k = 4) to reach a capacity closer to actual traffic. However, as soon as the load exceeds the optimal one l^*, k is increased until reaching a stable value (1.47), which happens after 60 minutes of operation. The inset table in Figure 6-13a details the values of k after one hour of operation for all traffic configurations. It is worth noting that the self-tuned threshold-based algorithm operates with zero traffic loss for all the cases.

Parallel to the threshold-based operation, traffic variance analysis (Algorithm 6-2) is conducted in order to compute the true variance of the traffic. Figure 6-13b shows the computed traffic variation as a function of time for all traffic configurations. Round markers highlight when the derivative of traffic variance reached a small *eps* = 0.01 and labels show the final computed variance value. The low error between computed and true variances is noticeable. Such estimation is achieved within two hours in all the cases.

After two hours of operation, *Phase II* (Algorithm 6-5) can start and an RL method with a generic pre-trained model for the true traffic variance is set to operate. The tuning of parameter ρ ($\Delta\rho$ = 0.1) and the resulting QoS are shown in Figure 6-14a and b, respectively, for traffic variance equal to 12%. To detect whether the measured QoS is considerably below or above the desired *qa* value, a significance level *cfl* = 0.05 was used to be compared against the obtained p-value from the binomial tests. We observe that ρ decreases up to a magnitude that produces QoS below 99%; just after that, ρ increases and remains stable from that point on. As shown in Figure 6-14a, the time to converge to the best ρ is 3960, 1440, and 3600 min (2.75, 1, and 2.5 days) for Q-learning, D3QN, and TD3, respectively.

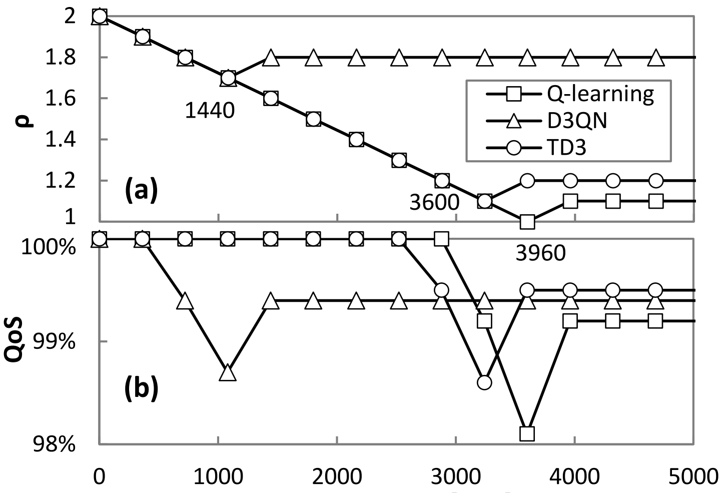

Figure 6-14 Phase II: QoS (a) and ρ (b) evolution.

The above analysis, however, needs to be complemented with the overprovisioning to extract meaningful conclusions. Figure 6-15 presents the overprovisioning obtained by every RL method before and after tuning ρ in *Phase II*. For reference purposes, the overprovisioning introduced by the threshold-based algorithm during *Phase I* is also included as a dotted line. The large benefits in terms of overprovisioning reduction for the RL-based operation with regard to the threshold-based algorithm are remarkable—up to 45% of capacity allocation reduction and 11 Tb/day of total capacity savings for one single flow. After ρ tuning, D3QN shows the worst performance, as Q-learning and TD3 achieved significantly lower overprovisioning (24%, ~3 Tb/day). Figure 6-15 also shows the obtained overprovisioning when the specific model (trained offline with the collected traffic) is loaded in *Phase III* after 10 days of operation. We observe that Q-learning and TD3 reduce overprovisioning slightly, whereas a larger reduction is achieved with D3QN; we conclude that the former RL methods are less dependent on an accurate model of the specific traffic to achieve optimal capacity allocation.

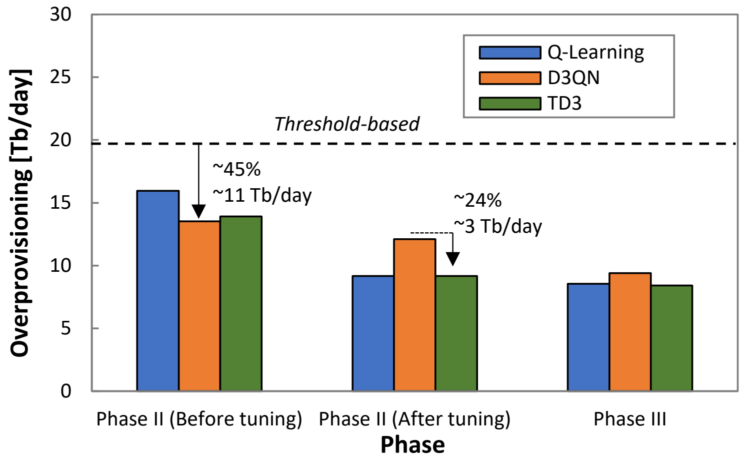

Figure 6-15. Overprovisioning reduction.

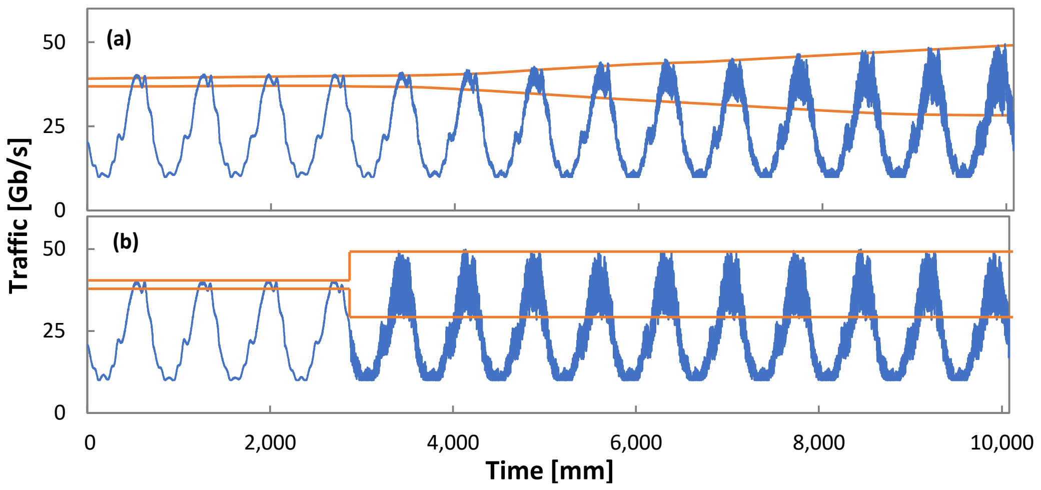

Figure 6-16 Phase III: Traffic variance change scenarios. Gradual increase (a) and sudden increase (b).

Finally, let us analyze the performance of Algorithm 6-6 to detect traffic changes while flow is operated in *Phase III*; recall that such detection immediately triggers

Phase II. To this end, we generated four different scenarios, combining two different types of changes in traffic variance while keeping traffic profile unchanged. We evaluate *gradual* and *sudden/increase* or *decrease* traffic variance changes. Figure 6-16 illustrates two out of four scenarios: *gradual increase* (variance gradually increases from 1% to 25% along 5 days) and *sudden increasing* (from 1% to 25% in just one minute); an inverse trend is configured for *gradual* and *sudden decrease* scenarios.

Table 6-4 details the time to detect the traffic change when the variance range was configured as [*var_l*, *var_h*] = [−10%, +10%]; the current traffic variance and minimum reward *rw_l* was set to 5% of the minimum observed reward (see Algorithm 6-6). We observe that the proposed mechanism ensures prompt reaction under any of the studied changes—immediate detection is achieved when a sudden change happens, and no more than one hour is required for gradual change detection.

Table 6-4: Phase III: Analysis under traffic changes

Traffic Change Scenario	**Detection Time (min)**	**QoS at Detection Time (%)**			**Reward Degradation (Min from Detection)**		
		Q-L	**D3QN**	**TD3**	**Q-L**	**D3QN**	**TD3**
Gradual increase	45	99.30	100	100	419	595	585
Gradual decrease	650	99.86	99.44	99.72	3,354	2,440	2,233
Step increase	1	99.17	99.86	99.86	332	413	433
Step decrease	1	99.03	99.44	99.44	494	683	212

To evaluate the promptness of detection, Table 6-4 considers the observed QoS at the detection time, as well as the elapsed time between detection time and the time when reward begins to degrade (reveals whether the RL module is working properly). Note that the detection happens when the QoS is still above the target value in all the cases. This is proof of anticipation of the change detection, which is key to guarantee robust and reliable RL-based operation.

6.6 Concluding Remarks

The Flow Capacity Autonomous Operation (CRUX) problem has been introduced to deal with online capacity allocation of traffic flows subject to dynamic traffic changes; it guarantees precise QoS requirement assurance and minimizes capacity overprovisioning. RL-based operation was proposed to learn the best policy for the traffic characteristics and QoS requirements of a given flow. RL allows adaptive and proactive capacity allocation once the optimal policy is learnt. However, pure RL operation lacks robustness during online learning (e.g., at the beginning of flow operation and in the event of traffic changes) and might result in undesirable traffic loss. However, this can be avoided using simpler reactive threshold-based capacity allocation.

In view of the above, an offline + online learning lifecycle was proposed, aiming at providing guaranteed performance during the entire lifetime of the traffic flow. The proposed management lifecycle consists of three phases. Firstly, a self-tuned threshold-based approach was proposed to operate just after the flow is set up and until enough evidence of the traffic characteristics are available (*Phase I*). Secondly, an RL operation based on models with a pre-trained generic traffic profile but meeting specific traffic variance that was measured during Phase I was executed (*Phase II*). Lastly, an RL operation with models trained for the real measured traffic, while allowing an online RL to adapt to smooth traffic changes (*Phase III*). In addition, during *Phase III* online traffic analysis and RL performance tracking was conducted to detect sharper traffic changes that might require moving back to *Phase II* to keep high reliability.

The proposed lifecycle was implemented under three different RL models, namely, Q-learning, D3QN, and TD3. While Q-learning allows for simple and easy-to-learn definition of policies under discrete spaces of states and actions, D3QN and TD3 enable the application of more complex policies based on deep learning models with continuous state space (D3QN) and continuous action space (TD3).

Numerical evaluation of the proposed offline + online lifecycle under different RL techniques was carried out, reproducing realistic traffic flows in a simulation environment. For benchmarking purposes, comparative results against basic threshold-based operation and online RL operation were also presented. The main conclusions extracted from the numerical evaluation are summarized in Table 5, where colors are used to highlight the results. As expected, online RL produces moderate to high loss (reaching peaks of 1–10 Gb/s) at the beginning of the network operation. Among the different methods, Q-learning reached the required QoS operation earlier (up to 6 times faster than TD3) at the expense of moderate to large overprovisioning (up to 40% larger than TD3). On the other hand, D3QN and TD3 needed more time to converge to the required QoS operation but resulted in considerably better capacity allocation efficiency.

The analysis of the numerical results of the proposed lifecycle leads to several conclusions. Firstly, zero traffic loss and QoS assurance is guaranteed from path set-up regardless of the chosen RL method. Secondly, *Phase II* allows a very efficient and robust operation based on pre-trained generic models that were tuned with specific traffic characteristics. *Phase II* clearly outperformed threshold-based operation in terms of capacity utilization since it remarkably reduced overprovisioning (up to 45%). Thirdly, all the methods reached outstanding capacity efficiency (more than 50% of capacity reduction with respect to threshold-based operation) without losing QoS performance in *Phase III*; Q-learning and TD3 behaved slightly better than D3QN. Finally, the continuous analysis and tracking conducted during *Phase III* to detect traffic changes allowed a prompt detection of sharp changes (between 1 and 650 minutes), triggering *Phase II* from several hours to days before online RL operation suffered any significant degradation.

Table 6-5: Summary of results for policy-based and RL operation with and without offline learning

Approach	**Concept**		**Threshold-based**	**Q-Learning**	**D3QN**	**TD3**
Policy-based	Traffic loss		Zero traffic loss			
	QoS assurance		Since path set-up			
	Over-provisioning		Very large			
Online RL Operation	Traffic loss			Moderated loss	Moderated loss	High loss
	QoS assurance			After 2 days	After 2 days	After 5 days
	ρ range for QoS assurance			Wide	Narrow	Narrow
	Over-provisioning	conservative ρ		Large	Small	Small
		optimal ρ		Moderate	Small	Small
Offline + Online RL Operation	Traffic loss		Zero traffic loss	Zero traffic loss	Zero traffic loss	Zero traffic loss
	QoS assurance		Since path set-up	Since path set-up	Since path set-up	Since path set-up
	ρ fine tuning effectiveness			Large	Moderated	Large
	Over-provisioning Gain	Phase I	None			
		Phase I-> Phase II		Moderated	Large	Large
		Phase II		Large	Small	Large
		Phase II-> Phase III		Small	Large	Small
	Reliability (Phase III-> Phase II)			High	High	High

Chapter 7

Revisiting Autonomous vLink Capacity Operation

In this chapter, we revisit the scenario described in Chapter 5 for vLink capacity management when the vLink was supported by a lightpath based on the DSCM. Specifically, in view of the results obtained in Chapter 5 for vLink capacity management, here we propose a RL model for vlink capacity management. We next go a step beyond and consider intent cooperation, where the intents deployed for the individual PkCs take actions based on the traffic in the connection (as in Chapter 6) and cooperate with the vLink intent, which aggregates the capacity of the individual PkCs to decide the capacity of the vLink.

7.1 Introduction

Recall that in Chapter 5 the vLink intent was based on short-term traffic forecasts to predict future capacity needs. Although this approach can help to anticipate potential capacity exhaustion by allocating capacity in advance, when the traffic volume decreases, the reduction of capacity can lead to undesired capacity fluctuations and to increase queuing. In this chapter, we propose a vLink intent based on RL to manage the capacity of the vLink. As demonstrated in Chapter 6, RL fits well with IBN as it entails learning on how to map situations to actions to maximize rewards, without specifically programming the learner. In turn, the algorithm in the transponder, making decisions on the configuration of the SCs, can be based on policies received from the SDN controller. This approach aims at managing the capacity of the vLink as a function of the current and predicted traffic volume, while avoiding queuing (and traffic losses) and keeping moderated SC configuration changes by removing oscillating capacity allocation actions.

Recall that the vLink intent targets at making decisions proactively to reach some performance defined for the vLink. A related concept is that of independent operation vs coordinated operation. Independent operation occurs when the decisions that are made on a network entity (in this case the vLink) are based on measurements collected for the same entity. However, since in a network infrastructure many entities are sharing the set of common resources, pure independent operation is rare, as it can lead to overall suboptimal resource utilization and even to result in poor performance because of the natural competence for resources. Therefore, some kind of coordination among entities should be devised.

Although PkCs and related vLinks can work independently making decisions based on the observed input traffic, some coordination might facilitate the overall operation. For instance, as a result of the capacity required by the PkCs, the capacity of the vLink needs to be reconfigured. Nonetheless, if the available capacity of the vLink is exhausted, competition for the available capacity of the vLink would lead to poor performance for both PkCs. A possible solution to avoid conflicts and countereffects between intent agents competing for common resources is to consider cooperation among them to ensure that they can achieve their operational goals.

The rest of the chapter is organized as follows. Section 7.2 extends the intent agent proposed in Chapter 5 and adapt it, so the intent can be based on RL. In addition, details of the definition of the reward function for the definition of the RL solutions are given. In Section 7.3, we propose a cooperative intent operation approach between PkC and vLink intents. The discussion is supported by the experiments and numerical results presented in Section 7.4. Finally, Section 7.5 draws the main conclusions of our work.

7.2 Autonomic vLink Capacity Adaptation

In this section, we extend the intent agent in Figure 5-2 with the architecture in Figure 7-1; note the similarities with the architecture in Figure 6-1 for flow capacity autonomous operation. In Figure 7-1, a RL-based vLink intent analyzes monitoring data, specifically *input traffic x(t)* and *current vLink capacity z(t)*, that is collected periodically (e.g., every minute). Based on such analysis, the vLink intent agent determines the *target capacity z'(t+1)* that should be allocated for the next period by using the learned optimal policy. With such capacity, an agent running at the optical transponder (Tx side) decides the *actual capacity z(t+1)* to be allocated, which will depend on the characteristics of the optical layer. The operation can be based on policies and other parameters received from the SDN controller.

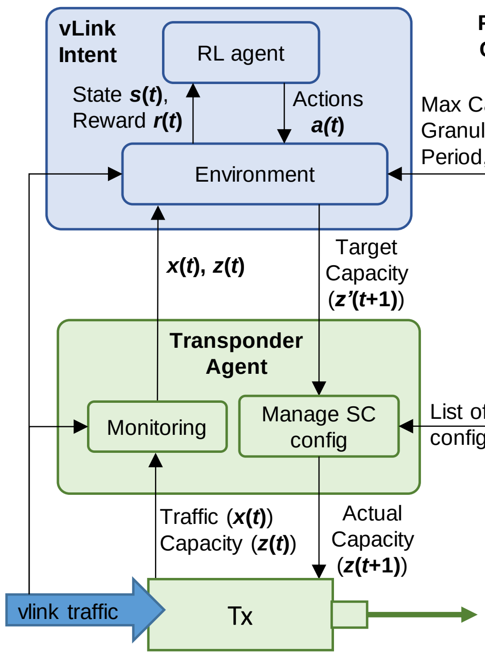

Figure 7-1 RL-based Autonomous vLink Operation Architecture.

The goal is to adjust the vLink capacity to guarantee that the vLink load $l(t)$ (defined as $x(t)$ / $z(t)$) does not exceed but is close to a given maximum l_{max}; this will minimize over-provisioning (defined as $z(t)$-$x(t)$) while limiting the average maximum delay for the traffic. In this scenario, the learning process can be focus on the traffic variation and its evolution with time, which is key for a tight load adjustment and for avoiding high delay and traffic loss due to insufficient capacity allocation.

The environment in the intent agent is in charge of computing the state $s(t)$, whereas $s(t)$ is obtained as a function of both $l(t)$ and l_{max}. Given $s(t)$, the RL agent selects the action $a(t)$ with highest total reward with probability 1-ε (*exploitation*) or randomly with probability ε (*exploration*) [SuBa98], where exploration is encouraged during an initial learning phase and a decay strategy is implemented. Action $a(t)$ consists in a capacity volume Δz to be added to or subtracted from the current vLink capacity. The reward function $r(t)$ is a linear function with three penalty components (ordered by importance): *i*) traffic loss ($x(t) > z(t)$), *ii*) l_{max} violation ($l(t) > l_{max}$), and *iii*) over-provisioning ($z(t)$ - $x(t)$). Thus, the maximum reward is achieved when neither loss nor l_{max} violation is observed, and over-provisioning is minimized.

7.3 Cooperative Intent Operation

Let us imagine now the case where the traffic that the vLink is supporting comes from a number of PkCs, which capacity is being managed by specific PkC intents. In this case, the capacity to be ensured in the vLink can be easily computed as the summation of the capacity required by every PkC. Therefore, in this section, we extend the previous stand-alone intent-based vLink capacity adaptation and focus on evaluating the potential benefits of a hierarchical cooperation with PkC intents. Figure 7-2 shows the architecture, where PkC intent agents implement a RL-based method similarly to the previously used for the vLink. The aggregation of the target capacity requested for every PkC is used as target capacity for the vLink.

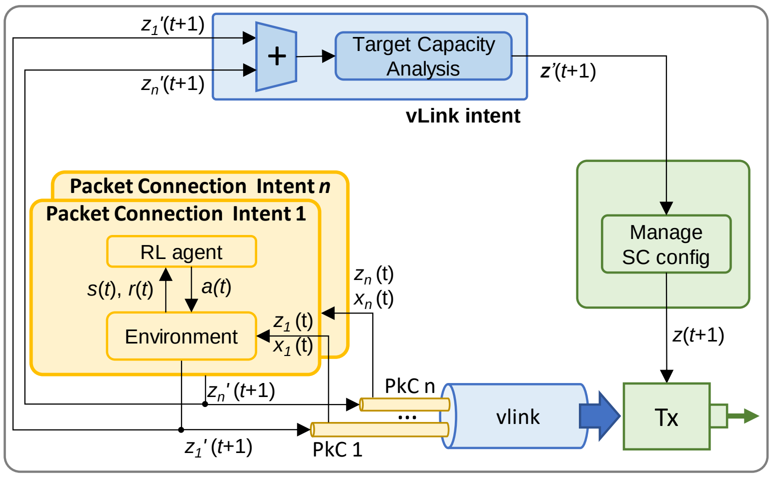

Figure 7-2 Extended architecture with hierarchical intent cooperation.

For PkCs specifically, let us consider different operational goals than those used for the vLink; every PkC has a different requirement in terms of maximum delay budget d_{max} that needs to be guaranteed. This entails changes in the reward function *r(t)*, where a new component adds a large penalty if the measured delay in the packet connection exceeds the required d_{max}. Moreover, no penalty for maximum load violation is considered.

7.4 Illustrative Intent-Based Applications

In this section, we first present the results obtained assuming a RL-based vlink intent and then, the results assuming cooperation between the vLink and the PkC intents.

7.4.1 Autonomous vLink Capacity Operation

A Python-based simulator reproducing the architecture in Figure 7-1 has been implemented for evaluation purposes. As in Chapter 5, realistic vLink input traffic was generated using the flow simulator and parameters described in [Ru18]. The target load l_{max} was set to 80%.

Q-learning, D3QN, and TD3 RL methods were implemented, adapting state and action spaces to either discrete or continuous space depending on the method (see

Chapter 2). The FFNNs for D3QN and TD3 methods were configured with 2 layers each with 100 neurons implementing ReLU activation function [ZhQi05]. For the sake of fairness, Δz was setup to 10 Gb/s in all the methods. In addition, a threshold-based approach was implemented for benchmarking purposes, which reactively adds or releases capacity to keep *l(t)* in the range [0.7-0.8].

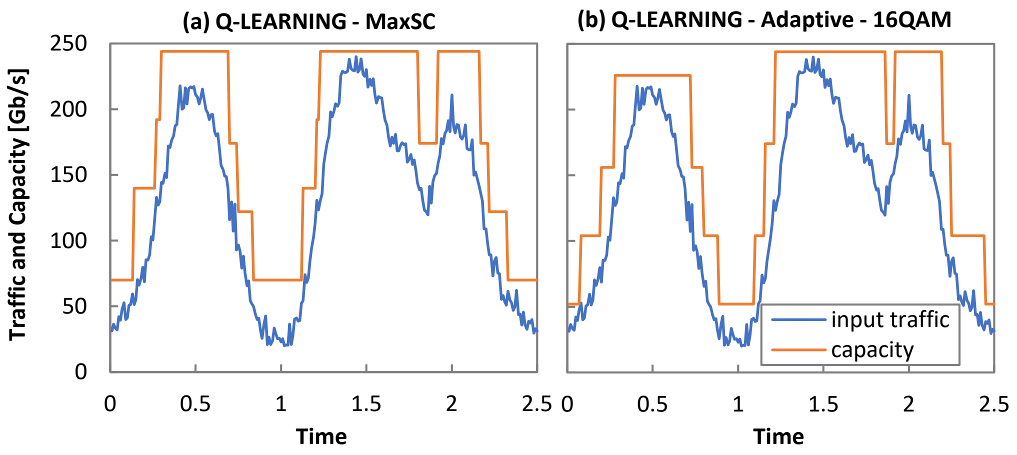

Figure 7-3 Optical connection managed by the vLink intent. Total capacity vs time for the High Traffic profile.

To facilitate comparison with the results the obtained in Chapter 5, let us first assume that the RL-based vlink intent was based on Q-learning. The obtained results are presented in Figure 7-3a-b and Table 5-3 (down). Initial exploration probability ε was set to 1, reducing every episode by a multiplicative factor of 0.98. The Q-learning algorithm was configured with a learning rate of 0.05 and a discount factor of 0.95.

Table 7-1: Summary of results for Optical Connection Configuration Managed by vlink Intent based on Q-learning

	Q-Learning			
	High Traffic Profile		**Low Traffic Profile**	
	maxSC	**adapt-16Q**	**maxSC**	**adapt-16Q**
#Changes per day	7.2	5.6	0	1.6
Energy savings [%]	31	26	47	46
Packet Loss [MB]	0	0	0	0
Queue (max) [MB]	0	0	0	0
Queue (avg) [MB]	0	0	0	0
Cap. Exhaust. per day	0	0	0	0

The results confirm that intent-based vlink capacity management based on RL results in a good solution for smooth capacity evolution, eliminating completely packet loss and time in vlink queue, while energy savings are still over 26% and 46% for the *High* and *Low Traffic* profiles, respectively.

Let us now compare the performance of the different RL methods. Figure 7-4 shows the performance of the threshold-based approach and RL-based methods (note that latter ones need a sufficiently large number of episodes to guarantee robust and efficient operation).

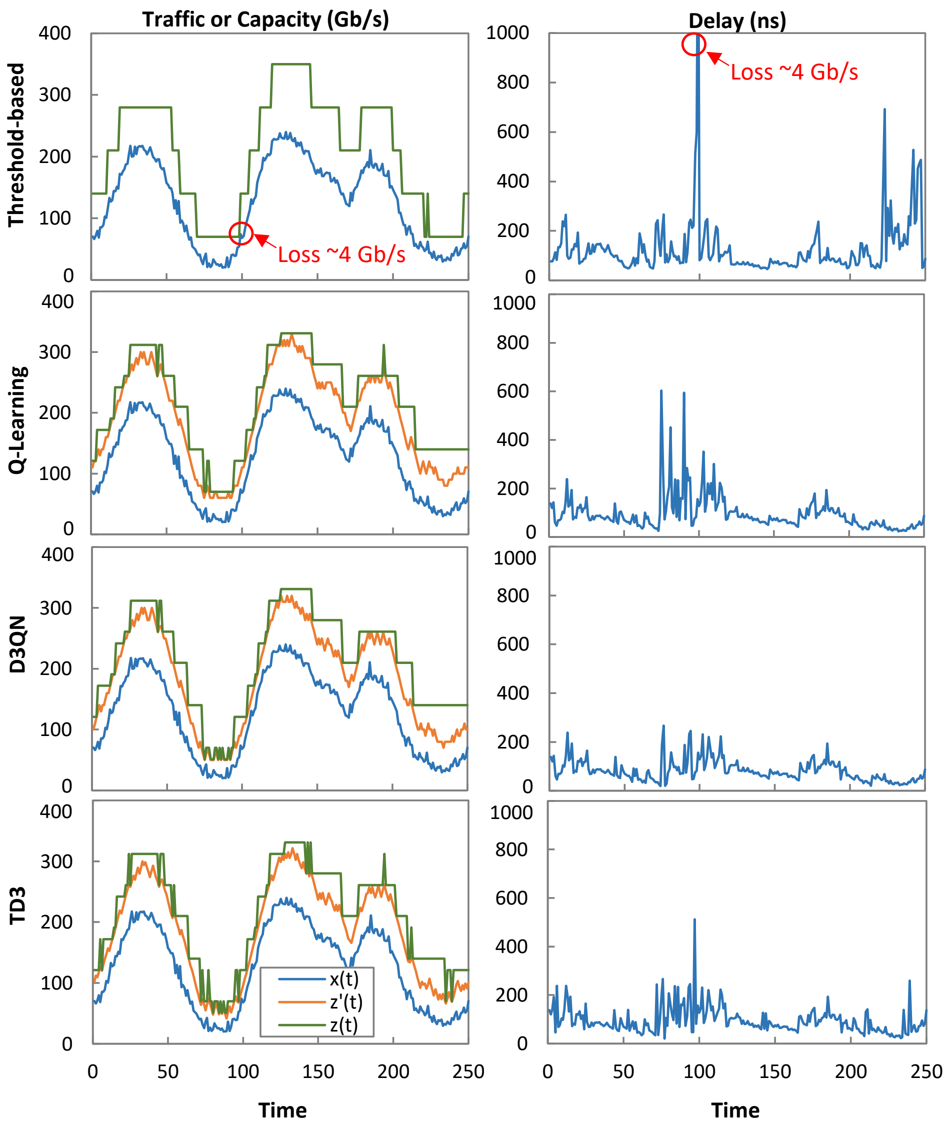

Figure 7-4 Autonomic vLink Capacity Adaptation (a) and obtained delay (b).

The measured input traffic *x(t)*, target capacity *z'(t)* in the case of RL-based methods, and allocated capacity *z(t)* are plotted for a typical day. We observe that the threshold-based method with an *a priori* good configuration produces poor performance (traffic loss and high delay) as a result of its reactive nature. In contrast, all RL-based methods learned policies to avoid losses and they adapt better to the traffic characteristics. Specifically, D3QN achieves low maximum delay (at least, half of the other RL methods). However, the main conclusions to be extracted from delay analysis is that although the reward function explicitly controls the load, which is closely related to delay performance, a finer delay control (e.g., keeping delay below a target maximum) requires *ad-hoc* delay analysis components to be considered in the reward function. Table 7-2 summarizes the results. In general, RL methods require higher overprovisioning than the threshold-based approach, but such overprovisioning is necessary to achieve the target performance. Therefore, these results validate the usefulness of RL for the proposed vLink operation use case.

Table 7-2 vLink Capacity Adaptation Summary

Method	**Loss (Gb/s)**	**Over-Provisioning (Tb/day)**	**Num SC Changes**	**Delay (µs)**		
				min	**avg**	**max**
Thr-based	4.05	19.2	18	45	129	1629
Q-Learning	0	21.6	54	23	95	603
D3QN	0	22.6	34	19	82	267
TD3	0	20.8	70	21	96	512

The drawbacks rely on the need for a larger number of SC changes (activations and deactivations) compared to the threshold-based approach. E.g., among the RL-based methods, the lowest overprovisioning is achieved by TD3 at the expense of doubling the number of SC changes with respect to D3QN, which requires double number of SC changes than the threshold-based approach. Hence, the selection of the RL method is not trivial and it might depend on limitations of the hardware, e.g., the SC activation time.

Finally, it is worth noting that RL-based operation at the vLink level cannot provide differentiated delay performance for the different PkCs supported by the vLink. On the contrary, implementing the RL-based operation at the PkC would provide specific performance to the individual PkC but would require from specific cooperation between PkC and vLink intent agents.

7.4.2 Cooperative Intent Operation

Let us assume the numerical evaluation scenario detailed in the previous section where phree PkCs A, B, C with maximum traffic 120, 60, and 60 Gb/s and different delay budgets generate the same aggregated vLink traffic as in Figure 7-4. We focus on the TD3 RL method and similarly as for vLink intent operation, we run it until achieving a robust and accurate operation.

The accuracy of the proposed cooperative scheme to predict vLink traffic is illustrated in Figure 7-5a. The vLink traffic is compared against the prediction from the PkC intents; the models learned by different PkCs intent agents for the short 1-min scope can be aggregated and used by the vLink for a much longer time scope with remarkable accuracy. Figure 7-5b shows the delay at the source node for all PkCs, assuming that PkCs leave through 100/200 Gb/s interfaces. We observe that RL-based operation at the PkC level allows achieving the targeted differentiated delay performance. From Figure 7-5, we observe that the requested target capacity for every PkC is accurate and well-fitted so, the sum of all target capacities to be considered by the vLink intent agent results into an overall capacity that meets PkCs needs.

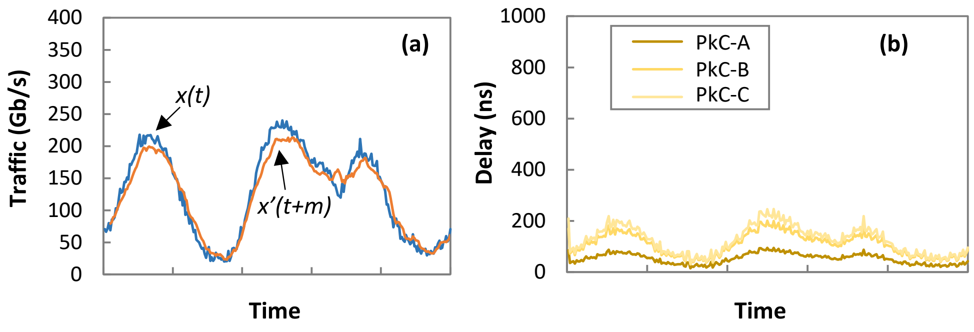

Figure 7-5 PKC-vLink intent cooperation performance.

Figure 7-6 and Table 7-3 compare hierarchical cooperation named *hierarchical* and vLink model. Results of the vLink allocated capacity and introduced delay are presented.

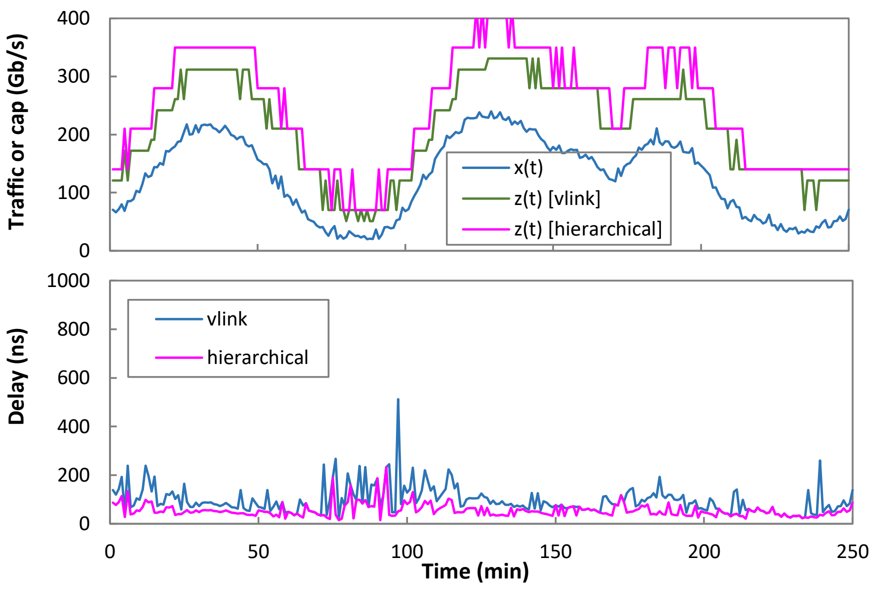

Figure 7-6 Comparative results

Table 7-3 Cooperative IBN summary

Method	**Over-Provisioning (Tb/day)**	**Num SC Changes**	**Delay (ns)**		
			min	**avg**	**max**
vLink	20.8	70	21	96	512
Hierarchical	29.8	50	15	54	233

In view of the graphs, the requirements from the PkCs to achieve differentiated delay performance result in a higher capacity that cannot be successfully learnt by the vLink intent. Interestingly, when PkC operation is intent-based, the number of SC changes at the optical layer reduces noticeably. This fact points out the benefits of hierarchical intent cooperation to simplify multilayer operation. Moreover, the delay contribution introduced by the vLink is greatly reduced. We can conclude that hierarchical intent cooperation is the option that provides the best trade-off between the achievement of the operational goals and resource utilization and management.

7.5 Concluding Remarks

In this final chapter, intent agents based on RL were proposed to adjust the capacity of a vLink as a function of the input traffic. Next, cooperative intent operation between pkC and vLinks was proposed, where the capacity required by the vLink comes directly from the capacity of the supported PkCs. Numerical results were presented and discussed. The solutions presented extended the ones in Chapter 5 for vLink autonomous operation.

Chapter 8

Closing Discussion

8.1 Main Contributions

This Ph. D. thesis focuses on applying ML techniques for the autonomous and reliable operation of multilayer optical networks. The main contributions are summarized as following:

- First, in Chapter 4, we compared estimated and measured QoT in the optical transponder by using a QoT tool based on GNPy. We showed that the changes in the values of input parameters of the QoT model representing optical devices can explain the deviations and degradation in performance of such devices. we used reverse engineering to estimate the value of those parameters tat explain the observed QoT. We showed by simulation a large anticipation in soft-failure detection, localization and identification of degradation before effecting the network. Finally, for validating our approach, we experimentally observed the high accuracy in the estimation of the modeling parameters.
- In Chapter 5, we studied the autonomous operation of optical connections based on digital subcarrier multiplexing. We proposed several solutions for the autonomous operation of DSCM systems. In particular, the combination of two modules running in the optical node and in the optical transponder activate and deactivate subcarriers to adapt the capacity of the optical connection to the upper layer packet traffic. The module running in the optical node is part of our IBN solution and implements prediction to anticipate traffic changes. Our comprehensive study demonstrated the

feasibility of DSCM autonomous operation and showed large cost savings in terms of energy consumption. In addition, Chapter 5 provides a guideline to help vendors and operators to adopt the proposed solutions.

- Chapter 6 is devoted to the autonomous packet flow capacity management. In this chapter we applied RL techniques and proposed a management lifecycle consisting of three different phases: 1) a self-tuned threshold-based approach for setting up the connection until enough data is collected, which enables understanding the traffic characteristics; 2) RL operation based on models pre-trained with generic traffic profiles; and 3) RL operation based on models trained with the observed traffic. We showed that RL algorithms provide poor performance until they learn optimal policies, as well as when the traffic characteristics change over time. The proposed lifecycle provides remarkable performance from the starting of the connection and it shows the robustness while facing changes in traffic.
- In Chapter 7 we took advantage of the experience from Chapter 6 and revisited the solutions proposed in Chapter 5 for autonomous vLink operation supported by DSCM systems. The contributions of this chapter are twofold: 1) and the one hand, we proposed a solution based on RL, which showed superior performance with respect to the solution based on prediction; and 2) because vLinks support packet connections, coordination between the intents of both layers was proposed. In this case, the actions taken by the individual PkCs are used by the vLink intent. The results showed noticeable performance compared to independent vLink operation.

8.2 List of Publications

8.2.1 Publications in Journals

[JOCN22] L. Velasco, **S. Barzegar**, F. Tabatabaeimehr, and M. Ruiz, “Intent-Based Networking for Optical Networks [Invited Tutorial],” IEEE/OSA Journal of Optical Communications and Networking, vol.14, pp. A11-A22, 2022.

[SENSORS21] **S. Barzegar**, M. Ruiz, and L. Velasco, “Packet Flow Capacity Autonomous Operation based on Reinforcement Learning,” MDPI Sensors, vol. 21, pp. 8306, 2021.

[TNSM21] **S. Barzegar**, M. Ruiz, A. Sgambelluri, F. Cugini, A. Napoli, and L. Velasco, “Soft-Failure Detection, Localization, Identification, and Severity Prediction by Estimating QoT Model Input Parameters,” IEEE Transactions on Network and Service Management, vol. 18, pp. 2627-2640, 2021.

[JSAC21] L. Velasco, **S. Barzegar**, D. Sequeira, A. Ferrari, N. Costa, V. Curri, J. Pedro, A. Napoli, and M. Ruiz, "Autonomous and Energy Efficient Lightpath Operation based on Digital Subcarrier Multiplexing," IEEE Journal on Selected Areas in Communications, vol. 39, pp. 2864-2877, 2021.

8.2.2 Publications in Conferences

[OFC21.1] **S. Barzegar**, M. Ruiz and L. Velasco, "Reliable and Accurate Autonomous Flow Operation based on Off-line Trained Reinforcement Learning," in Proc. IEEE/OSA Optical Fiber Communication Conference (OFC), 2021.

[OFC21.2] F. Tabatabaeimehr, **S. Barzegar**, M. Ruiz and L. Velasco, "Combining Long-Short Term Memory and Reinforcement Learning for Improved Autonomous Network Operation," in Proc. IEEE/OSA Optical Fiber Communication Conference (OFC), 2021.

[ECOC20] **S. Barzegar**, M. Ruiz and L. Velasco, "Reinforcement Learning -based Autonomous Multilayer Network Operation," in Proc. European Conference on Optical Communication (ECOC), 2020.

[ICTON20] **S. Barzegar**, Marc Ruiz, and Luis Velasco, "Soft-Failure Localization and Time-Dependent Degradation Detection for Network Diagnosis," in Proc. IEEE International Conference on Transparent Optical Networks (ICTON), 2020.

[OFC20] **S. Barzegar**, E. Virgillito, M. Ruiz, A. Ferrari, A. Napoli, V. Curri, and L. Velasco, "Soft-Failure Localization and Device Working Parameters Estimation in Disaggregated Scenarios," in Proc. IEEE/OSA Optical Fiber Communication Conference (OFC), 2020.

[ICTON19] **S. Barzegar**, M. Ruiz, and L. Velasco, "Adaptation of the residual signal for filter failure detection in scenarios with multiple filter types," in Proc. IEEE International Conference on Transparent Optical Networks (ICTON), 2019.

8.3 List of Research Projects

8.3.1 European Funded Projects

- **B5G-OPEN**: Beyond 5G - OPtical nEtwork continuum, H2020-ICT-2020-2 (G.A. 101016663).
- **METRO-HAUL:** METRO High bandwidth, 5G Application-aware optical network, with edge storage, compute and low Latency, H2020-ICT-2016-2 (G.A. 761727).

8.3.2 National Funded Projects

- **IBON:** AI-Powered Intent-Based Packet and Optical Transport Networks and Edge and Cloud Computing for Beyond 5G, Ref: PID2020-114135RB-I00, 2021-2024.
- **TWINS:** cogniTive 5G application-aware optical metro netWorks Integrating moNitoring, data analyticS and optimization, Ref: TEC2017-90097-R, 2018-2020.

8.3.3 Pre-doctoral Scholarship

- Pre-doctoral scholarship related to ICREA Academia 2015-2020 and 2021-2025 awards.

8.4 Collaborations

I had the opportunity to collaborate with:

- OPTCOM group at Politecnico di Torino on the estimation of configuration parameters for QoT (G.1).
- Infinera on the application of Reinforcement Learning to DSCM systems (G.2).
- Consorzio Nazionale Interuniversitario per le Telecomunicazioni (CNIT) and Universidad de la República on the application of Reinforcement Learning to packet networks (G.3).

8.5 Topics for Further Research

First, some of the algorithms and architectures devised in this Ph. D. thesis are being implemented experimentally in the framework of the B5G-OPEN project.

In addition, we are working on distributed decision-making following the concept of Multi-Agent Systems (MAS) [MAS]. MAS is a subfield of AI and it can be defined as a set of individual agents that share knowledge and communicate with each other in order to solve a problem that is beyond the scope of a single agent. In the scope of networking, we proposed that agent nodes make autonomous decisions real-time based on guidelines received from the SDN controller. Such decision-making will be performed based on its own observed data, as well as on the data and models received from other nodes. To illustrate this concept, we have first focused on flow routing. As in Chapter 6, we are assuming packet flows carrying traffic with unknown characteristics entering in a packet node. However, in this work, flows need to be routed to the destination though several output interfaces, while ensuring some given QoS, e.g., in terms of end-to-end delay, and optimizing resource utilization.

Figure 8-1 represents an example of flow routing operation in a node in the targeted multilayer scenario. The packet node agent has received from the SDN controller three possible routes for a given traffic flow and it has to decide which one or combination of several are the allow to reach some QoS performance (in this case, the end-to-end delay), while minimizing some cost function. In this case, we use RL to implement a service agent for the traffic flow. In such a figure, the traffic of the flow is routed through two different interfaces (in this case both supported by the optical layer) among the three available ones for the flow. Here, we assume that the traffic flow actually consists of multiple sub-flows, which are routed independently so the packets belonging to each sub-flow follow the same route. In the destination, the end-to-end delay is measured (e.g., using in-band telemetry) and some statistics are computed (e.g., maximum and weighted average) and sent to the node agents participating in the routing of the flow.

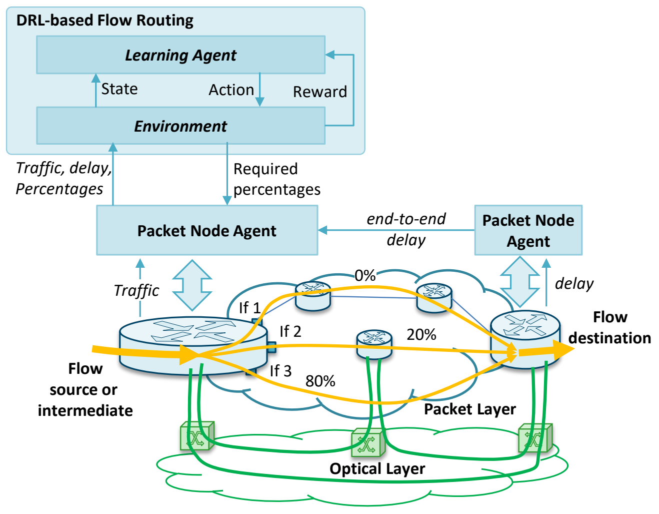

Figure 8-1 Example of distributed flow routing based on RL

Initial results show promising results of the proposed approach

List of Acronyms

PLC	Packet Layer Connections
FEC	Forward Error Correction
TRX	Transponders
BER	Bit Error Rate
QoT	Quality of Transmission
NL	Non-Linear
OA	Optical Amplifier
WSS	Wavelength Selective Switch
MDA	Monitoring and Data Analytics
ROADM	Reconfigurable Optical Add / Drop Multiplexer
GSNR	Generalized Signal to Noise Ratio
ASE	Amplified Spontaneous Emission
NLI	NL Interference
EDFA	Erbium Doped Fiber Amplifier
NF	Noise Figure
ML	Machine Learning
SNR	Signal to Noise Ratio
OSNR	Optical Signal to Noise Ratio
FS	Filter Shift
FT	Filter Tightening

OSA	Optical Spectrum Analyzer
GN	Gaussian-noise
OLS	optical line system
A/D WSS	Add/Drop Wavelength Selective Switch
QAM	Quadrature Amplitude Modulation
QPSK	Quadrature Phase-Shift Keying
RL	Reinforcement Learning
DQN	Deep Q-Network
DNN	Deep Neural Network
D3QN	Dueling Double DQN
TD3	Twin Delayed Deep Deterministic Policy Gradient
SDN	Software-Defined Networking
IBN	Intent-Based Networking
DB	database
rMSE	relative Mean Square Error
DSCM	Digital Subcarrier Multiplexing
SC	subcarriers
DSP	Digital Signal Processing
SR	Symbol Rates
Tx	Transmitter
Rx	Receiver
MF	Modulation Format
EON	Elastic Optical Networks
vLink	virtual Link
RSA	Routing and Spectrum Allocation
AI	Artificial Intelligence
RMSA	Routing, Modulation and Slot Assignment
SLA	Service Level Agreement
VIO	Virtual Infrastructure Orchestrator
MLFO	ML Function Orchestrator
TMN	Telecommunications Management Network

PBNM	Policy-Based Network Management
UI	User Interface
PLD	ML Pipeline Deployment
NBI	Northbound Interface
WF1	Deployment Workflow
ARIMA	Autoregressive Integrated Moving Average
FFNN	Feed-forward Neural Networks
CNN	Convolutional Neural Networks
RNN	Recurrent Neural Networks
LSTM	Long Short-Term Memory
DC	Data Center
PkC	Packet Connection

References

[Ag18]	C. Aggarwal, "Neural Networks and Deep Learning: A Textbook," Springer, 2018.
[APV17.1]	A. P. Vela *et al.*, "BER Degradation Detection and Failure Identification in Elastic Optical Networks," IEEE/OSA J. of Lightwave Technology, vol. 35, pp. 4595-4604, 2017.
[APV17.2]	A. P. Vela *et al.*, "Distributing Data Analytics for Efficient Multiple Traffic Anomalies Detection," Elsevier Computer Communications, vol. 107, pp. 1-12, 2017.
[APV18]	A. P. Vela *et al.*, "Soft failure localization during commissioning testing and lightpath operation," IEEE/OSA J. of Optical Comm and Networking, vol. 10, pp. A27-A36, 2018.
[Be20]	A. Bernal *et al.*, "Near Real-Time Estimation of End-to-End Performance in Converged Fixed-Mobile Networks," Elsevier Computer Communications, vol. 150, pp. 393-404, 2020.
[Bo18]	M. Bouda *et al.*, "Accurate Prediction of Quality of Transmission Based on a Dynamically Configurable Optical Impairment Model," IEEE/OSA J. of Optical Communications and Networking, pp. A102-A109, 2018.
[Bo21]	L. Bonati *et al.*, "Intelligence and Learning in O-RAN for Data-Driven NextG Cellular Networks," IEEE Communications Magazine, vol. 59, pp 21-27, 2021.
[Br16]	P. Brockwell *et al.*, "Introduction to Time Series and Forecasting," Springer: Berlin/Heidelberg, Germany, 2016.

[Ca02] G. Casella *et al.*, "Statistical Inference," Duxbury Press: Pacific Grove, USA, 2002.

[Ca18] M. Cantono *et al.*, "On the Interplay of Nonlinear Interference Generation with Stimulated Raman Scattering for QoT Estimation," IEEE/OSA Journal of Lightwave Technology (JLT), vol. 36, pp. 3131-3141, 2018.

[Ch12] R. Chmogrow *et al.*, "Error Vector Magnitude as a Performance Measure for Advanced Modulation Formats," IEEE Photonics Technology Letters, vol. 24, pp. 61-63, 2012.

[Ch19.1] X. Chen *et al.*, "DeepRMSA: A deep reinforcement learning framework for routing, modulation and spectrum assignment in elastic optical networks," IEEE/OSA J. Lightwave Technology, vol. 37, pp. 4155-4163, 2019.

[Ch19.2] X. Chen *et al.*, "Building Autonomic Elastic Optical Networks with Deep Reinforcement Learning," IEEE Commun. Mag., vol. 57, pp. 20–26, 2019.

[Ch21] X. Chen *et al.*, "A Multi-Task-Learning-based Transfer Deep Reinforcement Learning Design for Autonomic Optical Networks," IEEE J. on Sel. Areas in Communications, vol. 39, pp. 2878-2889, 2021.

[Cl21] A. Clemm *et al.*, "Intent-Based Networking - Concepts and Definitions," IRTF draft work-in-progress, 2021.

[Cu19] V. Curri *et al.*, "Synergetical Use of Analytical Models and Machine-Learning for Data Transport Abstraction in Open Optical Networks," in Proc. IEEE International Conference on Transparent Optical Networks (ICTON), 2019

[Da15] M. Dallaglio *et al.*, "Routing, Spectrum, and Transponder Assignment (RSTA) in Elastic Optical Networks," IEEE/OSA J. of Lightwave Technology, vol. 33, pp. 4648-4658, 2015.

[EON16] V. López and L. Velasco, *Elastic Optical Networks: Architectures, Technologies, and Control*, in Optical Networks book series, ISBN 978-3-319-30173-0, Springer, 2016.

[Fe20] A. Ferrari *et al.*, "GNPy: an open source application for physical layer aware open optical networks," IEEE/OSA J. of Optical Communications and Networking, vol. 12, pp. C31-C40, 2020.

[FGML19]	Focus group on Machine Learning for Future Networks including 5G, "Unified architecture for machine learning in 5G and future networks," Technical Specification ITU-T FG-ML5G-ARC5G, 2019.
[Fi18]	M. Filer *et al.*, "Multi-Vendor Experimental Validation of an Open Source QoT Estimator for Optical Networks," IEEE/OSA Journal of Lightwave Technology (JLT), vol. 36, pp. 3073-3082, 2018.
[FINISAR]	Flexgrid High Resolution Optical Channel Monitor (OCM) [On-line] www.finisar.com, accessed June 2018.
[Fl20]	C. Fludger, "Performance oriented DSP design for flexible coherent transmission," in Proc. OFC, 2020.
[Fr17]	F. Frey *et al.*, "Estimation of Trends for Coherent DSP ASIC Power Dissipation for different bitrates and transmission reaches," in Proc. Photonic Networks, 2017.
[Fu18]	S. Fujimoto *et al.*, "Addressing Function Approximation Error in Actor-Critic Methods," in Proc. ICML, 2018.
[Gi18]	Ll. Gifre *et al.*, "Autonomic Disaggregated Multilayer Networking," IEEE/OSA J. of Optical Communications and Networking, vol. 10, pp. 482-492, 2018.
[GuTh19]	V. Le Guen and N. Thome, "Shape and Time Distortion Loss for Training Deep Time Series Forecasting Models," In Proc. NeurIPS, 2019.
[Ha16]	H. Hasselt *et al.*, "Deep Reinforcement Learning with Double Q-learning," in Proc. AAAI Conference on AI, 2016.
[Infinera]	Infinera: "The Ultimate Guide to Nyquist Subcarriers," [on-line] https://www.infinera.com/wp-content/uploads/ The-Ultimate-Guide-to-Nyquist-Subcarriers-0208-WP-RevA-0719.pdf.
[Is02]	S. Ishak *et al.*, "Performance Evaluation of Short-Term Time-Series Traffic Prediction Model," J. of Transportation Engineering, vol. 128, pp. 490-498, 2002.
[ITU00]	"Principles for a Telecommunications Management Network," ITU-T, Rec. M.3010, 2000.
[ITU20]	"Framework for data handling to enable ML in future networks including IMT-2020," ITU-T Y.3174, 2020.

[Kl13] M. Klinkowski *et al.*, "Elastic Spectrum Allocation for Time-Varying Traffic in FlexGrid Optical Networks," IEEE J. on Selected Areas in Communications, vol. 31, pp. 26-38, 2013.

[Kr17] D. Krause *et al.*, "Design considerations for a digital subcarrier coherent optical modem," in Proc. OFC, 2017.

[Li20] Z. Li *et al.*, "Demonstration of Fault Localization in Optical Networks Based on Knowledge Graph and Graph Neural Network," in Proc. OFC, 2020.

[Lu20] H. Lun *et al.*, "Soft Failure Identification for Long-haul Optical Communication Systems Based on One-dimensional Convolutional Neural Network," IEEE/OSA J. of Lightwave Technol., vol. 38, pp. 2992-2999, 2020.

[Ma21] H. Mahmoud, "Parametric versus Semi and Nonparametric Regression Models," International Journal of Statistics and Probability, vol. 10, pp 90–109, 2021.

[MaCh01] D. Mandic and J. Chambers, "Recurrent Neural Networks for Prediction: Learning Algorithms, Architectures and Stability," Wiley, 2001.

[Mo17] F. Morales *et al.*, "Dynamic core VNT adaptability based on predictive metro-flow traffic models," IEEE/OSA J. Optical Comm and Networking, vol. 9, pp. 1202–1211, 2017.

[Mu19] F. Musumeci *et al.*, "A Tutorial on Machine Learning for Failure Management in Optical Networks," IEEE/OSA J. of Lightwave Technol., vol. 37, pp. 4125-4139, 2019.

[Ne17] P. Neves *et al.*, "Future mode of operations for 5G–The SELFNET approach enabled by SDN/NFV," Comput. Stand. Interfaces 2017, 54, 229–246.

[Pa14] F. Paolucci *et al.*, "Multipath Restoration and Bitrate Squeezing in SDN-based Elastic Optical Networks," Photonic Network Communications, vol. 28, pp. 45-57, 2014.

[Pa18] T. Panayiotou *et al.*, "Leveraging Statistical Machine Learning to Address Failure Localization in Optical Networks," IEEE/OSA J. of Optical Communications and Networking, vol. 10, pp. 162-173, 2018.

[Pa19] T. Panayiotou *et al.*, "A Data-Driven Bandwidth Allocation Framework with QoS Considerations for EONs," IEEE/OSA

Journal of Lightwave Technology (JLT), vol. 37, pp. 1853–1864, 2019.

[Po11] W. Powell, “Approximate Dynamic Programming, 2nd ed,” Wiley: New Jersey, USA, 2011.

[Po12] P. Poggiolini, “The GN Model of Non-Linear Propagation in Uncompensated Coherent Optical Systems,” IEEE/OSA Journal of Lightwave Technology (JLT), vol. 30, pp. 3857 - 3879, 2012

[Po14] P. Poggiolini *et al.*, “The GN-Model of Fiber Non-Linear Propagation and its Applications,” IEEE/OSA Journal of Lightwave Technology (JLT), vol. 32, pp. 694 - 721, 2014

[Po17] Y. Pointurier, “Design of Low-Margin Optical Networks,” IEEE/OSA Journal of Optical Communications and Networking, vol. 9, pp. A9-A17, 2017.

[Qi14] M. Qiu *et al.* “Digital subcarrier multiplexing for fiber nonlinearity mitigation in coherent optical communication systems,” OSA Optics Express, vol 22, pp. 18770-18777, 2014.

[Ra16] T. Rahman *et al.,* “Digital Subcarrier Multiplexed Hybrid QAM for Data-rate Flexibility and ROADM Filtering Tolerance,” in Proc. OFC, 2016.

[Ra18.1] D. Rafique and L. Velasco, “Machine Learning for Optical Network Automation: Overview, Architecture and Applications,” IEEE/OSA Journal of Optical Communications and Networking (JOCN), vol. 10, pp. D126-D143, 2018.

[Ra18.2] D. Rafique *et al.*, “Analytics driven fault discovery and diagnosis for cognitive root cause analysis,” in Proc. OFC, 2018.

[Ra19] D. Rafique *et al.*, “Machine Learning for Optical Network Automation: Overview, Architecture and Applications,” IEEE/OSA J. of Optical Comm and Networking, vol. 10, pp. D126-D143, 2018.

[Ru18] M. Ruiz *et al.*, “CURSA-SQ: A Methodology for Service-Centric Traffic Flow Analysis,” IEEE/OSA J. of Optical Comm and Networking, vol. 10, pp. 773-784, 2018.

[Ru20.1] M. Ruiz *et al.*, “Modeling and Assessing Connectivity Services Performance in a Sandbox Domain,” IEEE/OSA J. of Lightwave Technology, vol. 38, pp. 3180-3189, 2020.

[Ru20.2]	M. Ruiz *et al.*, “Knowledge Management in Optical Networks: Architecture, Methods and Use Cases [Invited],” IEEE/OSA J. of Optical Comm and Networking, vol. 12, pp. A70-A81, 2020.
[Sa15]	N. Sambo *et al.*, “Next Generation Sliceable Bandwidth Variable Transponders,” IEEE Communications Magazine, vol. 53, pp. 163-171, 2015.
[Se18]	E. Seve *et al.*, “Learning Process for Reducing Uncertainties on Network Parameters and Design Margins,” IEEE/OSA J. of Optical Communications and Networking, pp. A298-A306, 2018.
[Sh05]	R. Shumway *et al.*, “Time Series Analysis and Its Applications”, Springer Texts in Statistics, 2005.
[Sh18]	B. Shariati *et al.*, “Real-time Optical Spectrum Monitoring in Filterless Optical Metro Networks,” in IEEE/OSA Optical Fiber Communication Conference (OFC), 2018.
[Sh19]	B. Shariati *et al.*, “Learning from the Optical Spectrum: Failure Detection and Identification [Invited],” IEEE/OSA J. of Lightwave Technology, vol. 37, pp. 433-440, 2019.
[ShSt17]	R. Shumway and D. Stoffer, “Time Series Analysis and Its Applications,” Springer International Publishing, 2017.
[St04]	J. Strassner, “Policy-Based Network Management: Solutions for the Next Generation,” Morgan Kaufmann, 2004.
[Su20]	H. Sun *et al.*, “800G DSP ASIC Design Using Probabilistic Shaping and Digital Sub-Carrier Multiplexing,” IEEE/OSA J. of Lightwave Technology, vol. 38, pp. 4744-4756, 2020.
[SuBa18]	R. Sutton and A. Barto., “Reinforcement Learning: An Introduction, 2nd ed,” MIT Press: Cambridge, MA, USA; p. 1054, 2018.
[SuBa98]	R. Sutton and A. Barto, “Reinforcement learning: an introduction,” MIT Press, 1998.
[Ta21]	F. Tabatabaeimehr *et al.*, “Cooperative Learning for Disaggregated Delay Modeling in MultiDomain Networks,” IEEE Transactions on Network and Service Management, vol. 18, pp. 3633-3646, 2021.
[TIP]	Telecom Infra Project. [On-line] https://www.telecominfraproject.com/

[Tr21] S. Troia *et al.*, "On Deep Reinforcement Learning for Traffic Engineering in SD-WAN," IEEE J. Sel. Areas Commun., vol. 39, pp. 2198–2212, 2021.

[Ty06] A. Tychopoulos *et al.*, "FEC in optical communications - A tutorial overview on the evolution of architectures and the future prospects of outband and inband FEC for optical communications," IEEE Circuits and Devices Magazine, vol. 22, pp. 79-86, 2006.

[Va20] S. Varughese *et al.*, "Low Complexity Soft Failure Detection and Identification in Optical Links using Adaptive Filter Coefficients," in Proc. OFC, 2020.

[Ve12] L. Velasco *et al.*, "Modeling the Routing and Spectrum Allocation Problem for Flexgrid Optical Networks," Photonic Network Comm, vol. 24, pp. 177-186, 2012.

[Ve13] L. Velasco *et al.*, "Saving CAPEX by Extending Flexgrid-based Core Optical Networks towards the Edges," IEEE/OSA Journal of Optical Communications and Networking (JOCN), vol. 5, pp. A171-A183, 2013.

[Ve14] L. Velasco *et al.*, "In-Operation Network Planning," IEEE Communications Magazine, vol. 52, pp. 52-60, 2014.

[Ve17] L. Velasco *et al.*, "Designing, Operating and Re-Optimizing Elastic Optical Networks," (Invited Tutorial) IEEE/OSA J. of Lightwave Technology, vol. 35, pp. 513-526, 2017.

[Ve18.1] L. Velasco *et al.*, "An Architecture to Support Autonomic Slice Networking [Invited]," IEEE/OSA J. of Lightwave Technology, vol. 36, pp. 135-141, 2018.

[Ve18.2] L. Velasco *et al.*, "Building Autonomic Optical Whitebox-based Networks," IEEE/OSA J. of Lightwave Technology, vol. 36, pp. 3097-3104, 2018.

[Ve19.1] L. Velasco *et al.*, "Monitoring and Data Analytics for Optical Networking: Benefits, Architectures, and Use Cases," IEEE Network Magazine, vol. 33, pp. 100-108, 2019.

[Ve19.2] L. Velasco *et al.*, "A Learning Life-Cycle to Speed-up Autonomic Optical Transmission and Networking Adoption," in IEEE/OSA Journal of Optical Communications and Networking, vol. 11, pp. 226-237, 2019.

[Ve20] L. Velasco *et al.*, “Supporting Time-Sensitive and Best-Effort Traffic on a Common Metro Infrastructure,” IEEE Communications Letters, vol. 24, pp. 1664-1668, 2020.

[Ve21] L. Velasco *et al.*, “End-to-End Intent-Based Networking,” IEEE Communications Magazine, vol. 59, pp. 106-112, 2021.

[VeRu17] L. Velasco and M. Ruiz, *Provisioning, Recovery and In-operation Planning in Elastic Optical Networks*, Wiley, 2017.

[Wa16] Z. Wang *et al.*, “Dueling Network Architectures for Deep Reinforcement Learning,” in Proc. ICML, 2016.

[Zh11] Y. Zhang *et al.*, “Digital subcarrier multiplexing for flexible spectral allocation in optical transport network,” OSA Optics Express, vol. 19, pp. 21880-21889, 2011.

[Zh20] C. Zhang *et al.*, “Interpretable Learning Algorithm Based on XGBoost for Fault Prediction in Optical Network,” in Proc. OFC, 2020.

[ZhQi05] P. Zhang and M. Qi, “Neural network forecasting for seasonal and trend time series,” European J. of Operational Research, vol. 160, pp. 501-514, 2005.